



## **ING. AUTOMOTRIZ**

### **TRABAJO INTEGRACIÓN CURRICULAR PREVIA A LA OBTENCIÓN DEL TÍTULO DE INGENIERO EN AUTOMOTRIZ.**

#### **AUTORES:**

Vinicio Alexander Guachamín Quiña  
César Eduardo Ortega Feijoo

#### **TUTOR:**

Ing. Marcos Gutiérrez Ojeda PhD.

**EFFECTO DEL SWIRL Y DE LA COLISIÓN DIRECTA EN LOS FLUJOS DE  
ATOMIZACIÓN DE COMBUSTIBLE DE UN CONCEPTO DE MOTOR  
MULTI-INYECTOR PARA DIÉSEL, BIODIÉSEL Y HEPTANO**

JUNIO 2022



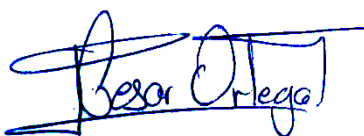
## CERTIFICACIÓN

Nosotros, Vinicio Alexander Guachamín Quiña y César Eduardo Ortega Feijoo, declaramos bajo juramento, que el trabajo aquí descrito es de nuestra autoría; que no ha sido presentado anteriormente para ningún grado o calificación profesional y que se ha consultado la bibliografía detallada.

Cedemos nuestros derechos de propiedad intelectual a la Universidad Internacional del Ecuador, para que sea publicado y divulgado en internet, según lo establecido en la Ley de propiedad Intelectual, reglamento y leyes.



Vinicio Alexander Guachamín Quiña



César Eduardo Ortega Feijoo

Yo, Marcos Xavier Gutiérrez Ojeda, certifico que conozco al autor del presente trabajo siendo el responsable exclusivo tanto de su originalidad y autenticidad, como de su contenido.



Marcos Xavier Gutiérrez Ojeda, PhD

## **DEDICATORIA**

El siguiente trabajo lo dedico a mi familia, que con su constante apoyo me han otorgado las herramientas necesarias para forjar mi futuro en la carrera de Ingeniería Automotriz, así mismo a mis compañeros de carrera que con su soporte y carisma diario han logrado que mi persona logre la meta que hace cinco años empecé. Finalmente, pero no menos importante, a mis seres queridos que Dios acogió en su brazo y que por distintas circunstancias no han podido estar presente a la fecha.

Vinicio Alexander Guachamín Quiña

## **DEDICATORIA**

Luego de varios años de esfuerzo y perseverancia dedico este proyecto a cada uno de mis familiares.

A mi esposa Katherine ya que fue mi pilar fundamentan en mis estudios, mi hijo Ismael quien es mi mayor motivación por el cual siempre pienso en superarme día a día, mis Padres Francisco y Esperanza, con sus bendiciones me han llevado por el camino del bien y que me han ayudado en el transcurso de mi carrera, Marquito y Elsi que de una u otra forma estuvieron pendientes de todo el proceso.

César Eduardo Ortega Feijoo

## **AGRADECIMIENTO**

Agradezco a Dios, quién me ha dado la sabiduría infinita para llegar a la cúspide de mi carrera. A mi madre quién ha sido mi compañera de vida y soporte en estos últimos años. A mi padre y hermana que a la distancia velan por mi seguridad e integridad. A mi familia, quién me ha apoyado en cada paso dándome consejos que mi persona necesitó en su etapa formativa. Agradezco a la Universidad Internacional del Ecuador, por otorgarme las herramientas necesarias para formarme como un profesional mediante docentes, compañeros y convenios que me han servido para crecer en todo ámbito. Finalmente, a mi tutor Ing. Marcos Gutiérrez por toda la increíble logística y opinión para culminar mi trabajo de titulación. Infinitamente gracias.

Vinicio Alexander Guachamín Quiña

## **AGRADECIMIENTO**

Agradezco a mis padres por siempre creer en mí y apoyarme sin límites, a mi esposa que siempre estuvo pendiente de mis avances, mi hijo que soy su ejemplo de vida por el cual no me rindo nunca, a la universidad la cual me dio la oportunidad de tener muchas experiencias en el transcurso de mi carrera.

Agradezco a todos mis maestros y tutores que me brindaron sus conocimientos y consejos dentro de las aulas quienes les he llegado a tener un gran aprecio, mis amigos que nos brindamos mucho apoyo y vivencias durante este proceso, espero que todas las personas que conocí durante mi proceso de formación profesional siempre guarden los buenos momentos que pasamos.

César Eduardo Ortega Feijoo

## ÍNDICE DE CONTENIDO

CERTIFICACIÓN .....	iii
DEDICATORIA .....	iv
DEDICATORIA .....	v
AGRADECIMIENTO .....	vi
AGRADECIMIENTO .....	vii
EFFECTO DEL SWIRL Y DE LA COLISIÓN DIRECTA EN LOS FLUJOS DE ATOMIZACIÓN DE COMBUSTIBLE DE UN CONCEPTO DE MOTOR MULTI-INYECTOR PARA DIÉSEL, BIODIÉSEL Y HEPTANO .....	1
RESUMEN .....	1
ABSTRACT .....	1
1. INTRODUCCION .....	2
2. FUNDAMENTACION TEORICA.....	2
3. MATERIALES Y METODOS.....	3
5. CONCLUSIONES .....	9
6. REFERENCIAS.....	10
7. ANEXOS.....	12



# EFECTO DEL SWIRL Y DE LA COLISIÓN DIRECTA EN LOS FLUJOS DE ATOMIZACIÓN DE COMBUSTIBLE DE UN CONCEPTO DE MOTOR MULTI-INYECTOR PARA DIÉSEL, BIODIÉSEL Y HEPTANO

Vinicio Guachamín<sup>1</sup>, César Ortega<sup>2</sup>, Marcos Gutiérrez<sup>3</sup>.

<sup>1</sup> *ingeniería Automotriz Universidad Internacional del Ecuador, email: [viaguachaminqu@uide.edu.ec](mailto:viaguachaminqu@uide.edu.ec)  
Quito - Ecuador*

<sup>2</sup> *ingeniería Automotriz Universidad Internacional del Ecuador, email: [ceortegafe@uide.edu.ec](mailto:ceortegafe@uide.edu.ec)  
Quito - Ecuador*

<sup>3</sup> *ingeniería Automotriz Universidad Internacional del Ecuador, email: [magutierrezoj@uide.edu.ec](mailto:magutierrezoj@uide.edu.ec)  
Quito - Ecuador*

## RESUMEN

Este documento describe el efecto que tiene un concepto de motor multi-inyector cuando los flujos de atomización de cuatro inyectores de un solo orificio, colisionan entre sí; y en otro escenario, provocan un remolino o mejor conocido como swirl. Estos efectos se comparan calculando el diámetro medio de Sauter tanto para diésel como para biodiésel, y tomando como referencia la atomización de un inyector con una tobera de cuatro orificios con el uso de heptano (C<sub>7</sub>H<sub>16</sub>), que es el sustituto del diésel con el que se llevan a cabo estudios de diésel con un reducido margen de error, por medio de la simulación de Dinámica de Fluidos con OpenFOAM® bajo condiciones reactivas. El propósito de este estudio es el determinar la configuración multi-inyector que ofrece el mayor nivel de atomización y de mezcla homogénea. Se encontró que el menor diámetro de atomizado de las moléculas de combustible se produce con la colisión directa de los flujos de atomización y que la mayor turbulencia se obtiene con flujos individuales y con el swirl debido a la mayor velocidad del fluido en el interior de la cámara donde es inyectado el combustible.

**Palabras clave:** diésel, biodiésel, heptano, swirl, inyector, atomización.

## ABSTRACT

This document describes the effect that a multi-injector engine concept has when the atomization sprays of four single-hole injectors collide with each other; and in another scenario, they cause a vortex or better known as a swirl. These effects are compared by calculating the Sauter mean diameter for both diesel and biodiesel, and taking as a reference the atomization of an injector with a four-hole nozzle with the use of heptane (C<sub>7</sub>H<sub>16</sub>), which is the substitute for diesel. The study of diesel based on heptane are carried out with a reduced margin of error and with a good standard, by means of Fluid Dynamics Simulation (CFD) with OpenFOAM® under reactive conditions. The purpose of this study is to determine the multi-injector configuration that offers the highest level of atomization and homogeneous mixing. It was found that the smallest atomized diameter of the fuel molecules occurs with the direct collision of the atomizing flows and that the greatest turbulence is obtained with individual flows and with the swirl due to the higher speed of the fluid in the chamber where the fuel is injected.

**Keywords:** diesel, biodiesel, heptane, swirl, injector, atomization

## 1. INTRODUCCION

Muchos de los estudios sobre cámaras de combustión y sistemas de inyección, se han enfocado en técnicas para mejorar la atomización del combustible y su homogenización con el aire. Una de las técnicas más generalizadas es la de generar un remolino, o mejor conocido como swirl, con los flujos de atomización; una técnica menos conocida y hasta cierto punto evitada, es la de la colisión directa de estos flujos. Entre las razones más comunes para evitar esta colisión directa, está la coalescencia de las moléculas atomizadas de combustible. Esto, a bajas presiones de inyección es bastante comprensible; sin embargo, a altas, la energía cinética que llevan consigo los flujos de atomización que interactúan entre sí, hacen que las moléculas choquen unas con otras y se dividan en moléculas más pequeñas.

## 2. FUNDAMENTACION TEORICA

Se sabe muy poco sobre la experimentación práctica en un motor con múltiples inyectores dentro de su cámara de combustión, incluso cuando desde 1995 Takeda y Niimura instalaron con éxito en un motor diésel tres inyectores diésel, uno montado verticalmente y los otros montados en diagonal desde la dirección lateral. En dicho estudio se obtuvo una mejora en el consumo específico de combustible y en la emisión de partículas; mientras que el NOx fue bajo, debido a la post-inyección por los inyectores laterales. Takeda formuló la teoría de que el aire no utilizado que quedaba en el centro de la cámara de combustión era efectivamente utilizado debido a los efectos de turbulencia que generaba la inyección y combustión de los inyectores laterales [1].

Más de 20 años después, el concepto de Okamoto y Uchida utilizó prácticamente la misma configuración que Takeda, un inyector se montó verticalmente en el cilindro y dos inyectores adicionales se montaron inclinados

en la circunferencia de la cavidad del pistón. La característica principal de su trabajo, menciona que los flujos de combustible de los inyectores laterales se dirigieron en la dirección del remolino para evitar la colisión directa entre flujos. Afirieron un rendimiento general mejorado del motor, incluida una reducción de NOx, como resultado del control de la liberación de calor durante la combustión [2]. En 2019, el estudio de Nyrenstedt, et. al., [3] proporcionó un enfoque adecuado para probar los beneficios de los conceptos de dos inyectores sobre el inyector único con el que cuentan los motores convencionales; se han sugerido múltiples inyectores para reducir la pérdida de calor y el desperdicio de combustible en el cilindro del motor a través de la reducción del impacto del flujo en las paredes del cilindro, porque los inyectores suministran combustible en un movimiento giratorio mientras se colocan en el borde del pistón.

Una falla importante de los estudios computacionales y propuestas de conceptos [2, 3] es la falta de resultados experimentales, que con validez estadística necesitan ser reproducidos. Takeda y Niimura [1], encontraron experimentalmente que el humo y el consumo de combustible empeoraban cuando la dirección de inyección relativa de los inyectores central y lateral chocaban entre sí, debido a una alta concentración de combustible en el centro del pistón donde se produjo la colisión y a una baja concentración de oxígeno; sin embargo, en 1995, el estudio de colisiones con flujos de combustible no tenía las posibilidades computacionales actuales para calcular y simular los flujos; y experimentalmente, fue difícil modificar los patrones de rociado en términos de longitud, ángulo y nivel de atomización dependiendo de la presión de inyección y de la electrónica para su control, esta limitación en ese tiempo, incluso contaba para simulaciones por computadora.

Los modelos de patrón de pulverización y atomización de combustible [4-6] son muy plausibles para cuantificar el diámetro de las gotas de combustible atomizado en términos del diámetro medio de Sauter (SMD) [7], pero en estos modelos no hay posibilidad de

estudiar la interacción entre flujos de atomización. Sin embargo, las simulaciones de dinámica de fluidos computacional (CFD) calculan, evalúan y representan flujos de atomización individuales [8, 9] con bastante precisión, así como es posible representar también, la interacción entre múltiples flujos de atomización; ya sea por colisión directa o por la generación de un swirl.

Este artículo presenta un nuevo enfoque de los conceptos y el modelado computacional de la interacción de los flujos de atomización de combustible, enfocándose en la atomización de las gotas a través de su colisión y la generación del swirl, refutando las conclusiones anteriores de que la colisión y el avance de los fluidos con su correspondiente desaceleración fusionan las gotas atomizadas [10]. El concepto motor multi-inyector presentado se analiza para demostrar que la interacción de los flujos de atomización reduce el diámetro de las gotas de combustible, en comparación con la inyección por parte de un solo inyector con varios orificios en la tobera. Nuestra investigación tiene como propósito ampliar el conocimiento actual y contribuir a una estandarización de las simulaciones CFD y modelos conceptuales con respecto a los conceptos de multi-inyector. El objetivo de este estudio es el determinar la configuración multi-inyector que ofrece el mayor nivel de atomización y de mezcla homogénea. Este artículo arroja nueva luz sobre los conceptos y modelos para mejorar la eficiencia de la combustión y principalmente los parámetros que mejoran la atomización del combustible, que como consecuencia produce una mezcla aire-combustible más homogénea.

La pregunta que debe hacerse es: ¿Contribuye el swirl y la colisión entre los flujos de combustible a alta presión en la cámara de combustión a una mayor atomización de las gotas de combustible? Como una respuesta, puede concebirse la hipótesis de que un flujo de combustible atomizado a alta velocidad que colisiona con otro da como resultado una mayor ruptura de las gotas de combustible.

En ausencia de instalaciones de prueba inmediatas en motores reales y habilitados para probar varias configuraciones con varios inyectores de combustible en el mismo

cilindro del motor; los conceptos y el modelado CFD siguen siendo actuales y se convierten en un factor decisivo en el proceso de desarrollo. En un intento por innovar la próxima generación de motores de combustión interna, proponemos este concepto de motor multi-inyector para mejorar la atomización de combustible por medio de la interacción, la colisión y el swirl de los flujos de inyección.

### 3. MATERIALES Y METODOS

Los datos e información usados para la presente investigación comprenden la caracterización del diésel y del biodiésel (Tab. 1), para calcular el diámetro medio de Sauter de las moléculas atomizadas de combustible; las propiedades del aire, bajo condiciones del ciclo de compresión de aire en un motor diésel (Tab. 2), la ecuación para calcular el diámetro medio de Sauter (Ec.1), y los parámetros para llevar a cabo la simulación con OpenFOAM® versión 9 con el solver reactingFoam (Tab. 3 y Fig. 4), considerando el heptano (C<sub>7</sub>H<sub>16</sub>) como sustituto del diésel por sus propiedades similares y datos más exactos para ser simulados [11]. La simulación se lleva a cabo con tres modelos en los que los flujos de atomización son independientes y salen de un mismo inyector (Fig. 1), los flujos colisionan entre sí saliendo de 4 inyectores opuestos entre sí (Fig. 2) y los flujos colisionan parcialmente unos con otros ocasionando el efecto swirl (Fig. 3).

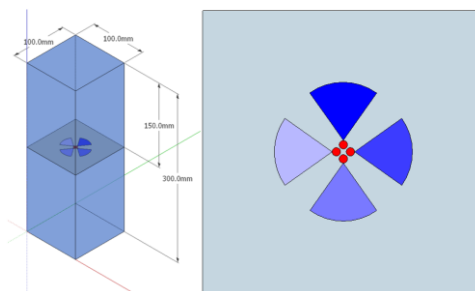


**Figura 1.** Modelo del estudio implementado con cuatro flujos de atomización independientes. Posición en mm de los orificios del inyector en una cámara tridimensional de 300 mm de alto: 1 (5, 150, 0), 2 (-5, 150, 0), 3 (0, 150, 5), 4 (0, 150 - 5).

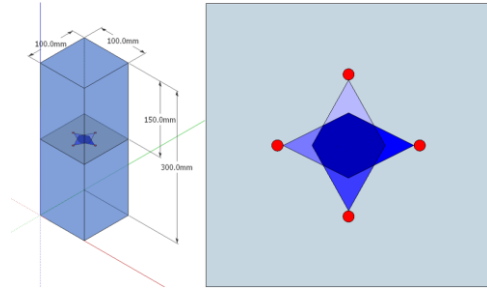


**Figura 2.** Modelo del estudio implementado con cuatro flujos de atomización que colisionan entre sí. Posición en mm de los orificios del inyector en una cámara tridimensional de 300 mm de alto: 1 (-25, 150, 0), 2 (25, 150, 0), 3 (0, 150, -25), 4 (0, 150, 25).

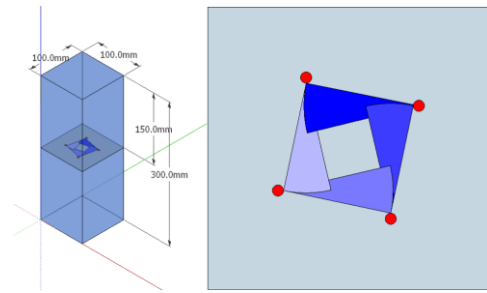


**Figura 3.** Modelo del estudio implementado con cuatro flujos de atomización que provocan un efecto swirl. Posición en mm de los orificios del inyector en una cámara tridimensional de 300 mm de alto; 1 (-25, 150, -15), 2 (25, 150, 15), 3 (15, 150, -25), 4 (-15, 150, 25).

Tipo de combustible	Diésel	Biodiésel
Densidad @ 37.8 °C [kg/m3]*	834.197	884.110
Viscosidad cinemática @ 37.8 °C [cSt]**	4.02	6.58
Viscosidad dinámica @ 37.8 °C [cP]***	3.353	5.817
Tensión superficial [N/m]****	0.023	0.028

**Tabla 1.** Propiedades del diésel. \*Valores medidos experimentalmente a 15.55°C y corregidos a 37.8°C [12]. \*\*Valores medidos experimentalmente. \*\*\*Valores calculados.

\*\*\*\*Tomado de Lahane, S., Subramanian, K.A.[4].

Densidad @ 915K & 61bar [kg/m3]* (valores al final de la compresión )	23.23
Viscosidad dinámica @ 915K & 61bar [cP]**	0.039

**Tabla 2.** Propiedades del aire. \*Valores calculados de acuerdo a la ley del gas ideal. \*\*Valores tomados de Willi Bohl, Wolfgang Elmendorf [13].

Según Hiroyasu et al. [7],  $X_{32}^{LS}$  y  $X_{32}^{HS}$  son el tamaño de las gotas de combustible atomizado para pulverizaciones incompletas y completas correspondientemente, que dependen principalmente de la velocidad de inyección y las condiciones del aire en el ambiente que se inyecta el combustible.  $X_{32}$  es el valor mayor de ambos. Esto significa que  $X_{32}$  es el mayor diámetro medio esperado de Sauter de las gotas de combustible atomizado. Este modelo matemático con las ecuaciones de apoyo se describe en detalle a continuación y en las fuentes [14] y [15].

$$X_{32} = \text{Max} (X_{32}^{LS}, X_{32}^{HS}) \quad \text{Ec. [1]}$$

Donde:

$$X_{32}^{LS} = 4.12 \times D_n \times Re^{0.12} \times We^{-0.75} \times \left(\frac{\mu_l}{\mu_a}\right)^{0.54} \times \left(\frac{\rho_l}{\rho_a}\right)^{0.18}$$

$$X_{32}^{HS} = 0.38 \times D_n \times Re^{0.25} \times We^{-0.32} \times \left(\frac{\mu_l}{\mu_a}\right)^{0.37} \times \left(\frac{\rho_l}{\rho_a}\right)^{-0.47}$$

$$Re = \frac{v_{inj} \cdot D_n}{\nu_l}$$

$$We = \frac{v_{inj}^2 \cdot D_n \cdot \rho_l}{\sigma_l}$$

$X_{32}$ : Diámetro medio de Sauter de las gotas de combustible atomizadas, como el valor máximo entre  $X_{32}^{LS}$  y  $X_{32}^{HS}$ .

$X_{32}^{LS}$ : Diámetro medio de Sauter de las gotas de combustible atomizadas para una atomización incompleta.

$X_{32}^{HS}$ : Diámetro medio de Sauter de las gotas de combustible atomizadas para una atomización completa.

Re: Número de Reynolds [-].

We: Número de Weber [-].

$\mu_l$ : Viscosidad dinámica del combustible [Pa-s].

$\mu_a$ : Viscosidad dinámica del aire [Pa-s].

$\rho_l$ : Densidad del combustible bajo las condiciones de inyección [kg/m<sup>3</sup>].

$\rho_p$ : Densidad del combustible bajo las condiciones de compresión del motor [kg/m<sup>3</sup>].

$\sigma_l$ : Tensión superficial [N/m].

vinj: Velocidad de la inyección [m/s].

Dn: Diámetro de los orificios de la tobera [m].

El diámetro X32 calculado se compara con el resultado de la simulación CFD, pero solo para la configuración con 4 flujos de atomización independientes. Por lo tanto, es posible evaluar la precisión del modelo matemático (Ec. 1) con la simulación CFD y analizar más a fondo la interacción entre múltiples pulverizaciones. Una formulación matemática de múltiples flujos de atomización que interactúan entre sí como en el caso de formulación del Diámetro Medio de Sauter, está fuera del alcance de esta investigación, ya que en OpenFOAM® se implementan algoritmos más precisos que consideran las condiciones volumétricas resolviendo las ecuaciones diferenciales de Dinámica de Fluidos. Por lo tanto, el diámetro resultante de las gotas de combustible atomizado bajo el efecto de la colisión de los flujos de atomización, no se considera analíticamente en esta investigación, pero se hace una simulación CFD detallada bajo condiciones reactivas para simular y entender su efecto.

Este método para simular la interacción por medio de la colisión y swirl entre flujos de atomización con las condiciones físicas y químicas de la cámara de combustión de un motor de combustión interna es una alternativa innovadora al desarrollo de modelos matemáticos, que en su mayoría son dependientes de condiciones de prueba específicas; esto también es una alternativa a procedimiento que consumen una alta cantidad de recursos, tanto para su modelado,

simulación y producción de prototipos de prueba.

El enfoque expuesto en esta investigación puede repetirse y adaptarse para ser verificado, mejorado o extendido a otras aplicaciones, considerando otros tipos de combustibles y motores.

Combustible	Diésel
Potencia del motor	110kW@2500rpm
Torque	20Nm@1400rpm
Presión de inyección [bar]	1500
Duración de la inyección [°]*	22.5
Duración de la inyección [s]*	0.0016
Presión de compresión [bar]**	61
Temperatura de compresión [K]	915
Temperatura de inyección del combustible [K]	310
$k$ [m <sup>2</sup> /s <sup>2</sup> ]**	0.275
$\varepsilon$ [m <sup>2</sup> /s <sup>3</sup> ]**	9.045
$\alpha$ & $\mu$ [kg/ m s]**	0.003353
Número de orificios	1
Coefficiente de descarga de la tobera*	0.8
Diámetro de los orificios de la tobera @ 1500bar [mm]**	0.4
Masa inyectada de combustible [kg]**	0.000077

**Tabla 3.** Parámetros del sistema de inyección para la simulación con OpenFOAM® versión 9.

\*Valores referenciales. \*\*Valores calculados basados en el modelo de simulación

kqRwallFunction for k, y epsilonWallFunction para  $\epsilon$  del software [8, 16].



**Figura 4.** Perfil del flujo másico de la inyección con 17 datos de entrada para la simulación.

El tiempo de inyección de 1.6ms corresponde al tiempo necesario para generar la potencia máxima del motor.

#### 4. RESULTADOS Y DISCUSION

Los diámetros mínimos de atomización del diésel (Fig. 5, Tab. 4) y biodiésel (Fig. 6, Tab. 4) calculados con la ecuación 1 son muy similares entre sí, y son medianamente similares a los obtenidos con el heptano (Tab. 5), como sustituto del diésel, por medio de la simulación con OpenFOAM®; sin embargo, los diámetros más grandes de atomización tienen una variación de casi el 50% entre los valores calculados y los simulados (Tab. 4, Tab. 5). Una limitación importante de la ecuación 1, es que solo es válido para un solo flujo y no es válido para estudiar la interacción entre flujos de atomización. Esto muestra también el potencial y la necesidad de refinar los modelos matemáticos y los procedimientos de simulación, para condiciones en los que varios flujos de atomización interactúan entre sí.

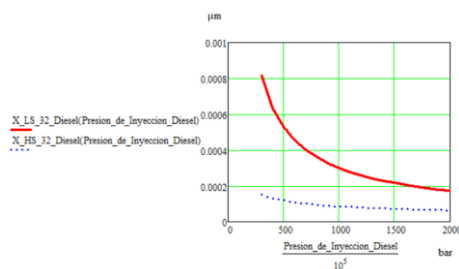


**Figura 5.** Diámetro medio de Sauter para el caso de diésel con diferentes presiones de inyección.

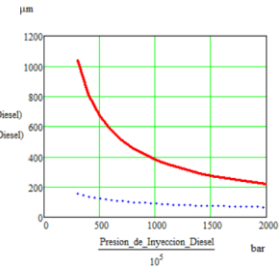


**Figura 6.** Diámetro medio de Sauter para el caso de biodiésel con diferentes presiones de inyección.

	Diésel	Biodiésel
$X_{32}^{HS}$	72.73 $\mu\text{m}$	75.13 $\mu\text{m}$
$X_{32}^{LS}$	216.94 $\mu\text{m}$	275.77 $\mu\text{m}$

**Tabla 4.** Diámetros de atomización de Sauter XHS y XLS para diésel y biodiésel. El diámetro máximo XHS de atomización corresponde al menor valor del diámetro de las moléculas atomizadas expresadas en  $\mu\text{m}$  y XLS corresponde al mayor del diámetro que puede llegar a ser atomizado.

	d0 mín.	d0	d0 máx.
Modelo del estudio implementado con cuatro flujos de atomización independientes.	64.26	113.46	145.45
Modelo del estudio implementado con cuatro flujos de atomización que colisionan entre sí.	59.37	112.88	146.22
Modelo del estudio implementado con cuatro flujos de atomización que provocan un efecto swirl.	65.54	113.41	145.26

**Tabla 5.** Diámetro medio de las gotas de combustible atomizado con las 3 configuraciones de estudio. Diámetro más probable – d0, diámetro máximo – d0 máx, y diámetro mínimo – d0 mín., simulado en OpenFOAM con heptano (C7H16).

El menor diámetro de las partículas atomizadas de combustible en el concepto multi-inyector, se obtiene con la configuración de 4 flujos chocan entre sí; sin embargo, con esta misma configuración se obtiene el valor más alto de las tres configuraciones para el diámetro máximo. El diámetro de las moléculas atomizadas de combustible con el

efecto swirl, es mayor en comparación con los flujos independientes y con la configuración que produce colisión.

La prueba de Chi Cuadrado (Fig. 7), muestra que, al no rechazarse la hipótesis nula, existe una independencia entre el diámetro de atomización de las moléculas de combustible y la configuración de los flujos de atomización. Esto indica que la interacción no siempre significa una mayor atomización, como se demostró con el swirl.

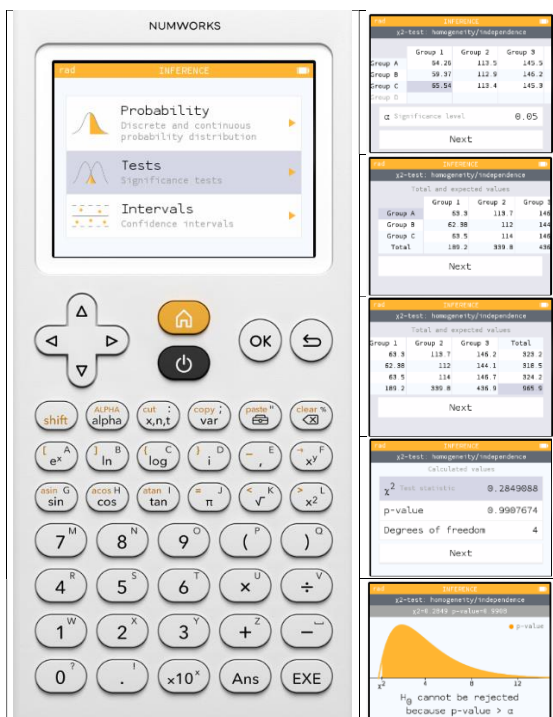


**Figura 7.** Prueba de Chi Cuadrado realizada con la calculadora científica Numworks [17].

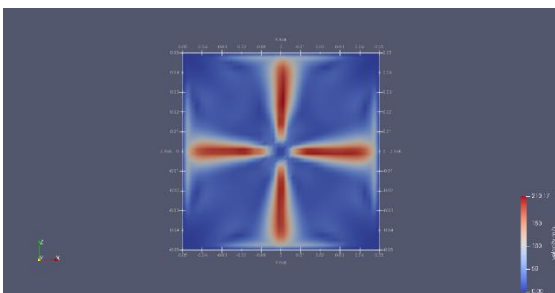


**Figura 8.** Velocidad de los flujos de atomización con la configuración de 4 flujos independientes, luego de 1.6ms.

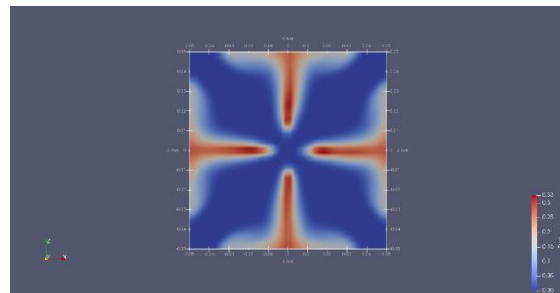


**Figura 9.** Concentración de combustible con la configuración de 4 flujos independientes, luego de 1.6ms.

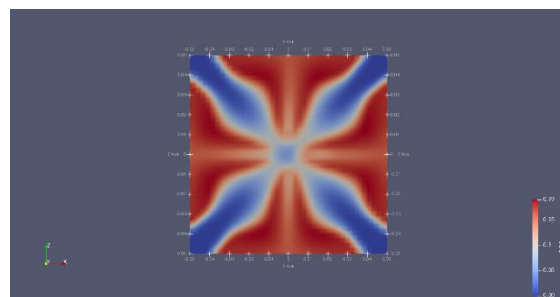


**Figura 10.** Concentración de CO2 con la configuración de 4 flujos independientes, luego de 1.6ms.

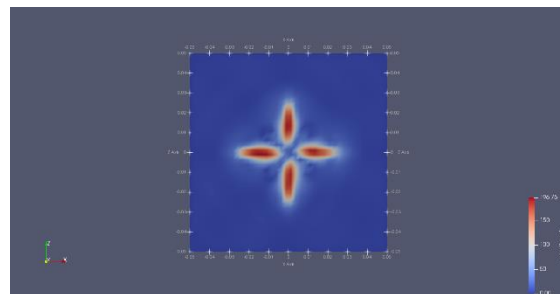


**Figura 11.** Velocidades de los flujos de atomización con la configuración de 4 flujos que colisionan entre sí, luego de 1.6ms.

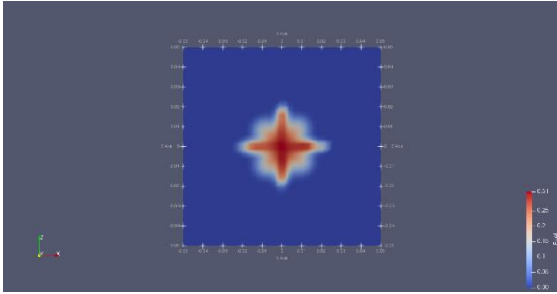


**Figura 12.** Concentración de combustible con la configuración de 4 flujos que colisionan entre sí, luego de 1.6ms.

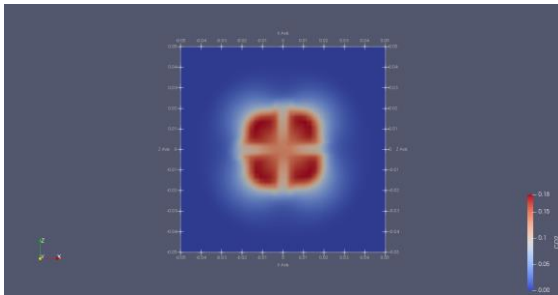


**Figura 13.** Concentración de CO2 con la configuración de 4 flujos que colisionan entre sí, luego de 1.6ms.

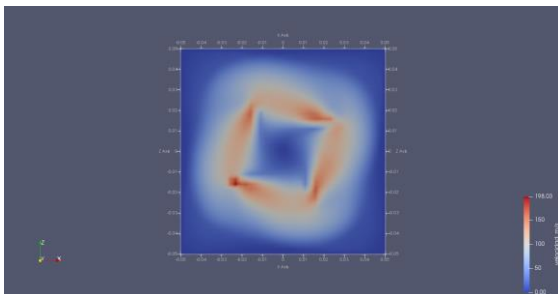


**Figura 14.** Velocidades de los flujos de atomización con la configuración de 4 flujos que provocan un efecto swirl, luego de 1.6ms.

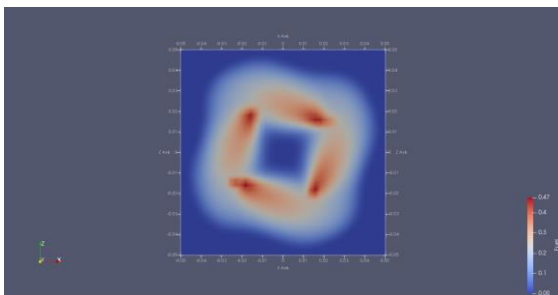


**Figura 15.** Concentración de combustible con la configuración de 4 flujos que provocan un efecto swirl, luego de 1.6ms.

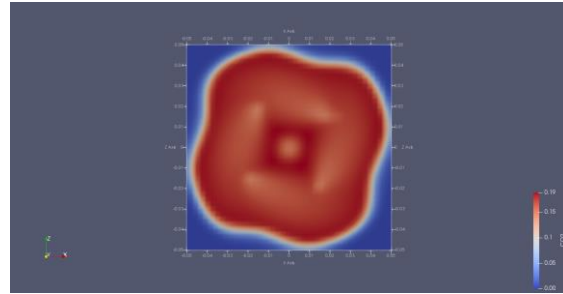


**Figura 16.** Concentración de CO2 con la configuración de 4 flujos que provocan un efecto swirl, luego de 1.6ms.

La configuración con flujos de atomización independientes muestra una mayor velocidad, principalmente porque tienen menos resistencia, en comparación con la configuración de colisión y de swirl. La concentración de combustible es mayor con el efecto swirl, lo que muestra un mayor efecto de coalescencia de moléculas en comparación con el efecto de la colisión. La concentración de CO2 es ligeramente menor con la configuración de colisión, lo que demuestra que en el centro de la cámara la concentración de combustible es mayor y la concentración de O2 es menor (Fig.8-Fig.16, Tab. 6); sin embargo, el diámetro de las moléculas atomizadas es menor. Con el efecto swirl, el espacio que ocupa el proceso de combustión en la cámara es mayor, como muestra la distribución de CO2 (Fig. 16).

Nuestro concepto concuerda con trabajos previos [1-3], sin embargo, la mayoría de ellos tienen un fuerte enfoque en el swirl resultante de la interacción de los flujos de atomización, y se analiza menos sobre la colisión de las gotas de combustible. En este sentido, Reitz en 1986 [10] llamó la atención sobre la coalescencia de las gotas de combustible atomizado. Hoy en día, con las tecnologías actuales y las instalaciones de CFD que implementan modelos matemáticos más desarrollados, se distingue la atomización aprovechada de las gotas de combustible que chocan entre sí.

Una de las limitaciones de este estudio, es la falta de pruebas experimentales que validen el concepto. Estas limitaciones revelan la dificultad de implementar este nuevo concepto en los motores y sistemas de inyección de



combustible actuales, y resaltan también la necesidad de desarrollar nuevos conceptos de motor y sistemas de inyección de combustible radicalmente nuevos.

	velocidad máxima de los flujos [m/s]	Concentración máxima de combustible [0-1]	Concentración máxima de CO2 [0-1]
Modelo del estudio implementado con cuatro flujos de atomización independientes.	210.17	0.33	0.19
Modelo del estudio implementado con cuatro flujos de atomización que colisionan entre sí.	196.75	0.31	0.18
Modelo del estudio implementado con cuatro flujos de atomización que provocan un efecto swirl.	198.03	0.47	0.19

**Tabla 6.** Velocidad máxima de los flujos de atomización y concentraciones de combustible y de CO2 con las tres configuraciones del estudio simulado en OpenFOAM con heptano (C7H16).

Investigación adicional sobre los flujos de atomización de combustible en reactivos y no reactivos, con condiciones precisas y exactas de la cámara de combustión, ayudaría a desarrollar modelos matemáticos y de simulación que sean menos discrepantes entre sí.

Estos resultados muestran que la interacción de las moléculas de combustible en la colisión reduce su diámetro, mientras que el swirl provoca un aumento del mismo, lo que significa que, el swirl ordena las moléculas, pero no las atomiza más.

## 5. CONCLUSIONES

Como se indicó en la introducción, nuestro propósito es ampliar el conocimiento y contribuir a una estandarización de la simulación CFD y de los modelos con respecto a los conceptos multi-inyectores, sacando a la luz las dependencias entre configuraciones y

discrepancias actuales para satisfacer de manera consistente cualquier falta de conocimiento.

Nuestro trabajo nos ha llevado a concluir por medio de la simulación CFD, que la interacción, como la colisión y el swirl de los flujos de atomización de combustible en condiciones reactivas, atomizan aún más las gotas de combustible y esto puede contribuir a una mejor y más homogénea mezcla aire-combustible en el cámara de combustión.

El diámetro reducido resultante de la simulación CFD de este estudio sugiere que la mayor atomización de las gotas de combustible se debe a la colisión y a la interacción de los flujos de atomización de combustible, además de las condiciones propicias en la cámara de combustión; tales como: la alta presión y alta temperatura, lo que conduce a una mayor ruptura, evaporación y desintegración de las moléculas de combustible.

La evidencia de este estudio respalda la idea de que la interacción de los flujos de atomización puede ayudar a reducir el diámetro de las gotas de combustible debido a la colisión y swirl resultante, y esto supera el efecto de la coalescencia de las gotas. Esto se puede explicar por la alta velocidad de los flujos de combustible, donde en lugar de detenerse y fusionarse, los flujos continúan su camino rompiéndose entre sí hasta que comienza el proceso de combustión. Se debe tener mucho cuidado cuando los flujos de combustible se representen como un flujo continuo de combustible; solo cerca de cada orificio de la boquilla hay una zona de alta densidad de combustible líquido, luego, durante la ruptura del flujo, se produce la colisión de las gotas de combustible atomizado con alta energía cinética. A esto hay que añadir el efecto de la presión y la temperatura durante las condiciones de reacción, es decir, las condiciones necesarias para el proceso de combustión.

Nuestra investigación en esta área aún está en curso y parece posible confirmar nuestra hipótesis experimentalmente con un motor de combustión real, capaz de proporcionar inyecciones multidireccionales de combustible.

Estamos seguros de que nuestra investigación mejora y aporta nuevos conocimientos sobre los conceptos de motores multi-inyectores, y refuerza la necesidad y la urgencia de contar con sistemas y procedimientos de combustión eficientes con tecnologías bien conocidas y actuales como los motores de combustión interna.

Actualmente nuestro trabajo estudió la interacción simultánea de cuatro flujos de atomización de combustible mediante simulaciones CFD con OpenFOAM®, cuyas ecuaciones, métodos y algoritmos han sido probados y validados con éxito en varios estudios previos. Sin embargo, nuestro trabajo tiene claramente algunas limitaciones en cuanto a la simulación y la validación del concepto mediante un procedimiento de prueba experimental.

Si los tiempos de inyección o la potencia del motor cambian; entonces también cambiarán el perfil de velocidades, concentración de combustible líquido, de CO<sub>2</sub>; así como también el diámetro de las moléculas atomizadas. Por esta razón si cambian los parámetros de funcionamiento del motor o de la inyección, será necesario una nueva simulación CFD por cada cambio.

Existen limitaciones en cuanto al diseño, construcción y prueba, con altos estándares de calidad y niveles industriales, para mostrar una relevancia física completa y una aplicabilidad pragmática del concepto que proponemos. Sin embargo, creemos que nuestro trabajo podría ser el marco de referencia para probar este y los conceptos anteriores de motores multi-inyectores, y en consecuencia, construir nuevos prototipos para tener nuevos motores en serie con mejores prestaciones.

El trabajo futuro debería concentrarse en mejorar la precisión de los modelos matemáticos y la calidad de la simulación CFD en condiciones reactivas. Por el momento este estudio, como otros, se concentra en la inyección simultánea. Pero a medida que la inyección principal se complementa con las pre y post-inyecciones, los modelos de conceptos de motor de multi-inyección también tienen la oportunidad de hacerlo; incluidas las ventajas y posibilidades de geometrías más desarrolladas de los orificios

de la tobera del inyector y de la cámara de combustión del motor.

## 6. REFERENCIAS

- [1] Takeda, Y. and Niimura, K., "Characteristics of Diesel Combustion and Emissions with a Multi-injector System," SAE Technical Paper 952511, 1995, <https://doi.org/10.4271/952511>.
- [2] Okamoto, T. and Uchida, N., "New Concept for Overcoming the Trade-Off between Thermal Efficiency, Each Loss and Exhaust Emissions in a Heavy Duty Diesel Engine," SAE Int. J. Engines 9(2):2016, doi:10.4271/2016-01-0729.
- [3] Nyrenstedt, G., Im, H., Andersson, A., and Johansson, B., "Novel Geometry Reaching High Efficiency for Multiple Injector Concepts," SAE Technical Paper 2019-01-0246, 2019, <https://doi.org/10.4271/2019-01-0246>.
- [4] Lahane, S., Subramanian, K.A., "Effect of different percentages of biodiesel–diesel blends on injection, spray, combustion, performance, and emission characteristics of a diesel engine," Fuel 139 (2015) 537–545, doi: 10.1016/j.fuel.2014.09.036.
- [5] Gutierrez, M., Castillo, A., Iniguez, J., and Reyes, G., "Spray Parameters of Fuel Blends of Recycled Lubricating Oil and Diesel," SAE Technical Paper 2018-01-1693, 2018, doi:10.4271/2018-01-1693.
- [6] Gutierrez, M., Castillo, A., Iniguez, J., Reyes, G., "Requirements for the fuel injection system to use of biodiesel," Dyna Vol. 93 n°4 416/420, 2018, doi: <http://dx.doi.org/10.6036/8656>.
- [7] Hiroyasu, H., Arai, M., and Tabata, M., "Empirical Equations for the Sauter Mean Diameter of a Diesel Spray," SAE Technical Paper 890464, 1989. doi:10.4271/890464.
- [8] Carlsson, P., "Tutorial dieselFoam," [http://www.tfd.chalmers.se/~hani/kurser/OS\\_CFD\\_2008/PerCarlsson/PC\\_Tutorial\\_dieselFoam\\_peered\\_NL\\_HN.pdf](http://www.tfd.chalmers.se/~hani/kurser/OS_CFD_2008/PerCarlsson/PC_Tutorial_dieselFoam_peered_NL_HN.pdf), accessed Apr. 2021.

- [9] Marcos Gutiérrez, "Modelling the spray development of fuel blends from recycled edible and lubricating oils using OpenFOAM®," *Tablet School Journal*. Nr.: 008. Vol.: 001. ISSN: 2661-6505. Art.: 2020-33-3313-0002. Feb 2021 <https://www.tablet-school.com/tablet-school-journal/>.
- [10] Reitz, R. and Diwakar, R., "Effect of Drop Breakup on Fuel Sprays," *SAE Technical Paper* 860469, 1986, <https://doi.org/10.4271/860469>.
- [11] A. L. Delgado-Mejía, L.C. Olmos Villalba. "Heptane and Dodecane as surrogates of diesel fuel, a comparison with CFD" *Revista CINTEX*, Vol. 20, N° 1, pp. 97-110, 2015.
- [12] Queiroz Santos, D., De Lima, A.L., De Lima, A.P., Borges Neto, W. et al., "Thermal Expansion Coefficient and Algebraic Models to Correct Values of Specific Mass as a Function of Temperature for Corn Biodiesel," *Fuel* 106:646650, 2013, doi:10.1016/j.fuel.2012.10.048.
- [13] Bohl, W., Elmendorf, W. "Technische Strömungslehre". 15th Edition, Vogel Business Media GmbH, 2014, Germany, ISBN 978-3-8343-3329-2.
- [14] Gutierrez, M., Castillo, A., Iniguez, J., and Reyes, G., "Spray Parameters of Fuel Blends of Recycled Lubricating Oil and Diesel," *SAE Technical Paper* 2018-01-1693, 2018, doi:10.4271/2018-01-1693.
- [15] Marcos Gutiérrez, "Modelling the spray development of fuel blends from recycled edible and lubricating oils using OpenFOAM®," *Tablet School Journal*. Nr.: 008. Vol.: 001. ISSN: 2661-6505. Art.: 2020-33-3313-0002. Feb 2021 <https://www.tablet-school.com/tablet-school-journal/>.
- [16] CFD Direct, "OpenFOAM 7 Released," <https://openfoam.org/version/9/>, accessed Apr. 2022.
- [17] Numworks "Numworks. The graphing calculator that makes everybody a math person.," <https://www.numworks.com/>, accessed Apr. 2022..

## 7. ANEXOS

Downloaded from SAE International by University Of Newcastle, Tuesday, August 07, 2018

**SAE TECHNICAL  
PAPER SERIES**

**952511**

---

# Characteristics of Diesel Combustion and Emissions with a Multi-injector System

Yoshinaka Takeda and Keiichi Niimura  
New ACE Institute Co., Ltd.

**SAE** *The Engineering Society  
For Advancing Mobility  
Land Sea Air and Space*  
**INTERNATIONAL**®

Fuels & Lubricants  
Meeting & Exposition  
Toronto, Ontario  
October 16-19, 1995

---

400 Commonwealth Drive, Warrendale, PA 15096-0001 U.S.A. Tel: (412)776-4841 Fax:(412)776-5760

The appearance of the ISSN code at the bottom of this page indicates SAE's consent that copies of the paper may be made for personal or internal use of specific clients. This consent is given on the condition however, that the copier pay a \$7.00 per article copy fee through the Copyright Clearance Center, Inc. Operations Center, 222 Rosewood Drive, Danvers, MA 01923 for copying beyond that permitted by Sections 107 or 108 of the U.S. Copyright Law. This consent does not extend to other kinds of copying such as copying for general distribution, for advertising or promotional purposes, for creating new collective works, or for resale.

SAE routinely stocks printed papers for a period of three years following date of publication. Direct your orders to SAE Customer Sales and Satisfaction Department.

Quantity reprint rates can be obtained from the Customer Sales and Satisfaction Department.

To request permission to reprint a technical paper or permission to use copyrighted SAE publications in other works, contact the SAE Publications Group.



**GLOBAL MOBILITY DATABASE**  
*All SAE papers, standards, and selected books are abstracted and indexed in the Global Mobility Database.*

No part of this publication may be reproduced in any form, in an electronic retrieval system or otherwise, without the prior written permission of the publisher.

**ISSN0148-7191**  
**Copyright 1995 Society of Automotive Engineers, Inc.**

Positions and opinions advanced in this paper are those of the author(s) and not necessarily those of SAE. The author is solely responsible for the content of the paper. A process is available by which discussions will be printed with the paper if it is published in SAE transactions. For permission to publish this paper in full or in part, contact the SAE Publications Group.

Persons wishing to submit papers to be considered for presentation or publication through SAE should send the manuscript or a 300 word abstract of a proposed manuscript to: Secretary, Engineering Activity Board, SAE.

**Printed in USA**

90-1203D/PG

952511

## Characteristics of Diesel Combustion and Emissions with a Multi-injector System

Yoshinaka Takeda and Keiichi Niimura  
New ACE Institute Co., Ltd.

### ABSTRACT

A conventional single cylinder direct injection diesel engine was fitted with three fuel injectors: one mounted vertically on the center, and the others mounted diagonally from the side direction. With this system, it was possible to control the fuel injection timing and injection quantity of each injector independently. It was also possible to independently control the fuel injection pressure of the center and side injectors. Using this system, it was possible to control the spatial and temporal distributions of the fuel injected into the combustion chamber, which are impossible to obtain with conventional injection equipment.

In this study, an improvement in particulates and specific fuel consumption was obtained, while maintaining low NO<sub>x</sub>, by injecting a small amount of fuel from the two side injectors after the main fuel injection from the center injector. Measurements were made in order to characterize engine performance and emissions, as influenced by the spatial fuel distribution inside the combustion chamber, by changing the relative fuel injection direction of the center and side injectors. Split fuel injection was also tested using all three injectors with a total of six injections during one cycle, which resulted in sharply decreased particulates but worsened specific fuel consumption.

### INTRODUCTION

In the direct injection diesel engine, the fuel is not evenly distributed inside the combustion chamber, and within regions where the fuel concentration is close to the stoichiometric mixture ratio, the combustion temperature is higher and hence more

NO<sub>x</sub> is produced. On the other hand, in regions where the fuel concentration is rich, the lack of oxygen causes smoke to occur. Therefore, in order to simultaneously decrease NO<sub>x</sub> and smoke emissions from a direct injection diesel engine, it is necessary to create a proper spatial distribution of the injected fuel, and to reduce as much as possible the regions of fuel concentration where NO<sub>x</sub> and smoke are generated. A single cylinder engine with one center-mounted injector was modified by adding two diagonally oriented side injectors.

Engine tests using the multi-injector system were carried out, and the effects of retarded fuel injection by the side injectors were investigated by changing injection direction, timing, quantity, pressure and nozzle specification (hole diameter) of side injectors. In doing so, the best conditions of side injection were sought by measuring the *NO<sub>x</sub> - Fuel Consumption* and *NO<sub>x</sub> - Particulate Matter (PM)* trade-off relationships.

Next, the relative fuel spray direction and injection quantity of the center and side injectors was varied in order to create a configuration for which the sprays collide and also for which they narrowly pass each other. These tests revealed the influences of spatial distribution of fuel on engine performance and emissions.

Lastly, split fuel injection using all three injectors was carried out. Up to six fuel injections per cycle were obtained, which permitted various novel injection rate patterns by changing each injection timing and interval.

With this particular multi-injector system, it was possible to operate the engine in several novel fuel injection 'modes,' which are difficult to achieve with conventional

injection systems using one injector. The aims of this research were not to develop a production-ready fuel injection system, but rather to carry out various fuel injection forms on a test engine, to deepen our understanding of diesel combustion, and to obtain knowledge useful for combustion improvement.

### EXPERIMENTAL EQUIPMENT

Figure 1 shows a schematic diagram of the multi-injector system. Both the center injector and side injectors have the capability to produce 'square' type fuel injection rate shapes which are typical of accumulator type injection systems. The start and end of injection are controlled by opening and closing a high-speed electromagnetic valve[1][2].

The fuel for the center injector is supplied by a high-pressure generator driven by a separate power source, and the fuel is supplied via an accumulator, which allows fuel injection at up to 250MPa. The fuel for the side injectors is supplied by a supply pump driven by the engine. These injectors use an additional accumulator and their maximum injection pressure is somewhat lower at 150MPa.

The fuel injection quantity and timing of each injector can be independently controlled on the basis of the engine crank angle signal. Moreover, the injection pressure of the center injector can be fixed independently of the injection

pressure of the side injectors and also can be adjusted independently of the engine speed.

The test engine is a single cylinder direct injection diesel engine, and the relevant engine specifications are shown in Table 1. This engine has a four-valve head with a bore of 135mm, and from previous test results[3] a 98mm diameter shallow dish type combustion chamber was selected.

Figure 2 shows the spray arrangement of each injector, and Table 2 shows the main specifications of each nozzle. The center injector is mounted vertically and is located on the cylinder centerline. The side injectors are installed at an inclination angle of 31° from vertical, and inside the combustion chamber the nozzle tip is about 9mm from the cylinder wall.

The center injector nozzle, having six holes, 0.17mm in diameter was selected for this work. The fuel spray direction was arranged so that the angle between one of the spray and the crankshaft centerline ( $\gamma$ ) was either 30° or 0°. Side injector nozzles having two holes of diameter 0.17mm were used, and also two comparative side nozzles having different diameter of 0.24mm (2 times area) and 0.12mm (1/2 the area) were tested. The hole-to-hole included angle ( $\alpha$ ) was either 30° or 90°, and  $\beta$ , the slant angle from horizontal, was 10°. The combustion chamber was recessed slightly to make a suitable clearance space for the side nozzles.

Gaseous emission and smoke concentration measurements were made using a sample probe located directly in the exhaust pipe. A chemiluminescent analyzer was used for measurement of NOx and a flame ionization type analyzer was used for THC measurements.

Since lower-than-usual smoke levels were expected, a special low-concentration type smoke meter, AVL 415,

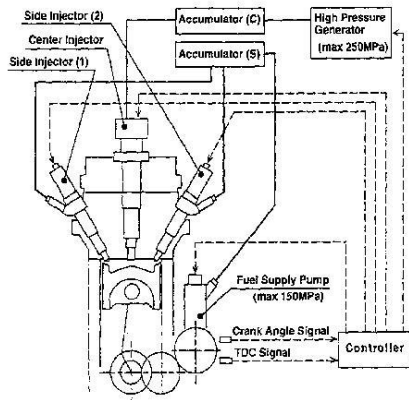


Figure 1 : Schematic diagram of the multi-injector 1.66 used in this study

Table 1 : Summary of test engine specifications

Engine type	DI, Single cylinder NA, 4-Stroke
Bore × Stroke	135mm × 140mm
Displacement	2004cm <sup>3</sup>
Cylinder head	2 inlet, 2 exhaust valves
Combustion chamber	°98 mm Shallow dish (with nozzle recess)
Compression ratio	$\epsilon = 16.5$
Swirl ratio	S/R=0.5 (impulse)
Injection system	Accumulator type

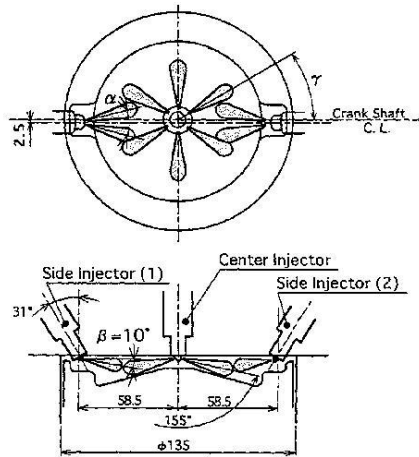


Figure 2 : Schematic of the spray arrangement for the center and side injectors

Table 2: Summary of nozzle specifications of the center and side injectors

	Center	Side (1)	Side (2)
Nozzle type	DLL-S	DLL-P	←
Hole diameter mm	φ0.17	← (φ0.24, φ0.12)	← ( ← )
Hole number	6	2	←
L/D	7.6	4.7	←
Needle lift mm	0.35	"	←
Sac volume mm <sup>3</sup>	1.28	0.44	←

was used in this work. Figure 3 shows a correlation of smoke concentration measured with this unit and a conventional Bosch type unit. From this figure, the smoke concentration measured by the AVL 415 type (FSN) was about 1~2 units higher than the value measured by the Bosch type (BSU).

Particulate Matter (PM) was sampled using a full flow dilution tunnel and the soluble organic fraction (SOF) and the insoluble organic fraction (INSOL) were quantified by the soxhlet extraction technique. A low-sulfur diesel oil was used for fuel (S=0.04%, other specifications are JIS 2 equivalent).

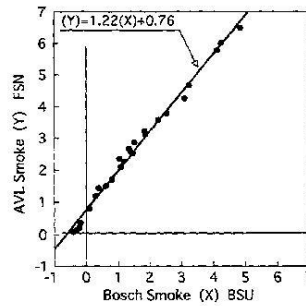


Figure 3 : Comparison of measured smoke values using Bosch type and AVL 415 type smoke meters

## INVESTIGATION AND RESULTS

### EFFECTS OF RETARDED SIDE INJECTIONS -

The fuel injection timing of the main (center) injector was held constant at 3° after top dead center (ATDC), which was characteristic of the lowest NO<sub>x</sub> concentration. Then the fuel injection timing, quantities, and pressures were varied, along with the different side nozzle included angles, and the resulting influences on engine performance and emissions were investigated.

With the center nozzle at  $\gamma=30^\circ$  and the engine speed fixed at 1.000RPM and excess air ratio at  $\lambda=1.4$ , the first set of tests were carried out. The fuel injection quantity will be described as the total of all three injectors, in this case for example,  $Q_{total} = 122\text{mm}^3/\text{cycle}$ .

**Side injection timing and direction** - The fuel injection quantity of the center injector was fixed at 80% of  $Q_{total}$  ( $98\text{mm}^3/\text{cycle}$ ), and the fuel injection quantity of the side injectors to 10% of  $Q_{total}$  each ( $12\text{mm}^3/\text{cycle}$ ) and then the fuel injection timing of the side injectors was varied from 24° BTDC to 18° ATDC. The injection timing of the side injectors was identical and the injection pressure was 100MPa for all three injectors.

Figure 4 shows the fuel injection conditions of the center and side injectors. The two different side nozzles were used as shown in Figure 5 (included angle  $\alpha=30^\circ$  or  $90^\circ$ ). Figure 6 shows the measured results of engine performance and emission characteristics. The 'X' marks in the figure show results when operating with only the center



injector at a fuel injection timing of 3° ATDC and quantity of 122mm<sup>3</sup>/cycle. When fuel sprays from the side injectors were directed more towards the center of the combustion chamber,  $\alpha = 30^\circ$ , it turned out that specific

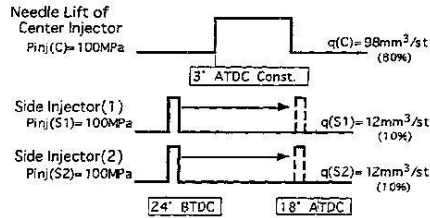


Figure 4 : Engine testing conditions (effects of side injection timing)

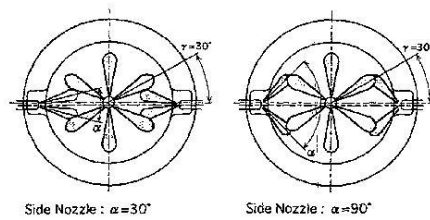


Figure 5 : Nozzle hole arrangements of center and side injectors

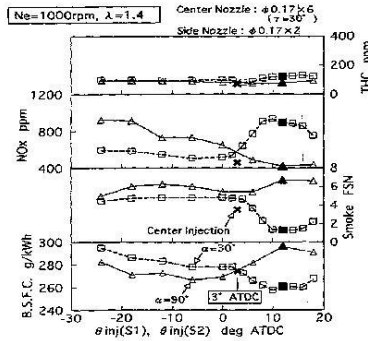


Figure 6 : Effects of side injection timing on engine performance and emissions

fuel consumption and smoke were improved if the side injection began after the center injection start. However, in this case NOx concentration increased, therefore if this configuration was left as is, NOx and smoke could not be decreased simultaneously. On the contrary, when the side injectors were directed more towards the combustion chamber wall,  $\alpha = 9^\circ$ , smoke improvement was not obtained. In particular, when the side injectors were activated after the center injection start, smoke was increased and fuel consumption grew worse.

At this point combustion observation photographs were obtained - examples of which are shown in Figure 7. With an identical geometry bottom-view visualization engine[4], high speed photography of the combustion event was made possible. Including the case with only the center injector ('X' marks in Figure 6), three cases can be compared,  $\alpha = 30^\circ$  ('■') and  $\alpha = 90^\circ$  ('▲') with side injection timing of 12° ATDC, 9 degrees after the center injection start.

From these combustion observation photographs, with  $\alpha = 30^\circ$ , fuel was injected from the side injectors into the center region of the combustion chamber after the spray from the center injector burned to a certain extent. Because of this, air which remained unused at the center of the combustion chamber could be used more effectively, thus providing a rationale for the measured results outlined above. On the other hand, with  $\alpha = 90^\circ$ , more fuel from the side injectors ended up in regions of the combustion chamber already containing combustion from the center injector spray, which resulted in a local shortage of oxygen, which was hence thought to be detrimental to smoke and fuel consumption.

Hence, if the fuel sprays are arranged so that the fuel from the side injectors will have a better possibility to utilize any air that remains at the center of the combustion chamber, or effectively utilize unused air as a result of the turbulent disturbance effects of the side injection and its combustion, there exists a possibility for specific fuel consumption and smoke improvement.

Figure 8 shows a comparison of the heat release rate and the needle lift of each injector with narrow angle ( $\alpha = 30^\circ$ ) side injectors at 12° ATDC, 9 degrees after the center injection start for only the center injector ('X' marks in Figure 6). As seen in the figure, the ignition delay of fuel injected by the side injectors is very short - combustion starts almost immediately after injection - and the diffusion combustion is activated. Because of this, specific fuel consumption and smoke were improved, but the average

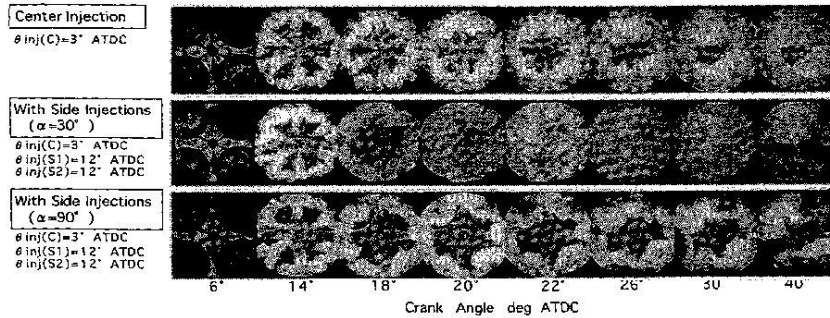


Figure 7 : Photographs of combustion with retarded side injection

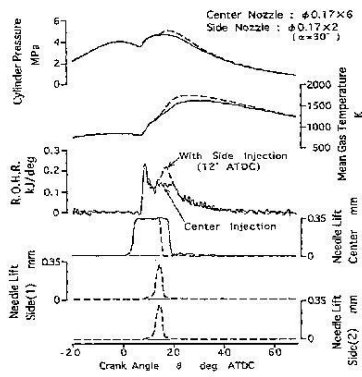


Figure 8 : Comparison of heat release rates for center injection only and when accompanied by side injection

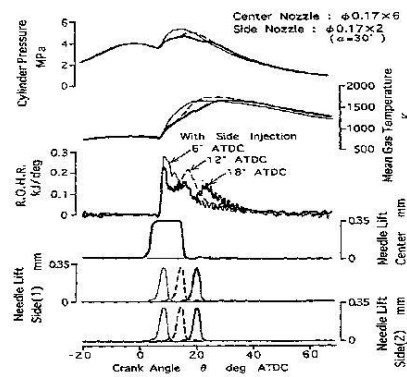


Figure 9 : Comparison of heat release rates and mean gas temperatures for various side injection timings

age gas temperature increased, which can be considered to be one cause of the observed increase in NOx.

Figure 9 shows the heat release rate when the side injection timing was varied. When the injection timing from the side injectors was 6° ATDC, combustion of fuel injected by the side injectors combined with the premixed combustion of the center injection, and the overall amount of premixed combustion increased. On the other hand, at 18° ATDC, combustion of fuel injected by the side injectors

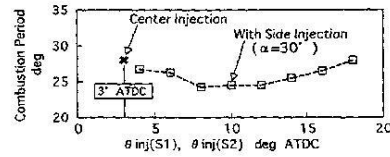


Figure 10 : Comparison of the combustion period at various side injection timings

occurs after the diffusion combustion peak of the center injection, thus the heat release rate shows three distinct peaks.

Figure 10 shows a comparison of the combustion period at various side injector timings. It can be seen that the combustion period was the shortest when injection from the side injectors took place 5° to 9° after the start of center injection. This injection period nearly corresponds to the point at which the minimum fuel consumption occurs in Figure 6 ( $\alpha = 30^\circ$ ). It is thus considered that the improvement in fuel consumption with the side injection was due to the fact that the combustion period was shortened.

**Nozzle specifications** - The side injector nozzle hole diameter was changed and the fuel injection conditions of three injectors were set as shown in Figure 4. The base side injector nozzle hole diameter was 0.17mm, and additional nozzles with diameter 0.24mm (2 times area) and 0.12mm (1/2 the area) were compared. The side injector spray direction was  $\alpha = 30^\circ$  for all three diameters. As shown in Figure 11, it can be seen that even though the hole diameter was changed, the same degree of improvements with the base side nozzle in fuel consumption and smoke emissions were obtained with retarded side injection after the center (main) injection.

From these results, it is concluded that the primary influence of the side injection event was not due to the injection itself, but rather caused by combustion of the fuel injected by the side injection.

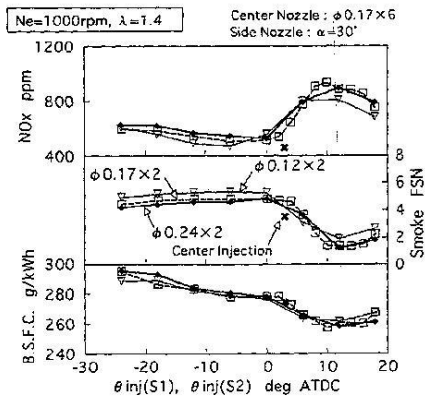


Figure 11 : Effect of side nozzle hole diameter on engine performance and emissions

**Side injection quantity** - The next series of engine tests involved the change at fuel quantity of side injection and varying the injection timing of the side injectors as before. These results are shown in Figure 12, and the injection quantity of the two side injectors was set to 5% and 20% of  $Q_{total}$  as well as the previous value (Figures 6 and 11), namely 10% of  $Q_{total}$ . The injection timing of the center injector was set to 3° ATDC as before, and the injection pressure was set to 100MPa for all three injectors, as before.

When the injection quantity of the side injectors was reduced to 5% of  $Q_{total}$ , approximately the same degree of smoke decrease could be obtained as with the 10% of  $Q_{total}$  case. At the same time, there was a smaller increase in NOx emissions associated with retarded side injection. In addition, there was a tendency for the point of minimum smoke emissions to shift to later timings as the side injector quantity was decreased.

Finally, when the side injector quantity was increased to 20%, the smoke level grew worse as a whole. Even when the side injection occurred after the main (center) injection, little improvements in smoke could be obtained compared to the center injection only case. In this case, the NOx concentration was similar to when the side injection quantity was set to 10%.

From the results obtained thus far, it is evident that when late injection was carried out by the side injectors, the lower the injection quantity was, the better the NOx -

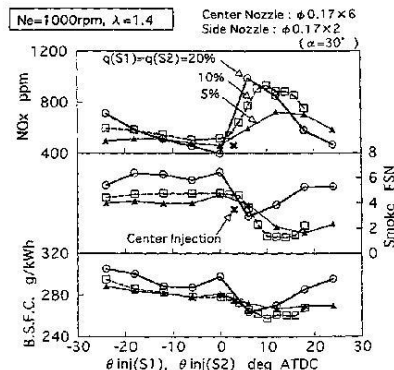


Figure 12 : Effect of side injection quantity on engine performance and emissions

Smoke trade-off became. If the side injection quantity was too large, NOx and smoke both became worse.

**Side injection pressure** - The effect of varying the side injection pressure was investigated by setting the injection quantity of the side injectors to either 10% or 5% of  $Q_{total}$  and varying the injection pressure from 40 to 140MPa. The injection timing and injection pressure of the center injector were  $3^\circ$  ATDC and 100MPa, respectively. The injection timing of the side injectors was set to the timing that corresponded to the maximum smoke improvement for each injection quantity.

As shown in Figure 13, when the injection pressure of the side injectors was increased, smoke improvement effects were enhanced. However, NOx concentration and fuel consumption worsened. When the injection pressure was reduced to 40MPa at a side injection quantity of 5%, fuel consumption and smoke clearly decreased, even though the NOx concentration was somewhat higher, compared to center injection only case ('X' marks in the figure). One contribution to the increased fuel consumption at the higher injection pressure is the increased driving loss to the fuel supply pump of the side injectors.

**Effects of retarded side injections on NOx-Fuel Consumption and NOx-PM tradeoff** - In the previous section, fuel consumption and smoke were shown to improve due to the retarded side injection timing, which was after the main injection via the center injector had started. NOx concentration however, was shown to worsen, and the

NOx-Smoke(PM) and NOx - Fuel Consumption trade-off still were not improved. After the side injector quantity and pressure were changed and further engine tests were carried out, it was found that if the injection quantity of the two side injectors was smaller the injection pressure was lower, there was a higher possibility for improvement in the NOx-Smoke(PM) and NOx - Fuel Consumption trade-offs.

Considering these results, the injection quantity of the side injectors was set to 5% ( $6 \text{ mm}^3/\text{cycle}$ , each) of  $Q_{total}$ , and the injection pressure was set to 40MPa. The side injection timing was set to  $\Delta\theta = 18$  degrees after the start of center injection, which was characteristics of the best NOx, smoke, and fuel consumption in the engine tests. ( $\Delta\theta$  is defined in Figure 14) Under these conditions, the NOx - PM and NOx - Fuel Consumption trade-offs were measured and compared with the center injection only case.

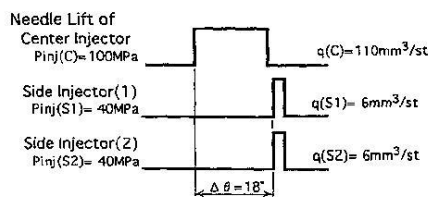


Figure 14 : Injection pattern for investigation of the effects of retarded side injection

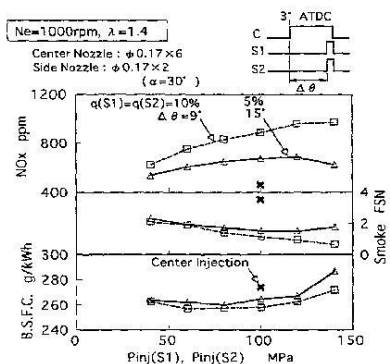


Figure 13 : Effects of side injection pressure on engine performance and emissions

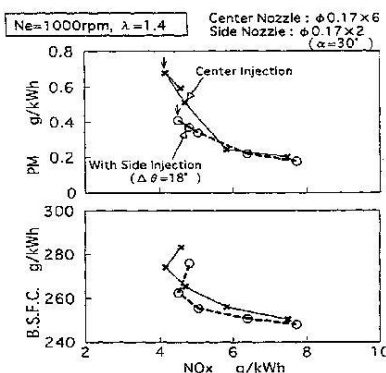


Figure 15 : Effects of retarded side injection on NOx, particulates and fuel consumption

Once the relative injection conditions of the side injectors were determined for this trade-off investigations, the timing of the entire combination of injection was adjusted and measurements were made. Figure 14 shows the injection timing and other data, and Figure 15 shows the resulting  $NO_x$  - Fuel Consumption and  $NO_x$  - PM trade-offs. These figures show that retarded injection by the side injectors could decrease the fuel consumption and particulates simultaneously while maintaining low  $NO_x$  (specific  $NO_x$  emissions of 4 to 5g/kWh).

Figure 16 shows the results of separating the particulate emissions into the soluble organic fraction (SOF) and insoluble fraction (INSOL). At this operating condition, the insoluble fraction was the main component of particulate emissions. The top plot, showing the center injection only case, reveals a sharp rise in insoluble particulates with timing retard. The soluble fraction was basically constant. With retarded injection by the side injectors, the SOF was relatively constant, while the INSOL was lower overall. Thus, the improvement in smoke with side injection caused particulates to decrease.

Further analysis was carried out on the center injection only case and with addition of late side injection at  $\Delta\theta = 18$  degrees (denoted by  $\downarrow$  in Figure 15). Figure 17 shows a comparison of the heat release rate and mean gas temperature. When the side injection occurs after the peak of diffusion combustion of the center injection, small heat release peaks occurred at the end of the diffusion combustion peak of the center injection. Because of this, the mean

cylinder gas temperature during the initial part of combustion was almost the same as with center injection only, and this was assumed to be one of the reasons that low  $NO_x$  levels could be maintained. Moreover, with late side injection, fresh air which remained in the combustion chamber presumably activated combustion of unburned fuel. At the same time, oxidation of smoke generated by the center injection was similarly activated. It turned out that this effect could be obtained even at the relatively retarded timing used at this test condition.

**EFFECTS OF SPATIAL DISTRIBUTION OF THE SPRAY** - For these tests, the timing of the center injector and side injectors were all set to  $3^\circ$  ATDC and the total fuel injection quantity,  $Q_{total}$ , was set to  $122mm^3/cycle$  ( $\lambda = 1.4$ ). Engine tests were then carried out by changing the fraction of total fuel in the two side injections. The injection quantity of both side injectors was equal and the injection pressure was 100MPa for both the center and side injectors. The injection test pattern is summarized in Figure 18.

Recall that for the  $\alpha = 30^\circ$  side injectors, the spray was injected more towards the center of the combustion chamber. As shown in Figure 19, the center injector was positioned at  $\gamma = 0^\circ$  and also rotated to  $\gamma = 30^\circ$  for comparison. With  $\gamma = 0^\circ$ , one of the center sprays was directed

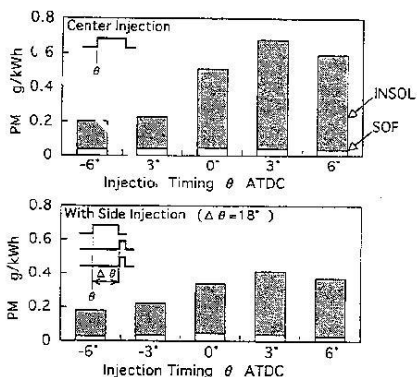


Figure 16 : Effects of retarded side injection on soluble and insoluble fraction of particulate emissions

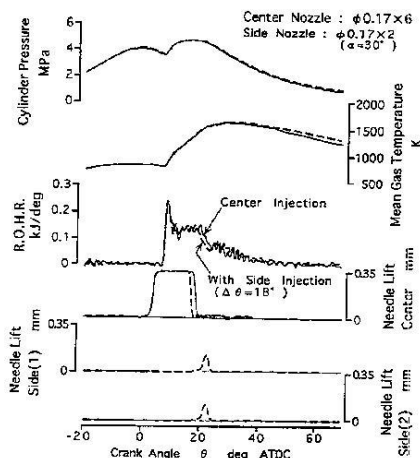


Figure 17 : Comparison of the heat release rate and mean gas temperature for center injection only and accompanied by late side injection

into the same area as the two sprays from the side injectors and they narrowly passed each other. When the center injector was rotated to  $\gamma = 30^\circ$ , the two sprays from the side injectors collided diagonally with two sprays from the

center injector.

The results of the engine tests are shown in Figure 20. Comparing fuel consumption, the  $\gamma = 0^\circ$  orientation was better, and even at the various side injection quantities this tendency did not change. Smoke emissions were also better at  $\gamma = 0^\circ$ , however NOx was higher. The dependence of smoke on side injection quantity shows an interesting trend. Smoke emissions of the  $\gamma = 0^\circ$  case were nearly equal to the case of no side injection (the horizontal axis data is 0%), and were nearly constant throughout the range of side injection quantity. With  $\gamma = 30^\circ$ , however, as the side injection quantity increased, the smoke emission level increased.

Further tests were performed under the condition that the quantity of fuel injected from each injector hole was equal. The center injector had six holes, and each side injector had two. Therefore, the fraction of total fuel injected by the side injectors amounted to 0.40 and the data points at a value of 40% in Figure 20 will be discussed next. Figure 21 shows the heat release rate for the  $\gamma = 0^\circ$  and  $\gamma = 30^\circ$  center injector orientations. Because the fuel quantity injected from each injection hole was equal, the injection duration of each injector was also almost the

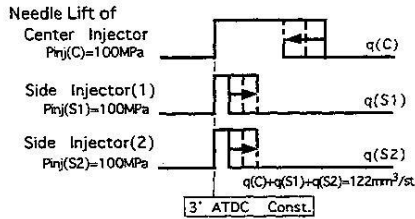


Figure 18 : Engine test conditions for determining the effects of varying the side injection quantity

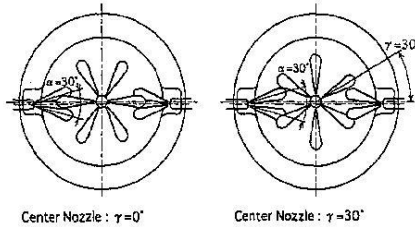


Figure 19 : Center and side injector orientations

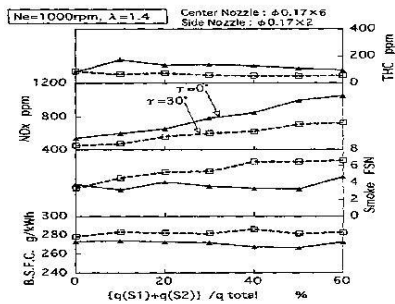


Figure 20 : Effects of center nozzle orientation and side injector quantity on fuel consumption and emissions

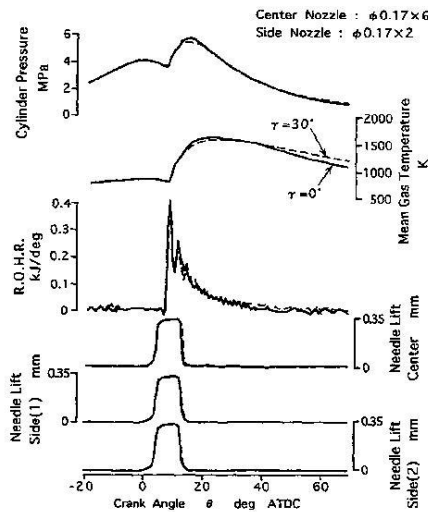


Figure 21 : Comparison of heat release rates, mean gas temperatures and needle lifts for the two center injector orientations

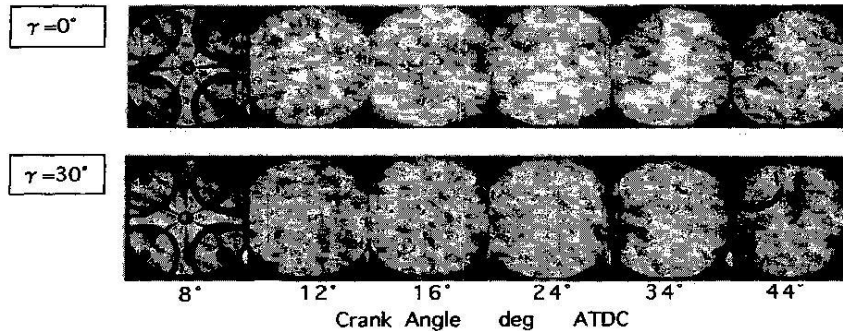


Figure 22 : Combustion photographs comparing the two center injector orientations

same. There was a tendency at the  $\gamma = 0^\circ$  orientation for a slightly higher heat release rate at the initial period of diffusion combustion, however, there was almost no difference in heat release rates during premixed combustion.

With the fraction of total fuel injected by the side injectors again at 40%, observation of the  $\gamma = 0^\circ$  and  $30^\circ$  configurations was performed using a bottom-view type visualization engine [4] and high-speed combustion photography. Specifications of the visualization engine were nearly identical to the engine used for the performance tests. Results for the two center injector positions are shown in Figure 22. The images show quite clearly that with  $\gamma = 0^\circ$ , the center spray did not collide with the side sprays, but rather managed to pass by. The reason smoke did not increase in this case may be attributed to the fact that turbulence at the spray surface was strong and the air entrainment of each spray was maintained to a certain extent. In addition, the increased  $\text{NO}_x$  concentration was presumably due to an increase in size of nearly stoichiometric regions brought on by the increased overlap of the lean peripheral spray areas.

At the  $\gamma = 30^\circ$  orientation on the other hand, there was assumably a tendency for the fuel-rich 'core' region of the center and side injectors to overlap and also for the amount of air entrainment to decrease on the whole, which in turn caused smoke to worsen. Such overlap assumably did not exist at  $\gamma = 0^\circ$  though, and so even though the side injector quantity was increased, smoke emissions were roughly the same. With the  $\gamma = 30^\circ$  case the core-region overlap presumably caused an increase in fuel-rich regions which brought on the increase in smoke.

As reasoned above, in terms of fuel consumption and smoke, the  $\gamma = 0^\circ$  center injector orientation showed better characteristics. In this case, however, the side nozzle was directly exposed to the fuel spray and resulting flames from the center injector, and this caused durability problems. Other than the tests in this section, the  $\gamma = 30^\circ$  center injector orientation was exclusively used.

**TRIAL OF SIX INJECTIONS** - A limited number of tests were conducted with split injection using all three injectors (the center and two side injectors) and six total injections per cycle. The quantity of fuel injected by each hole was again held equal and the quantity of the two injections were kept the same for each injector. Without changing these injection parameters, engine tests were carried out, changing the order and interval of each injection. At certain conditions, an example of which is shown in Figure 23, it was possible to obtain low  $\text{NO}_x$  and low particulates. The injection pressure was 100MPa for all six injections, the center nozzle was at  $\gamma = 30^\circ$  and the  $\alpha = 30^\circ$  side injectors were used.

After the relative position of each injection was fixed, the injection timing of the entire pattern was adjusted and emissions and fuel consumption were measured. This allowed comparison of the  $\text{NO}_x$  - Fuel Consumption and  $\text{NO}_x$  - Particulate trade-off curves to the center injector only case. The results are shown in Figure 24. From this figure, it is evident that one may sharply decrease particulates at the region of low  $\text{NO}_x$  by utilizing multiple injection. Moreover, in this test range there is no increase in

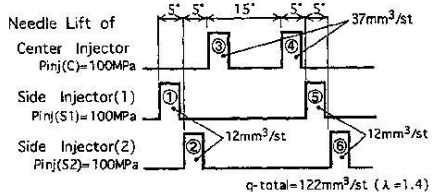


Figure 23 : Injection pattern for investigation of the effects of six injections

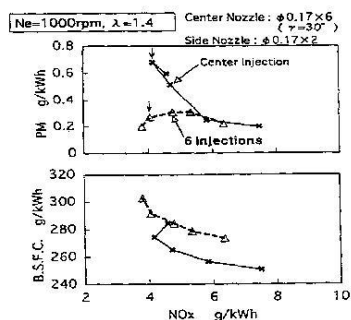


Figure 24 : Effects of six injections on NOx, particulates and fuel consumption

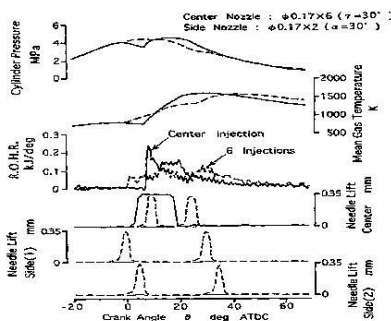


Figure 25 : Comparison of heat release rates, mean gas temperatures and needle lifts for the center injection only case and the six injections case

PM at lower NOx levels, thus making it possible to decrease NOx further, but in that case fuel consumption worsened.

Figure 25 shows the cylinder pressure, mean gas temperature, heat release rate and needle lift histories at the 4g/kWh NOx emission point (denoted by ↓ in Figure 24). With multiple injection the peaks of heat release rate corresponding to each injection overlapped and resulted in a somewhat complicated pattern. Compared to the center injector only case, the fairly large premixed combustion peak disappeared and thus the heat release rate was lower overall, and the combustion period lengthened. In addition, the cylinder pressure increased very gradually near top dead center (TDC) and the cylinder pressure pattern was similar to constant pressure combustion.

## SUMMARY AND CONCLUSIONS

A conventional single cylinder test engine with one center-mounted injector was retrofitted to allow use of three independent injection systems by adding two diagonally-mounted side injectors. With this system, independent control of the fuel injection quantity and timing of each injector was possible, as was independent adjustment of the injection pressure for the center and side injectors. The use of this system made it possible to have more control over the spatial and temporal fuel distributions in the combustion chamber, which is not possible conventional fuel injection equipment.

(1) Engine tests using the multiple injector system were began by investigating some effects of retarded side injection, after which the following results were obtained:

(a) With main injection corresponding to 80% of the total fuel quantity by the center injector, fuel consumption and smoke could be improved by injecting the remaining 20% of the fuel into the center part of the combustion chamber with the retarded injections from the two side injectors.

(b) With the aid of high-speed combustion observation, it was theorized that unused air remaining at the center of the combustion chamber was effectively utilized by the turbulence effects due to the injection and combustion from the side injectors. Furthermore, it was found that the combustion period could be shortened by side injection.

(c) When the side injection sprays were directed more towards the combustion chamber wall, smoke was worsened. This was attributed to being a lack of oxygen



caused by the center injection sprays burning in the same location.

(d) When the optimum parameters were sought for retarded injection from the side injectors, it was found that about 5% of the total injection quantity at about 40MPa injection pressure worked well. It was also found that the best side injection timing was a rather late 18 degrees after the start of center injection.

(e) Under the optimum conditions, retarded side injection resulted in an improvement in both smoke (PM) and fuel consumption while maintaining low NOx.

(2) Next, by changing the relative injection direction of the center and side injectors, a comparison was made of the case that the sprays collided with one another to the case that they did not collide. It was found that when the sprays collided, smoke and fuel consumption grew worse. This was because regions of very high fuel concentration at the center of the sprays overlapped which caused an increase in total size of such regions.

(3) Lastly, six times per cycle multiple injection was tested, and the best combination of injection parameters in terms of NOx, fuel consumption, and particulates were sought by varying the order and interval of each injection. It was found that compared to the center injection only case, it was possible to greatly decrease PM at the low NOx region. There was however, a fuel consumption penalty.

This report describes one type of novel multiple injector system, capable of producing various injection patterns, and how it was used to gain some insight into combustion improvement and emissions decrease. Diesel engine combustion is complicated though, and many unsolved issues still remain for further investigation.

## ACKNOWLEDGMENTS

The authors received valuable direction and support from many people throughout the course of this investigation. In particular, Dr. Shinji Kobayashi and Mr. Kohji Shimizu of the Japan Automobile Research Institute (JARI) provided invaluable assistance with the combustion observation tests.

## REFERENCES

- [1] T. Minami, I. Yamaguchi, M. Shintani, K. Tsujimura, T. Suzuki, "Analysis of Fuel Spray Characteristics and Combustion Phenomena under High Pressure Fuel Injection," SAE Paper 900438, (1990).
- [2] S. Shundoh, T. Kakegawa, K. Tsujimura, S. Kobayashi, "The Effect of Injection Parameters and Swirl on Diesel Combustion with High Pressure Fuel Injection," SAE Paper 910489, (1991).
- [3] M. Komori, S. Shundoh, K. Tsujimura, T. Kakegawa, T. Sakai, S. Kobayashi, "Combustion Improvement of Diesel Engine by High Pressure Fuel Injection," The 9th Internal Combustion Engine Symposium, p. 103-108 (1991) [in Japanese].
- [4] S. Kobayashi, S. Shundoh, T. Nakahira, M. Komori, K. Tsujimura, "Visualization of Diesel Combustion with High Pressure Fuel Injection by Laser Shadowgraph Technique," Journal of the Visualization Society of Japan,



## New Concept for Overcoming the Trade-Off between Thermal Efficiency, Each Loss and Exhaust Emissions in a Heavy Duty Diesel Engine

Takeshi Okamoto and Noboru Uchida  
 New Ace Inst. Co., Ltd.

### ABSTRACT

To overcome the trade-offs of thermal efficiency with energy loss and exhaust emissions typical of conventional diesel engines, a new diffusion-combustion-based concept with multiple fuel injectors has been developed. This engine employs neither low temperature combustion nor homogeneous charge compression ignition combustion. One injector was mounted vertically at the cylinder center like in a conventional direct injection diesel engine, and two additional injectors were slant-mounted at the piston cavity circumference. The sprays from the side injectors were directed along the swirl direction to prevent both spray interference and spray impingement on the cavity wall, while improving air utilization near the center of the cavity. Results obtained with a heavy-duty single cylinder engine equipped with multiple injectors indicated that it was possible to achieve the desired heat release rate profile by independent control of injection timing and duration (fuel injection pressure was kept in constant) for each fuel injector. Furthermore, smoke emissions were reduced by improved in-cylinder air utilization, which was possible through a different air-fuel mixture formation process than that found in conventional single-injector diesel engines. Results showed reduced friction loss, heat loss and NO<sub>x</sub> (nitrogen oxides) emissions, while maintaining indicated thermal efficiency by suppressing the peak cylinder pressure, bulk average temperature, and spray flame impingement to the cavity wall. Additionally, a simultaneous reduction in smoke and NO<sub>x</sub> emissions was achieved, without any deterioration in CO (carbon monoxide) and THC (total hydrocarbon) emissions, even compared with conventional diesel combustion. "CONVERGE" three-dimensional numerical simulation results also suggested that rapid homogenization of local equivalence ratio by improved mixture formation could result in the simultaneous reduction of smoke and NO<sub>x</sub> emissions, even with EGR.

**CITATION:** Okamoto, T. and Uchida, N., "New Concept for Overcoming the Trade-Off between Thermal Efficiency, Each Loss and Exhaust Emissions in a Heavy Duty Diesel Engine," *SAE Int. J. Engines* 9(2):2016, doi:10.4271/2016-01-0729.

### INTRODUCTION

Many measures for thermal efficiency improvement have been studied and proposed over the years. A larger proportion of constant volume combustion by an increased fuel injection rate, advanced injection timing, HCCI (homogeneous charge compression ignition) combustion [1], PCI (premixed compression ignition) combustion [2] etc., have been investigated, since the thermal efficiency of the Otto cycle is ideally higher than other reciprocating engine cycles [3]. An increase in compression ratio or specific heat ratio also contributes toward increasing theoretical cycle efficiency. Furthermore, low temperature combustion by means of higher boost and higher EGR rate conditions have attracted attention in recent years because of the associated theoretical thermal efficiency improvement and heat loss reduction [4]. Nevertheless, drastic improvement in brake thermal efficiency has not been achieved yet, because simultaneous reduction in individual energy losses is difficult utilizing conventional measures, i.e. heat loss, pumping loss, exhaust loss and mechanical friction, and brake thermal efficiency [5].

However, very large two-stroke marine engines have already achieved brake thermal efficiencies exceeding 50%, in spite of engine size effects. In comparison with commercial diesel vehicles engines, marine engines operate at relatively lower fuel injection pressures of about 90MPa, and lower effective compression and expansion ratios of 14.0:1 and 17.0:1 respectively [6], which suppress peak cylinder pressure and averaged cylinder temperature. The resulting near-constant pressure (theoretical Diesel, not Otto) combustion cycle exhibits very low mechanical loss and heat loss. That is, finding the new balance point between cycle efficiency and individual losses is more important than simply raising the theoretical efficiency.

Direct control of the heat release rate profile in a current automotive diesel engine is generally difficult due to hardware constraints, e.g. limited fuel injection rate, only one injector, even if both the fuel injection pressure and timing can be precisely controlled. On the other hand, large two-stroke marine diesel engines usually have two or more injectors per cylinder, for which injection can be phased to control the heat release rate profile and thus obtain nearly constant pressure combustion (Diesel cycle.) Furthermore, heat loss can be decreased more than in conventional diesel engines by avoiding flame impingement to the cavity walls by directing fuel sprays in the

tangential direction, since the injectors are mounted at circumference of the cavity. As a result, these marine engines achieve very high brake thermal efficiency with minimum heat and friction losses due to lower averaged cylinder pressure and temperature.

Several studies dealt with diesel engine equipped with multiple injectors, e.g. PREDIC [7] and MULDIC [8] concepts were proposed to potentially control PCCI combustion. These concepts were able to control PCCI combustion by optimizing the spray distribution in the cylinder during ignition delay, however, smoke emissions increased when the opposed sprays collided with each other. Other results showed that NOx and smoke emissions were simultaneously reduced by avoiding interference between pilot and main sprays injected by different injectors [9].

For a new combustion concept by means of multiple fuel injectors, two major advantages over conventional diesel combustion were presumed. Firstly, both combustion phase and cumulative heat release rate profile can be controlled because of the additional degrees of freedom in injection rate shaping, without any interference between temporally overlapped sprays from different injectors, resulting in independent air entrainment and ignition timing. Secondly, in-cylinder air utilization can be improved with properly allotted air for each injector by temporal and spatial control of the sprays. In this study, the optimum heat release rate profile for increasing brake thermal efficiency was first calculated by a zero-dimensional thermodynamic simulation. Then, to test and verify the heat release history, a single-cylinder engine equipped with three common-rail injectors was utilized for engine performance and emissions tests. The injection setup was designed to concurrently reduce heat loss to the wall and to improve exhaust emissions.

### OPTIMUM TIME-RESOLVED HEAT RELEASE RATE CALCULATION BY ZERO-DIMENSIONAL THERMODYNAMIC MODEL

The theoretical thermal efficiency can be improved by a higher degree of constant volume combustion, higher compression ratio and/or higher specific heat ratio. However, a subsequent increase in brake thermal efficiency is not always obtained if these parameters are increased and exhaust loss is decreased, since heat and mechanical losses also typically increase. To quantitatively simulate not only thermal efficiency but also each energy loss, i.e. heat loss, mechanical loss, and exhaust loss, a zero-dimensional thermodynamic diesel engine model was developed [10]. This model allowed observation of the effect of the heat release rate history, engine specifications, and operating conditions on the energy balance, to find an optimum heat release rate profile.

Figure 1 shows a process diagram of calculations performed by the zero-dimensional model. This model is based on standard fuel-air reciprocating engine cycles like Otto, limited pressure dual cycle (Sabathe cycle) and Diesel cycle. First the P-V diagram is selected and the pressure ratio and cut-off (isobaric combustion) ratio are adjusted to maintain the appropriate input energy. Theoretical IMEP (indicated mean effective pressure), bulk mean temperature, and heat release rate can be calculated from this diagram. Heat loss was

determined by Newton's law of cooling, in which the heat transfer coefficient is estimated by Woschni's correlation [11]. Apparent (gross) IMEP was calculated by subtracting the heat loss from the theoretical IMEP. Mechanical loss and FMEP (friction loss mean effective pressure), were then calculated by the Chen-Flynn friction model [12], which depends on maximum cylinder pressure and mean piston speed. And finally, BMEP (brake mean effective pressure) was determined by subtracting FMEP from apparent IMEP. Other assumptions for calculation of heat balance are as follows:

- PMEP (pumping loss mean effective pressure) was neglected by assuming in-cylinder temperature and pressure as initial value from EVO (exhaust valve open) to IVC (intake valve close) timing.
- Instantaneous in-cylinder pressure and temperature were calculated at each crank angle presuming the fuel-air cycle. Maximum in-cylinder temperature did not exceed adiabatic flame temperature, which takes thermal dissociation into account.
- Specific heat ratio ( $\gamma$ ) was calculated by utilizing the approximation formula based on the temperature and gas composition at the prior step.
- To limit the rate of pressure rise in the constant volume combustion phase, its duration was set to 1 degree crank angle.
- The combustion efficiency was considered as 100%. That is, the injected fuel was completely transformed into heat energy, given by the fuel's LHV (lower heating value).
- Combustion commenced at 1 degree before top dead center (BTDC), except the Diesel cycle started at TDC.

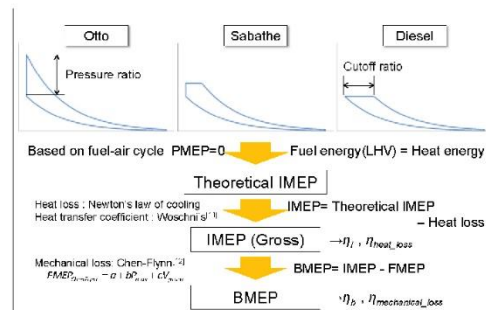


Fig. 1. Process diagram of zero-dimensional thermodynamic simulation model

Figure 2 shows a comparison of experimental and calculated energy balance and cylinder pressure history at an engine speed of 1000rpm, injection quantity of 240mm<sup>3</sup>/stroke (BMEP of about 1.9MPa in this experimental data), boost pressure of 391.3kPa (absolute), intake temperature of 323K and EGR rate of 50%. In calculation, the pressure ratio was determined from the maximum in-cylinder pressure (Pmax) to match experimental data. The cut-off ratio was then calculated by subtracting the total heat energy inputs during the constant volume combustion phase from the total fuel energy. Figure 2 shows that although PMEP and unburned fuel were not accounted for in the model, the calculation results coincide well with measurements.

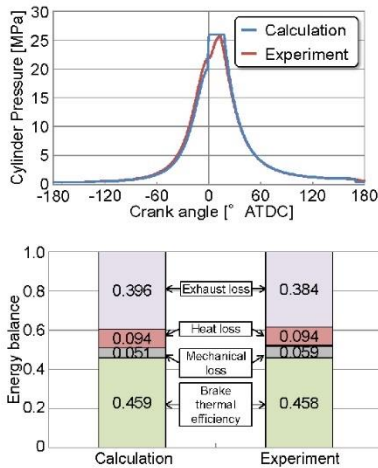


Fig. 2. Comparison of experimental and calculated cylinder pressure histories and energy balance

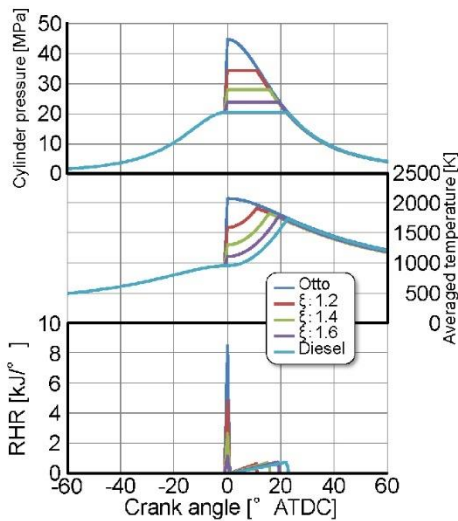


Fig. 3. Comparison of calculated cylinder pressure, temperature and heat release rate for the different idealized cycles and cut-off ratios

Figure 3 shows a comparison of calculated in-cylinder pressure, bulk temperature, and heat release rate at various combination of pressure ratio and cut-off ratio (volume ratio in constant pressure combustion term). These conditions span the Otto, Sabathe, and Diesel cycles, and are carried out under the same conditions as in Fig. 2. Cylinder pressure and temperature rise sharply with heat release rate at top dead center for Otto cycle. The dual cycle heat release rate consists of

the initial acute part and the following “delta” part. Furthermore, as the cut-off ratio increases, the initial acute heat release rate diminishes (finally becoming zero for the Diesel cycle), and the delta heat release period lengthens. The transition from Otto cycle to Diesel cycle anticipates a simultaneous reduction in mechanical loss and heat loss by suppressing the rapid increase in pressure and temperature, even though the proportion of constant volume combustion decreases.

Consideration of compression ratio is appropriate for investigation into the optimum combustion profile to achieve higher brake thermal efficiency (BTE). One should be aware that higher compression ratio may be associated with higher heat loss and lower mechanical efficiency due to increased pressure and temperature. So, the combined effects of compression ratio and heat release rate history on the BTE were then investigated by means of the zero-dimensional model under the same operating conditions as above. Figure 4 shows the effects of compression ratio and cut-off ratio on theoretical thermal efficiency, (gross) indicated thermal efficiency, heat loss and mechanical loss (again normalized by total fuel energy). Theoretical thermal efficiency increased when the compression ratio was increased from 14.0:1 to 22.0:1 and/or cut-off ratio was decreased. However, both heat and mechanical losses also increased, as presumed above.

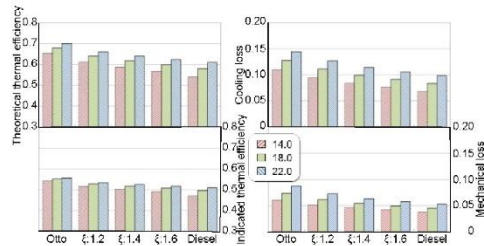


Fig. 4. Effect of compression ratio and cut-off ratio on theoretical thermal efficiency, heat loss, indicated thermal efficiency and mechanical loss

Figure 5 shows a comparison of BTE and Pmax for various combinations of compression ratio and cut-off ratio. These results show that a higher BTE is achieved at a compression ratio of 18.0:1 and cut-off ratio of 1.6 (right-most red crown) under the constraint of Pmax = 25MPa, compared to the combination of lower compression ratio and higher cut-off ratio. The center (red) line corresponds to 25MPa, the current maximum level for heavy-duty commercial vehicles. Thus, the optimum heat release rate profile to achieve the highest BTE depends heavily on not only Pmax constraints but also on each energy loss as a function of the instantaneous pressure and temperature. It is readily apparent that the Otto-like cycle could not result in optimum BTE because of the increase in other energy losses. Thus it becomes a kind of chicken-and-egg problem to determine the optimum heat release rate profile. So, given more degrees of freedom and real-time control of the heat release rate profile to maximize the cycle efficiency concurrent with minimizing energy losses at any operating condition, BTE could be improved further.

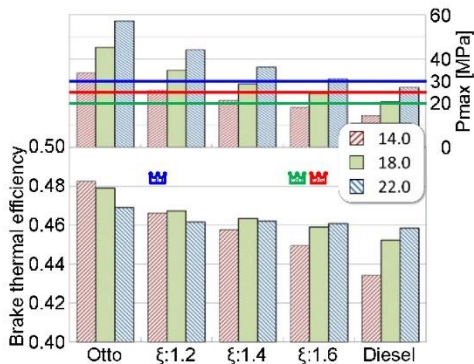


Fig. 5. Effect of compression ratio and cut-off ratio on Pmax and BTE

### COMPUTATIONAL INVESTIGATION OF DIRECT HEAT RELEASE RATE CONTROL BY MULTIPLE-INJECTOR SYSTEM

To arbitrarily control the heat release rate profile and vary the proportion of constant volume and constant pressure combustion, a new three-injector combustion system was developed. The single-cylinder test engine has one center mounted injector and two opposed side injectors. Three nozzle orifices of each side injector aimed in the swirl direction and slightly inward of the cavity wall, with the objective that no sprays interfere with each other. This nozzle system should have two main effects on combustion; one is to improve air utilization in the cylinder to reduce smoke, CO, and THC emissions by allocating the combustion volume for each fuel spray. The other is to reduce heat loss to the wall by suppressing direct impingement of the spray flame.

To verify the ability to arbitrarily obtain heat release rate histories like those obtained by the zero-dimensional model, a three-dimensional numerical simulation using CONVERGE (Convergent Science, Inc.) was then carried out for limited engine conditions. Spray and combustion sub-models utilized by CONVERGE are listed in Table 1.

Table 1. Sub-models used by CONVERGE

Phenomenon	Sub-model
Turbulence model	k- $\epsilon$
Combustion model	CTC
Ignition model	Shell
Droplet breakup	KH-RT

Figure 6 shows a comparison of predicted cylinder pressure, bulk gas temperature and heat release rate for the injection strategy shown at the bottom of the graph. Fuel was initially injected from the center

injector slightly before TDC, and successively from side injectors at independent and slightly staggered timings. The figure indicates that the combination of constant volume combustion by the center injector and constant pressure combustion by the side injectors specified by the zero-dimensional simulation was possible to be closely reproduced by the three injector system. These results confirm that suitable injection timing and injection duration of each injector could control the heat release rate profile as required. So, single cylinder engine tests were next conducted.

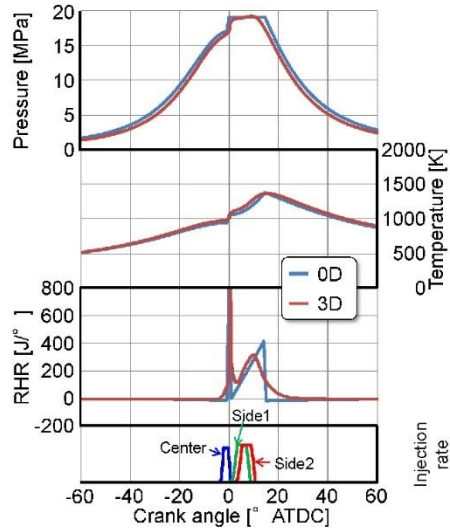


Fig. 6. Comparison of predicted cylinder pressure, bulk temperature and heat release rate between 0D and 3D for the given injection strategy

### ENGINE SPECIFICATIONS AND SCHEMATIC OF EXPERIMENTAL SYSTEM

To confirm the effect of combustion profile on engine performance and emission characteristics, a single cylinder 4 stroke direct-injection diesel engine, displacement volume of 2003.9cm<sup>3</sup>, was utilized in this study. Detailed specifications of the engine are shown in Table 2. The engine idealizes a turbocharged and after-cooled heavy-duty diesel engine by an externally driven supercharger and exhaust throttle. A hydraulic variable valve actuation system (Sturman Industries, DHVVA) and an electronically controlled high-pressure common rail injection system (Denso G3S modified) which enable a maximum injection pressure of 220MPa were equipped in the engine. The nozzle hole (orifice) diameter of center and side injector nozzles was fixed at  $\phi$ 0.177mm. The geometric compression ratio of the piston cavity was 18.0:1.

Table 2. Engine specifications

Item	Specification
Engine type	DI single cylinder 4 stroke
Bore × Stroke	φ135mm × 140mm
Displacement	2003.9cm <sup>3</sup>
Piston type	Steel Piston
Fuel injection system	Common rail system (Max 200MPa)
Nozzle	Center: φ0.177 × 8-150° Side : φ0.177 × 3
Valve actuation	Cam-less Hydraulic VVA
Geometric compression ratio	18.0:1
Swirl ratio	0.9

Figure 7 shows the orientation of the three injectors and the piston cavity. The center injector was situated vertically at the center of the bowl, like a conventional direct injection diesel engine, and the other two side injectors were slant-mounted near the periphery of the bowl. The opposed side injector sprays were directed along the swirl direction to minimize spray interference of two side injectors as well as wall impingement, while improving air utilization near the center of the cavity. However, Fuel sprays which are injected from center and side injector may interfere each other when fuel is injected at the same time or center injection timing is later than side injection timing. The piston cavity shape was designed to achieve a relatively large bore but deep bottom to avoid wall impingement by the side injectors, even at high compression ratios.

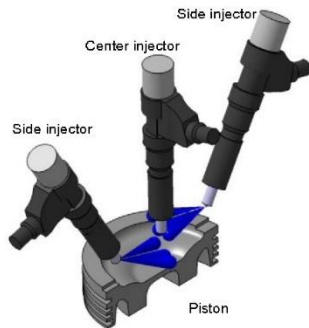


Fig. 7. Piston crown design, injector orientation, and spray directions

Figure 8 shows a schematic of the experimental equipment. This test system has high-capacity boost air supply and EGR systems. Intake air is available up to 500kPa (abs.) as provided by an externally driven supercharger. Note that the intake boost pressure, exhaust back pressure, and EGR rate are controlled independently. The intake manifold pressure and exhaust manifold pressure were made equal throughout the tests so that the external work done by the supercharging system could be ignored, and to exclude the effect of variations in actual turbocharger efficiency and EGR cooler efficiency with various boost pressures and EGR rates.

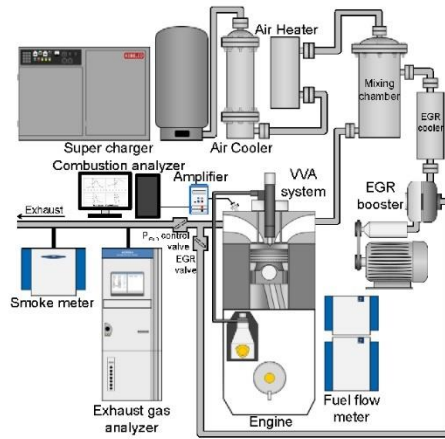


Fig. 8. Schematic of engine test cell

Figure 9 shows a diagram of the modified injector control system, to drive the additional side injectors. The current signal to drive the center injector was detected by a current probe and used to trigger the side injectors. A function generator synthesized the timing and duration of the side injectors based on the center injector trigger, and output the waveform to the electronic drive unit (EDU). Since all the injectors were connected to the system common rail, the injection pressure was the same for all injectors.

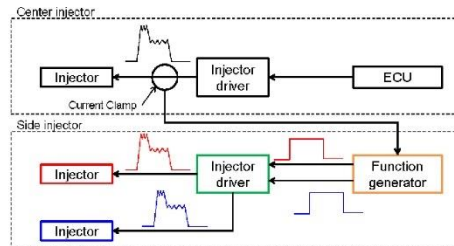


Fig. 9. Multi-injector control system

**Engine Operating Conditions**

Table 3 shows the baseline operating conditions for the engine tests. This condition is quite comparable to 45% load (BMEP of 0.9MPa) on the engine.

Table 3. Engine operating condition

Engine speed	1000rpm
Injection quantity	120mm <sup>3</sup> /str./cyl
Excess air ratio	2.5
Intake pressure	170kPa (abs.)
Intake temperature	323.15K

## RESULTS AND DISCUSSION

### Investigation into Added Degrees of Freedom for Control of Heat Release Rate History

Initial tests focused on investigation of the added degrees of freedom for shaping the heat release rate profile, and confirmation of the effects on engine performance and exhaust emissions. Comparison of experimental and three-dimensional predictions of cylinder pressure, bulk averaged temperature, apparent heat release rate, and nozzle needle lifts are shown in Figure 10. In both cases the pressure ratio (ratio of maximum in-cylinder pressure to TDC compression pressure) was 1.35. It is apparent that the desired constant volume -constant pressure combustion idealized by the zero-dimensional model (i.e. Fig. 3) can be achieved with an appropriate injection strategy for each injector. Results also suggest that this system allows more degrees of freedom to directly control the heat release rate shape, compared to conventional single injector combustion systems.

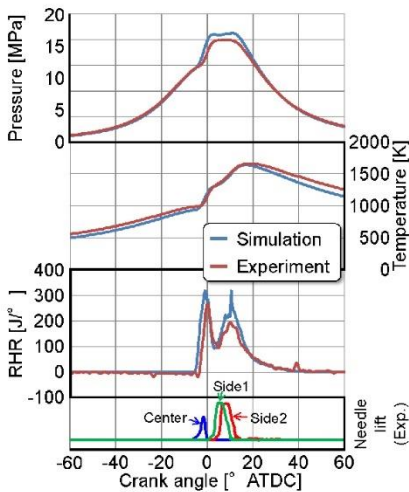


Fig. 10. Comparison of measured and 3D predictions of cylinder pressure, averaged temperature, and heat release rate for the given injection strategy

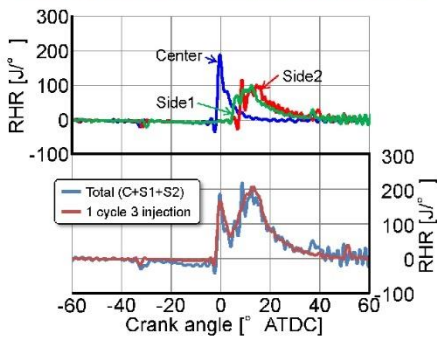


Fig. 11. Experimental investigation into interference between spray flames

Figure 11 compares single-cycle heat release rates. The top graph shows three heat release rates for combustion of a single injection by each injector. The blue line in the bottom graph indicates the sum of three heat release rates shown in the top graph, and the red line indicates the heat release rate for multiple injections with the same injection timing and duration as the top graph. These data indicate that the spray flames from the three injectors are predominantly independent, thus no or negligible interactive effects are seen on ignition timing or heat release rate history.

### Effects of Heat Release Rate History on Engine Performance

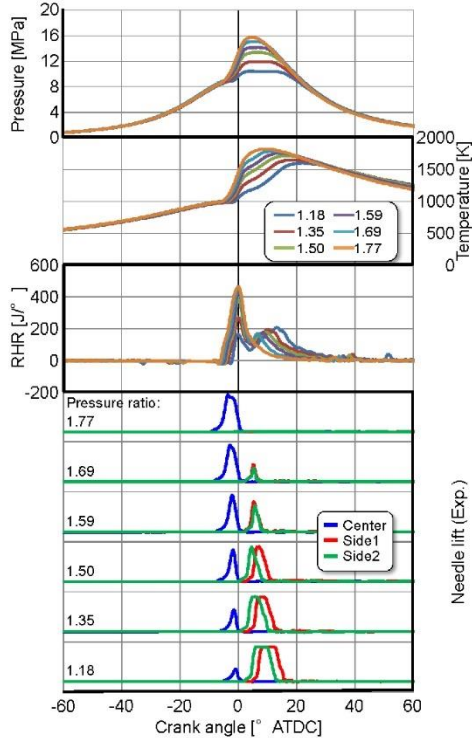


Fig. 12. Measured cylinder pressure, averaged temperature and heat release rate for various pressure ratios, and typical needle lift traces to achieve selected pressure ratios

As previously mentioned, multiple injectors offer additional degrees of freedom for heat release rate profile control. Therefore, the effects of heat release rate history on engine performance were then experimentally investigated. Figure 12 shows a comparison of cylinder pressure, averaged temperature, and heat release rate for various pressure ratios, and three injector needle lift profiles yielding pressure ratios of 1.77, 1.59 and 1.35 respectively. As shown in the figure, the desired combination of constant volume combustion and

constant pressure combustion can be achieved with an appropriate injection rate of each injector, without any changes in injection pressure and/or in-cylinder gas conditions.

The effects of pressure ratio on energy balance and constant volume combustion ratio are shown in Figure 13. Constant volume combustion ratio increased as pressure ratio increased. Meanwhile, cylinder temperature became higher at near TDC and lower at expansion process as pressure ratio increased, from the balance of cylinder temperature phase, heat loss decreased once and increased afterwards. Therefore, the pressure ratio for achieving maximum indicated thermal efficiency was lower than that for maximum constant volume combustion ratio. Moreover, the brake thermal efficiency trended similarly for various pressure ratios. This confirms that higher constant volume combustion ratios (e.g. Otto cycle) may not always be an ideal combustion profile. These results also validate conclusions drawn from the zero-dimensional thermodynamic model.

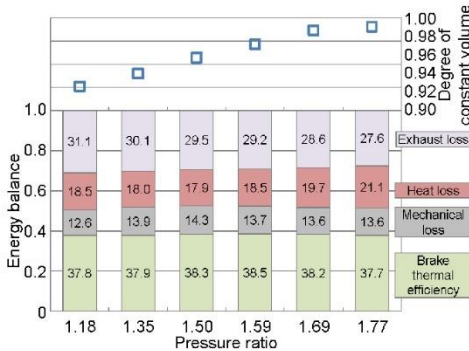


Fig. 13. Effects of combustion strategy on energy balance

#### Effects of Heat Release Rate History on Exhaust Emission Characteristics

It can be assumed that if the sprays interfere with each other, this may negatively impact exhaust emission characteristics. Therefore, the effects of multiple injector heat release rate control on exhaust emission characteristics was investigated with the test engine. Comparison of NO<sub>x</sub>, smoke, CO and THC emissions for various pressure ratios at the same operating condition as previously mentioned are shown in Figure 14. Surprisingly, NO<sub>x</sub> and smoke emissions were simultaneously reduced at lower pressure ratios, even though the combustion mechanism is still conventional diffusion combustion. Most notably, NO<sub>x</sub> emissions were drastically reduced to about 1/3 or less without significant deterioration in BTE. One of the reasons why such a breakthrough phenomenon was achieved for the emission characteristics could be simultaneous reduction in averaged temperature by altering the heat release rate and local equivalence ratio in the cylinder due to the decrease in fuel quantity for each spray. THC emissions increased with a decrease in side injector quantity, which drove the pressure ratio increase, except for the highest pressure ratio (which was achieved with no side injections). This result was caused by a decrease in spray penetration

from the side injectors, resulting in a deterioration in mixture formation at the center of cavity; however, the absolute value was not as bad as for the conventional single injector system.

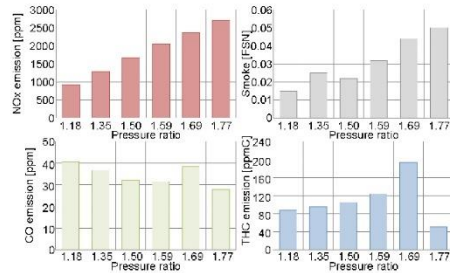


Fig. 14. Effects of combustion strategy on emission characteristics

#### Investigation into Simultaneous Reduction of NO<sub>x</sub> and Smoke Emissions Utilizing Three-Dimensional Numerical Simulation

In general, reduction in NO<sub>x</sub> and smoke emissions for conventional diesel combustion follow a trade-off relationship. Nevertheless, they were simultaneously reduced in this study following the decrease in pressure ratio by controlling the injection parameters (quantity, injection timing) of multiple injectors. Since the cause of this simultaneous reduction in NO<sub>x</sub> and smoke emissions was thought to be a decrease in local equivalence ratio due to a more appropriate mixture formation by the three-injector system, additional analysis was carried out. The 3D CONVERGE model was used to compare histograms of the instantaneous  $\phi$ -T (local equivalence ratio and temperature). Figure 15 compares the temporal and spatial variation of local equivalence ratio for the pressure ratio of 1.35 (multiple injectors, left) and 1.77 (single injector, right) at the same operating condition as the previously mentioned, and the corresponding  $\phi$ -T histograms are shown in Figure 16. From both figures, it is seen that the local equivalence ratio for the multiple injectors at 1.0° ATDC (just after the start of center injection), was diluted faster than that for the single injector because of lower injection quantity of the center injector. As shown at 9.0° ATDC (start of side injection) in Figure 15, the local equivalence ratio of the center injector sprays for the multiple injector system were well diluted at the circumference of the cavity, while that for single injector was still correspondingly higher anywhere in the cylinder because of deterioration in mixture formation by a relatively lower momentum of each spray. Sprays injected by the side injectors were earlier found to not interfere with the center spray, and were designed to spread towards the center of the cavity. As a result, the local equivalence ratio for the side injectors was also diluted faster in the same manner as the spray at 1.0° ATDC. By comparison to 20.0° ATDC, when heat release has essentially ended, the  $\phi$ -T histogram in Figure 16 for the multiple injector system shows higher intensity at lower temperature - lower equivalence ratio regions than the single injector case. Therefore, it is considered that the simultaneous reduction in NO<sub>x</sub> and smoke emissions was achieved by reduction in both averaged temperature and local equivalence ratio, by this unique multiple injector system.



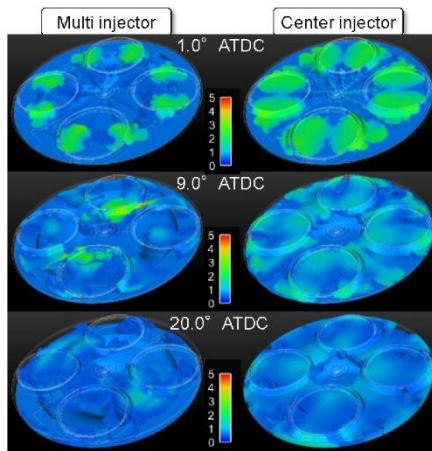


Fig. 15. Comparison of local equivalence ratio distribution as a mixture formation index for different injection strategies

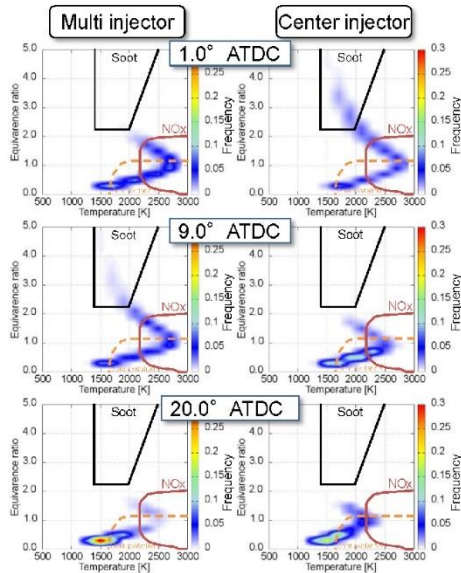


Fig. 16. Comparison of  $\phi$ -T histogram between different injection strategies

### Effect of Increased EGR Rate on Relationship between NOx and Smoke Emissions

Since improvement in exhaust emissions described thus far were exclusively achieved at normal air oxygen content, with no EGR, the effect of reduced oxygen content by increasing EGR rate on the relationship between NOx and smoke emissions of the multiple injector system was investigated. Comparison of NOx and smoke

emissions between the single injector and the multiple injector system at a pressure ratio of 1.5, where the indicated thermal efficiency was maximized, is shown in Figure 17 for various EGR rates. Data show both NOx and smoke emissions were improved with the multiple injector system, without any constraints on oxygen content.

Therefore, it was concluded that the NOx - particulate trade-off could be improved by the new mixture formation strategy, even at lower oxygen contents typical of a current diesel engine utilizing EGR for NOx emissions reduction.

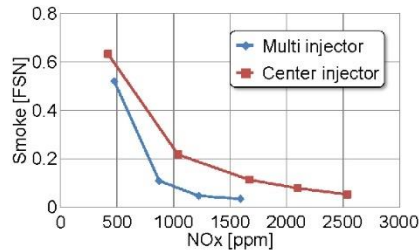


Fig. 17. Trade-Off between NOx and particulate emissions

## SUMMARY

The purposes in this study was to utilize added degrees of freedom to control heat release rate history for the improvement in brake thermal efficiency and improvement of in-cylinder air utilization to reduce both NOx and smoke emissions. To this end, numerical and experimental investigation into diesel combustion and emission characteristics by means of a single cylinder test engine equipped with three injectors and a newly designed combustion chamber were carried out.

The results obtained are summarized as follows:

1. Additional degrees of freedom allowed control of the heat release rate profile via suitable independently controlled injection strategy from three injectors.
2. The optimum heat release rate to achieve maximum BTE was concluded to be a dual (Sabathe) cycle, which combined an initial constant volume combustion with following constant pressure combustion, since heat and mechanical losses were minimized by the decrease of in-cylinder pressure and averaged temperature.
3. Simultaneous reduction in NOx and smoke emissions was achieved, even with conventional diffusion combustion, which could be caused by a decrease in averaged temperature resulting from control of heat release rate profile, as well as a decrease in local equivalence ratio with the new three-injector system.
4. A simultaneous reduction in NOx and smoke emissions was also achieved at high EGR rates (low O<sub>2</sub> concentration).
5. Direct control of the heat release rate profile and improvement in mixture formation utilizing this new multiple injector combustion concept should be an effective measure for both improvement in BTE and exhaust emission characteristics.

## REFERENCES

- Najt, P. and Foster, D., "Compression-Ignited Homogeneous Charge Combustion," SAE Technical Paper [830264](#), 1983, doi:[10.4271/830264](#).
- Kitabatake, R., Shimazaki, N., and Nishimura, T., "Expansion of Premixed Compression Ignition Combustion Region by Supercharging Operation and Lower Compression Ratio Piston," SAE Technical Paper [2007-01-3614](#), 2007, doi:[10.4271/2007-01-3614](#).
- Heywood, J. B., *Internal Combustion Engine Fundamentals*, McGraw Hill, Inc., 1988.
- Osada, H., Uchida, N., Shimada, K., and Aoyagi, Y., "Reexamination of Multiple Fuel Injections for Improving the Thermal Efficiency of a Heavy-Duty Diesel Engine," SAE Technical Paper [2013-01-0909](#), 2013, doi:[10.4271/2013-01-0909](#).
- Shimada, K., Uchida, N., Osada, H., Aoyagi, Y., "Energy Balance Analysis in a Heavy-duty Diesel Engine," *Transactions of Society of Automotive Engineers of Japan* Vol. 45, No. 4, pp. 621-626, 2014.
- Tayama, K., "Historical Development of Two Stroke Slow Speed Marine Diesel Engine," *Systematization survey of the National Science Museum*, Vol. 8, pp. 183-240, 2007.
- Nakagome, K., Shimazaki, N., Niimura, K., and Kobayashi, S., "Combustion and Emission Characteristics of Premixed Lean Diesel Combustion Engine," SAE Technical Paper [970898](#), 1997, doi:[10.4271/970898](#).
- Hashizume, T., Miyamoto, T., Hisashi, A., and Tsujimura, K., "Combustion and Emission Characteristics of Multiple Stage Diesel Combustion," SAE Technical Paper [980505](#), 1998, doi:[10.4271/980505](#).
- Wagner, U., Spicher, U., "Advanced Heterogeneous Diesel Combustion with Ultra-low Engine Emissions and Low Fuel Consumption Levels," *Proceedings of the Institution of Mechanical Engineers, Part D: Journal of Automobile Engineering*, 2013, doi:[10.1177/0954407012441888](#)
- Okamoto, T., Osada, H., Fukunaga, A., Shimada, K., Uchida, N., "Study of the improvement of brake thermal efficiency based on a zero-dimensional thermal efficiency model," 2014 JSAE Annual Congress (Spring) PROCEEDINGS No. 88-14, 2014.
- Woschni, G., "A Universally Applicable Equation for the Instantaneous Heat Transfer Coefficient in the Internal Combustion Engine," SAE Technical Paper [670931](#), 1967, doi:[10.4271/670931](#).
- Chen, S. and Flynn, P., "Development of a Single Cylinder Compression Ignition Research Engine," SAE Technical Paper [650733](#), 1965, doi:[10.4271/650733](#).

## CONTACT INFORMATION

<http://www.nace.jp>

[t\\_okamoto@nace.jp](mailto:t_okamoto@nace.jp)

[n\\_uchida@nace.jp](mailto:n_uchida@nace.jp)

## ACKNOWLEDGMENTS

The authors would like to thank to all the consortium member companies of the New A.C.E Institute for financial support for the "Breakthrough strategies to achieve BTE of 55% without any WHRs" research project, and to the Ministry of Land, Infrastructure, Transport and Tourism for funding support as the part of the project to promote Research and Development of Next Generation Environmentally Friendly Heavy-Duty Vehicles.

---

All rights reserved. No part of this publication may be reproduced, stored in a retrieval system, or transmitted, in any form or by any means, electronic, mechanical, photocopying, recording, or otherwise, without the prior written permission of SAE International.

Positions and opinions advanced in this paper are those of the author(s) and not necessarily those of SAE International. The author is solely responsible for the content of the paper.



جامعة الملك عبد الله  
للعلوم والتقنية

King Abdullah University of  
Science and Technology

## Novel Geometry Reaching High Efficiency for Multiple Injector Concepts

Item Type	Conference Paper
Authors	Nyrenstedt, Gustav; Im, Hong G.; Andersson, Arne; Johansson, Bengt
Citation	Nyrenstedt, G., Im, H., Andersson, A., & Johansson, B. (2019). Novel Geometry Reaching High Efficiency for Multiple Injector Concepts. SAE Technical Paper Series. doi:10.4271/2019-01-0246
Eprint version	Post-print
DOI	<a href="https://doi.org/10.4271/2019-01-0246">10.4271/2019-01-0246</a>
Publisher	SAE International
Rights	Archived with thanks to SAE International
Download date	13/12/2021 01:13:01
Link to Item	<a href="http://hdl.handle.net/10754/661309">http://hdl.handle.net/10754/661309</a>

## Novel Geometry Reaching High Efficiency for Multiple Injector Concepts

Author, co-author (Do NOT enter this information. It will be pulled from participant tab in MyTechZone)

Affiliation (Do NOT enter this information. It will be pulled from participant tab in MyTechZone)

### Abstract

Heat losses are known to decrease the efficiency of CI engines largely. Here, multiple injectors have been suggested to shrink these losses through reduction of spray wall impingement. Studies on multiple injectors have proven the concept's heat transfer reduction but also highlighted the difficulty of using a standard piston bowl. This study proposes a two-injector concept combined with a flat bowl to reduce heat losses further. To change the spray pattern, the two injectors are injecting in a swirling motion while placed at the rim of the bowl. Four injection timings have been investigated using Reynolds-Averaged Navier-Stokes simulations. This computational method quantified the amount of heat loss reduction possible. A conventional single injector concept is compared to two injector concepts with a standard and flat bowl. A Double Compression Expansion Engine (DCEE) concept, based on a modified Volvo D13 single-cylinder engine, was the base for all simulations. The DCEE can re-use the residual exhaust energy for a second expansion meaning increased importance of reduced heat losses. Heat release effects were discarded in the evaluation as an explanation for the reduced heat losses in order to isolate the effects of the changed spray pattern. Results showed a decrease in heat losses by 25.1 % or 4.2 % of the fuel energy as well as an increased IMEP of 4.5 % or 1.9 % of the fuel energy. Together with the increased exhaust energy, results showed a possible total engine efficiency increase of 2.6 % using the DCEE concept. This work successfully proves the benefits of using two injectors with a flat bowl over a standard bowl and the conventional one-injector strategy.

### Introduction

Research of modern CI engines focuses on reducing the CO<sub>2</sub> emissions by increasing the efficiency. New regulations restrict the carbon footprint further [1], meaning an increased strive for CO<sub>2</sub> emissions reduction. The CO<sub>2</sub> emissions are set to be reduced by 15 % until 2025 and 30 % in 2030. Particularly, the heavy-duty vehicles are targeted as the main contributor to CO<sub>2</sub>-emissions among vehicles [2]. A strive for increased energy efficiency follows.

Some engine alternatives have been suggested for increasing the efficiency of the IC engine. In later years there has been a trend for low-temperature combustion concepts including the Homogenous Charge Compression Ignition (HCCI) [3] and Partially Premixed Combustion (PPC) [4]. The idea of these concepts is to reduce the heat losses through a lower burned gas temperature.

The HCCI concept combines the benefits of a homogeneous charge with a compression ignition concept. Studies have suggested that increased efficiency follows from low heat losses [3] proving the benefits of this concept. Other studies [5] have presented some drawbacks of the HCCI, including ignition difficulties at low load and low combustion efficiency.

The PPC concept tries to solve the flaws of the HCCI through a later injection inducing a less homogenous charge. In [6], PPC combustion at different load conditions was investigated. It was concluded that an indicated efficiency of 57 % could be achieved. Low heat transfer, as well as low exhaust losses, were claimed. However, it was difficult to reach a high load with the PPC concept. This was caused by the too short ignition delays at higher pressure.

Another promising concept for solving the problems of the low-temperature theory as well as keeping a high efficiency at all loads is the Double Compression Expansion Engine (DCEE) [7]. By dividing the cycle into two cylinders, this concept is capable of performing a second expansion using the spare exhaust energy. It follows that high exhaust energy is beneficial for this concept as a contrary to typical IC engine concepts.

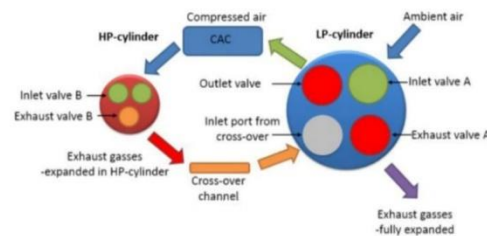


Figure 1. The DCEE concept outlined with the high-pressure (HP) and low-pressure (LP) cylinders [8]

Dividing the cycle into two cylinders also means that very high pressure can be used without the usual high friction losses. The low-pressure (LP) cylinder will compress the intake air before it is transferred to the high-pressure (HP) cylinder. Here, a second compression takes place leading to pressures as high as 300 bar. This compression is followed by a typical CI fuel injection and combustion. The first expansion takes place here in the HP-cylinder followed by a gas transfer to the LP-cylinder where a second expansion takes place.

Using the DCEE concept, Lam et al. demonstrated brake efficiencies of 56 % [8] as well as 52.7 % [9]. Further efficiency improvements have then been achieved by Shankar et al. [10] with the use of insulation to reduce heat losses. This study proves the importance of heat transfer reductions for this concept. The second expansion uses the extra exhaust energy. Thus, it becomes further significant to keep the heat losses low to increase exhaust energy.

A typical approach of achieving lower heat losses in a CI engine is to reduce wall impingement, i.e., to keep the high-temperature zones away from the cylinder walls. This lower flame/wall interaction can be achieved by increasing the injection time as well as reducing the injection pressure. However, there are some limitations to these ideas when going towards high load since more fuel needs to be injected. Another solution was proposed by Uchida et al. [11] using multiple injectors. Further evaluation has been done on this concept [12] showing a heat transfer reduction of 15 % or 2 % of the fuel energy through a changed flow pattern. However, this study highlighted the issues of an omega-shaped bowl when using two injectors. The central pip increases impingement and narrows the possibilities of directing the sprays. Notable is that this study also emphasized that the multiple-injector is not to be restricted to the DCEE concept but can be used in any engine with exhaust regeneration (e.g., a turbo).

To solve the issues of an omega-shaped bowl, a flat bowl where the central pip is removed is here proposed for the two-injector concept. This is expected to reduce the heat transfer further through the changed flow pattern as well as the smaller surface area. Since multiple injectors increase the cost of an engine, it is of interest to investigate the quantity of efficiency gain. In this computational study, the heat transfer is examined and compared with previous cases showing a substantial reduction through the changed flow pattern.

## Methodology

Three-dimensional RANS CFD simulations have been completed using the software Converge (version 2.4) during the compression stroke and expansion stroke of the high-pressure unit. No air exchange and so, no pumping losses have been taken into account in this study. More details about the methodology were reported in a previous study [12].

## Test Conditions

Only the combustion chamber has been chosen as the computational domain in this study, i.e., valves, intake and exhaust systems have not been considered. To compensate this, the chamber has been assumed to contain a specified composition of gases at the start of compression. The residual exhaust gases from the previous cycle in this composition have been considered to hold only water, carbon dioxide (CO<sub>2</sub>), nitrogen (N<sub>2</sub>) and oxygen (O<sub>2</sub>) since these are usually the main components in diesel engine exhaust. Since intake flow is not considered in this setup, an initial turbulence level was set.

The geometry studied here is a standard 4-stroke Volvo D13 engine but with an altered compression ratio (see Table 1). An engine speed of 1200 rpm was set for all different cases. All cases were simulated using Diesel surrogate as fuel, with different injection timings. Only the fluid domain was simulated, and wall temperatures were assumed to be constant.

Page 2 of 9

1/15/2019

Table 1, Engine Parameters

Engine parameters	
Cylinder volume	2.33 l
Stroke	158 mm
Bore	131 mm
Connecting Rod	267.5 mm
Compression Ratio	11.5:1
Engine Speed	1200 rpm
Intake Temperature	464.15 K
Nozzle hole diameter	240 μm
Number of injector holes	6
Standard umbrella angle	145 degrees
Lambda	3.2
Intake Pressure	5 bar

## CFD Models and Validation

N-heptane is here used as a surrogate for the multicomponent Diesel. The liquid phase spray is Diesel meaning only evaporated parcels are n-heptane. However, the lower heating value of diesel is used to account for the fuel energy. The physical properties of n-heptane are incorporated in the CFD code. Spray breakup model, used to capture the spray injection, was based on a Kelvin-Helmholtz Rayleigh-Taylor (KH-RT) approach [13]. All droplets are assumed to disperse and merge during the breakup process. The spherical shape is assumed for all droplets, and the Frossling droplet evaporation correlation [14] was used to calculate new droplet diameter during evaporation. The Rosslin-Rammler cumulative probability distribution was implemented to account for the size distribution of droplets in the domain.

In this study, a renormalized group k-epsilon RANS turbulence model was used to account for in-cylinder turbulence. Other physical sub-models follow the standard built-in capabilities in CONVERGE v2.4 [15].

A base grid size of 2 mm was used in all three directions for the mesh. Fixed embeddings for the injectors were added to account for the near-nozzle flow. The flow inside the nozzle is not considered in the study. Level 3 adaptive mesh refinement (AMR) was utilized based on velocity and temperature gradients inside the combustion domain. The resulting minimum cell size in all three directions after AMR implementation is calculated based on the standard formulation

$$\text{Min. cell size} = \frac{\text{Base grid}}{2^n} \quad (1)$$

where n is the level of refinement provided. The meshing strategy is further described in a previous CFD study [16].

All heat transfer calculations in this paper are using the O'Rourke heat transfer model [17] based on the law of the wall where a constant wall temperature of 500K is assumed. Since the models are validated against pressure and heat release, the heat transfer is also assumed validated. Only minor differences in heat losses were found with the use of radiation models. Thus radiation modeling was not included in this study.

The chemical models are an essential part of any engine combustion simulation in order to properly predict the ignition delay as well as combustion timing. A SAGE multi-zone combustion model [18] was used by mapping the grid cells to temperature bins of 5 K and equivalence ratio bins of 0.05 increments.

A skeletal n-heptane mechanism [19] with 110 species was used in this study. It has been demonstrated that this mechanism is relevant at a number of operating conditions, without further adjustments [19].

Since many simplifications and assumptions are needed for RANS CFD simulations, a validation process has been performed based on the setup discussed above. Simulation results have been compared to experiments conducted at the combustion engines group at Lund University.

At first, the compression ratio was adjusted to fit the motoring trace, motivated by that the connecting rod flex is not considered in the models. The effective compression ratio used was set to 11.41 instead of 11.5 which is in line with previous studies on connecting rod flex making the effective compression ratio lower [20].

Since no intake stroke is performed in the simulations, leftover exhaust gases were introduced in the chamber. These were assumed only to contain  $H_2O$ ,  $CO_2$ ,  $N_2$ , and  $O_2$ , since these are the major components. Residual gases are expected to be present from the previous cycle due to gas exchange inefficiencies. This affects the fluid specific heat ratio, which was decided through comparison with the experimental data before the start of combustion.

Considering the effective SOI and injection duration, the injection timing was changed to -0.2 CAD ATDC instead of -1 CAD ATDC. Similarly, the injection duration was changed from 7.2 CAD to 8.5 CAD. Ignition delay was optimized to fit experimental results.

After several adjustments on the injection timing and duration, the simulation was validated by comparison to experimental data as demonstrated in Figure 2. Furthermore, the Rate of Heat Release (RoHR) plot shows that the simulation is well-predicting the peak value.

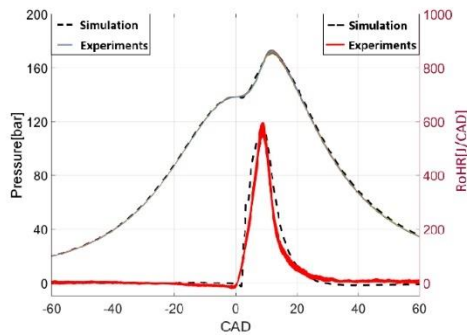


Figure 2. Pressure [bar] and RoHR [J/CAD] traces of the simulation case vs. experimental results

Pressure, RoHR and ignition delay matched experimental data well. This simulation case will be considered in the following analysis as the reference case. Heat transfer models were also assumed validated based on the Pressure and RoHR traces.

### Project Approach

This paper focuses on a flat bowl geometry to reduce the heat transfer for multiple-injector usage. Two new geometries are proposed and evaluated against a reference geometry as well as an earlier multiple injector study [12]. This means that three different geometries were tested, geometry 2 and 3 using a flat bowl for two outer injectors and geometry 1 using a standard bowl (see Figure 3) for both one centrally mounted injector and two outer injectors.

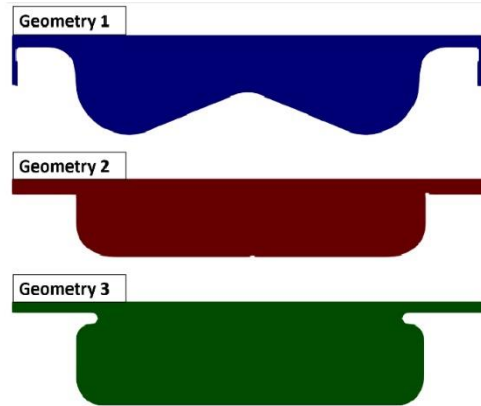


Figure 3. The three different bowl shapes displayed with Geometry 1 (standard), Geometry 2 (removed pip) and Geometry 3 (pips placed at the rim of the bowl)

Geometry 3 was decided with the knowledge that a flat bowl leads to a higher heat transfer through the cylinder head. So, the added pips were expected to drive the flow away from the head surface.

The two outer injectors are placed just at the rim of the bowl for all geometries (see Figure 4) while spraying towards the cylinder center. This gives a changed fluid motion proven to reduce heat transfer [12]. The umbrella angles used, 145 degrees for the reference case, 150 for the two-injector case using Geometry 1 and 160 degrees for the remaining cases, are based on reaching the minimum amount of heat transfer.

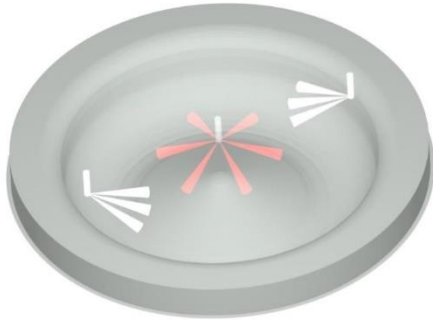


Figure 4. Injector and spray configuration showing the two outer injectors (white) as well as the standard central injector

Compensation has been made for the different bowls to maintain the same compression ratio for all cases. Notable is that the flat bowl will have a smaller surface area compared to the standard case. Since the crevices were found not to impact the heat transfer notably, they were removed for the changed geometry.

The fuel amount per cycle is the same for all cases, 150 mg or 30 bar FuelMEP, with a single injection, split equally between the injectors for the two-injector cases. Same number of holes mean same flow rate for the reference cases and the two-injector cases. Four different injection timings were tested, namely -7, -4, -1 and 2 CAD ATDC.

More cases than the ones listed here were tested, but only the most relevant are presented here due to space limitations. All cases were operated at lambda 3.2. In Table 2 the cases are shown. For Geometry 3, only one case SOI is presented here since the results did not show any improvements regarding heat transfer.

Table 2. Design of Experiment (DOE) with a sweep of injection timings and geometries

Cases	Injection timings [CAD ATDC]			
	-7	-4	-1	2
Geometry 1 1 and 2 injectors	-7	-4	-1	2
Geometry 2 2 injectors	-7	-4	-1	2
Geometry 3 2 injectors			-1	

## Results

This section emphasizes not only how heat transfer through the walls is reduced but also covers the reason for the reduction in heat transfer. The primary outcome is the reduced heat transfer when using multiple injectors with an altered bowl geometry. The definitions of mean effective pressures follow the standard set in a previous study [12].

Page 4 of 9

1/15/2019

## Reducing Heat Losses

The structure of the presented results in this section is as follows. Geometries are presented as 1-3 where \* indicates that only a centrally mounted injector is used. It follows that Geometry 1\* is the reference case. Results are grouped with injection timing for an easy comparison between the different geometries. Notable is that there are four cases for an SOI of -1 CAD ATDC as opposite to the three cases for other injection timings.

For all cases studied here, Geometry 2 with a flat bowl is more favorable regarding heat transfer. Results show that it is mainly a significant reduction in piston heat transfer (see Figure 5). The head heat transfer is a smaller part of the whole meaning that although there is an increase for Geometry 2, there is a total reduction in heat transfer. The heat loss through the liner is similar, and small, for all cases.

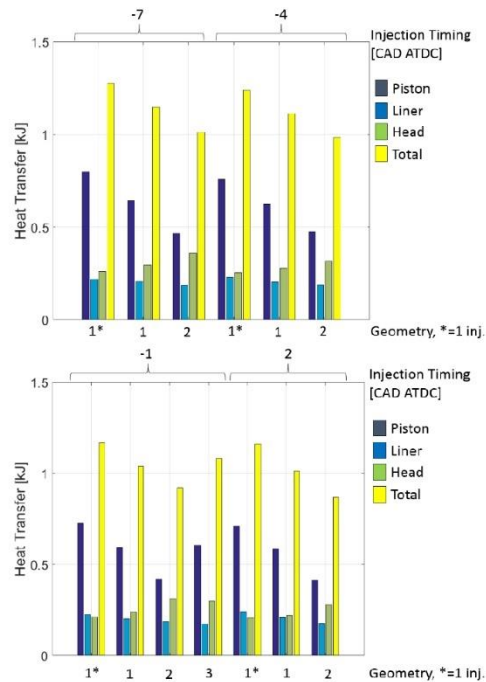


Figure 5. Total heat transfer [kJ] through the piston, liner, and head for the different cases

The heat transfer reduction is at most 25.1 % or 4.2 % of the fuel energy for the SOI of 2 CAD ATDC compared to the reference case. Compared to the two-injector case using Geometry 1, the reduction is instead 14.3 % or 1.9 % of the fuel energy. As opposed to what was seen in the two-injector case using Geometry 1, for Geometry 2 there is a significant gain in IMEP (see Figure 6). This improvement corresponds to a maximum of 4.5 % or 1.9 % of the fuel energy compared to the reference case, again for the SOI of 2 CAD ATDC.

Geometry 3 proves to not reduce the heat transfer more than 7.5 % compared to the reference case at -1 CAD ATDC SOI. It is a smaller reduction compared to what the standard geometry would give. However, the IMEP increases 1.7 % compared to the reference case as an opposite to the slight decrease in IMEP when using two injectors with the standard geometry. As opposed to the author's suggestion, Geometry 3 did not indicate a reduction in heat losses through the head.

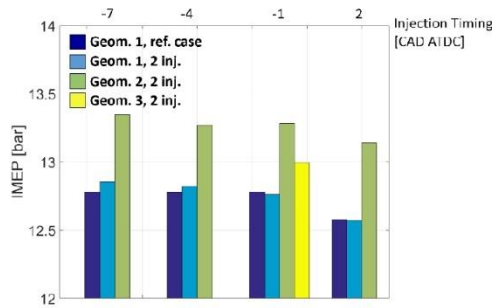


Figure 6. IMEP [bar] for all cases grouped by injection timing

The maximum efficiency in this sweep is found for an SOI of -7 CAD ATDC, and here the gain in IMEP is 4.4 % and the reduction in heat transfer 20.6 % for Geometry 2 compared to the reference case, all with fixed fuel injection. Since all different SOI proved a higher IMEP and lower heat transfer, the concept of using a flat bowl is concluded useful.

The heat transfer is seen to increase more rapidly at an early stage for the reference cases (see Figure 7). This is expected since the hot gases will reach the walls faster with the shorter distance between injector and wall. Comparing the two-injector cases with Geometry 1 and 2, it is seen that the heat transfer is rising earlier for Geometry 1 since the central pip is hit earlier due to the shorter traveling distance for the spray. Without the central pip, as in Geometry 2 and 3, the hot temperature gases will take a longer time to reach the walls.

The time of heat release will have an impact on heat losses. Consequently, the CA50, CAD at which 50 % of the heat is released, is of importance. Figure 8 shows that the CA50 is relatively constant, with only up to 0.5 CAD perturbation from standard case to two-injector case. The RoHR and Pressure (see Figure 9) also show only small differences between the cases and are so confirming that the heat release is itself not an explanation for the reduced heat losses.

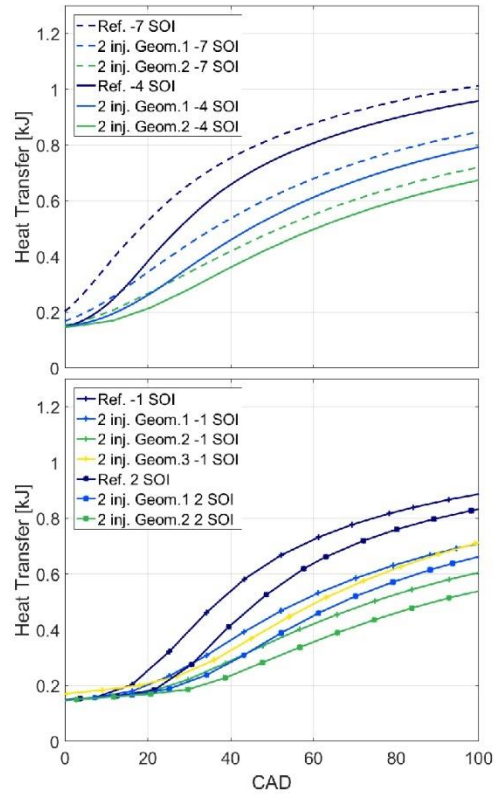


Figure 7. Accumulated heat transfer [kJ] as a function of crank angle

Better mixing can lead to complete combustion, but in this case, the reference case does not seem to have more complete combustion compared to the two-injector cases, looking at the RoHR (Figure 9). This means that if there are any losses regarding combustion, they are minor compared to the reduction in heat losses achieved by the two-injector concept.



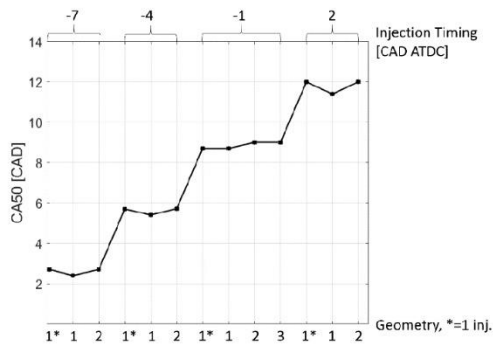


Figure 8, CA50 (CAD at which 50 % of the heat is released) for the different cases

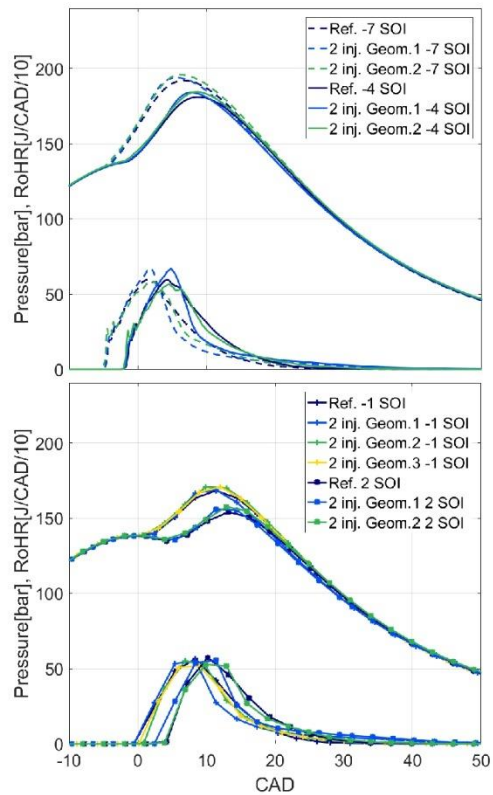


Figure 9, Pressure [bar] and RoHR/10 [J/CAD/10] as function of CAD

Wall area is another driver for heat transfer. Here the wall area (see Figure 10) is changing between the cases even as volume is kept identical. The wall area is smaller for Geometry 2 and 3 where the central pip is removed. This is, therefore, part of the explanation for the lower heat transfer. However, since Geometry 3 has a smaller wall area compared to Geometry 1 but still a higher heat transfer, the wall area is not the full explanation.

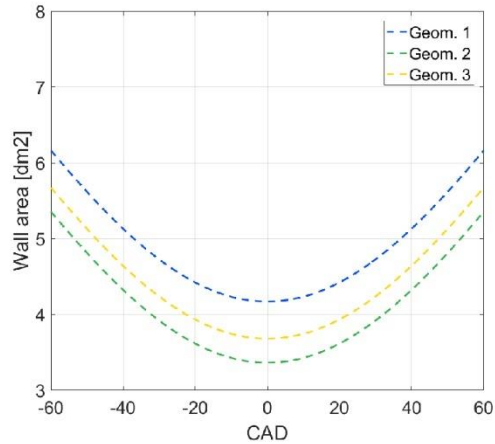


Figure 10, Wall area [dm2] as a function of crank angle

Gas temperature at the cylinder walls is a driver for heat transfer. As investigated earlier, the bulk of the heat losses are through the piston boundary. Figure 11 demonstrates that although the piston temperature is lower for Geometry 2 compared to the reference cases, it is not lower compared to the two-injector cases using Geometry 1. It follows that with a higher average fluid wall temperature, the heat transfer should be higher for Geometry 2. However, as seen before, this is not the case. Notable is that the wall temperature is already higher before combustion for Geometry 2 and 3 compared to Geometry 1. This means that there is a non-combustion related driver. Such a factor is the turbulence created by the altered flow due to the different bowl geometry.

A measure of the turbulence level at the boundary is the near-wall velocity, as plotted in Figure 12. The velocity is here concluded to be more dependent on the injector configuration than the bowl shape. Geometry 1 and 2 have similar near-wall velocities when using two injectors. For the reference case, the high velocity (around 20 m/s higher than the two-injector cases) is created from the spray pattern that is made for proper mixing. It follows that this near wall flow is causing high heat transfer for the reference case. Also, since the near-wall velocity is higher for Geometry 1, comparing two-injector cases of Geometry 1 and 2, it is concluded that this is part of the explanation for the increased heat losses.

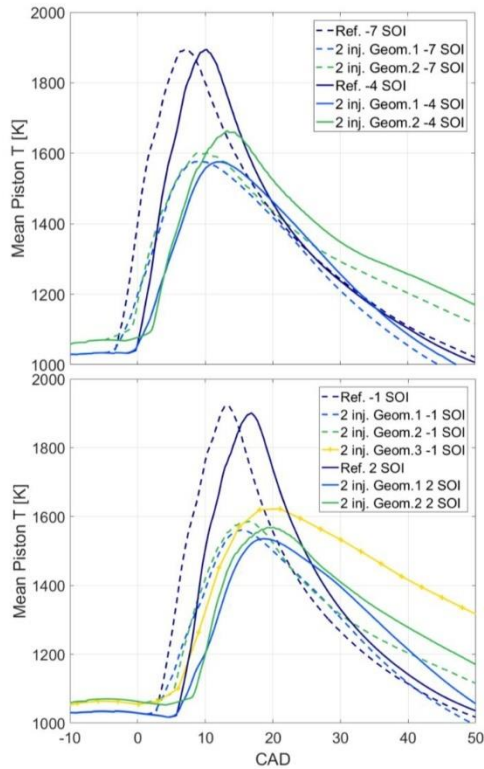


Figure 11. Average fluid wall temperature [K] as a function of crank angle

The longer tail of wall velocity for Geometry 3 explains the late increase in heat transfer for that case [see Figure 7] as opposed to the other cases. Wall area is large late in the cycle meaning that it is of greater importance to keep the near-wall velocity low at this time. In general, the peak of near-wall velocity coincides with the most rapid rise of heat transfer, showing its importance as a factor for heat transfer.

Wall area and near-wall velocity are together having a more significant impact on the heat transfer compared to the wall temperature for this study. Even if wall temperature is higher for Geometry 2 compared to Geometry 1, using two injectors, the heat transfer is lower and does not increase as rapidly. This suggests that it is instead the fluid flow, for the two-injector cases, causing the reduced heat transfer and not the high-temperature zones.

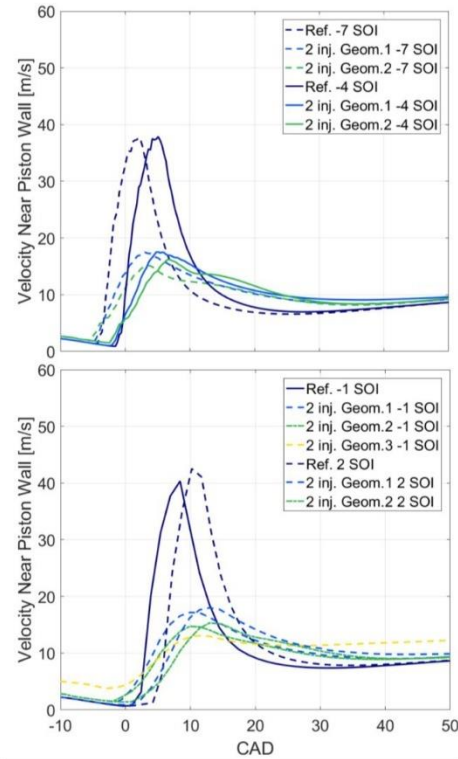


Figure 12. Near wall velocity [m/s] for piston as a function of crank angle

As discussed early in this paper, the exhaust energy is not to be treated as a loss for the DCEE concept. Instead, it should be interpreted as a necessary quantity for the second expansion in the LP cylinder. Significant gains in exhaust energy were found for the two-injector cases compared to the reference case. This is due to the reduced heat transfer. The most significant gain in exhaust energy compared to the reference case was found for an injection timing of 2 CAD ATDC. The percentage gain is 5.6 % for Geometry 2 and 5.0 % for Geometry 1 when two injectors are used compared to the reference case. This corresponds, respectively, to 2.3 % and 2.1 % of the fuel energy. It follows that also for the exhaust energy, Geometry 2 is the best option when using two injectors for all SOI but -1 CAD ATDC.

This extra exhaust energy can potentially be used in a concept such as the DCEE to deliver further work resulting in an improvement of efficiency up to 2.3 %-points, depending on the LP-cylinder efficiency, only by the increased exhaust energy. Assuming an LP-cylinder efficiency of 30 % gives an efficiency gain of 0.7 %-points

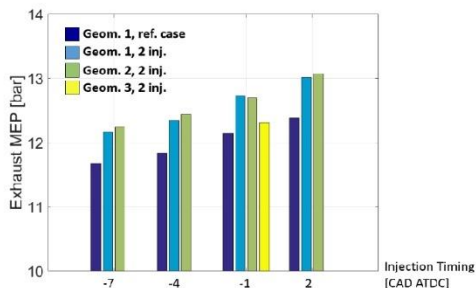


Figure 13. Leftover exhaust energy in the form of Exhaust MEP [bar]

The results of this CFD study showed that two injectors placed at the rim of the bowl could increase indicated efficiency directly if a flat bowl is used. In a concept using exhaust gas re-use, such as the DCEE concept, the efficiency gain can potentially be 4.2 %-points depending on how well the exhaust energy can be used.

The driver for this efficiency gain is seemingly a combination of two factors: wall area and fluid velocity at the vicinity of the wall. Near-wall temperature is not one of these factors since it was higher for the flat-bowl cases although they showed lower heat losses.

For future studies, it is interesting to see further how combustion is affected by the changed bowl shape. Emissions such as NO<sub>x</sub> and soot would be of interest to evaluate but are out of the scope of this study.

## Summary/Conclusions

CFD simulations were conducted to evaluate the level of convective heat transfer reduction by using two injectors in CI engines. While the study was motivated by the DCEE engine application, the two injector concept applies to general CI engine applications, especially when using a flat bowl since this increases the efficiency further. In summary, it was concluded that:

- Reduced heat losses of 25.1 % or 4.2 % of the fuel energy can be achieved by using multiple injectors placed at the rim of a flat bowl
- Increased indicated efficiency of 4.5 % or 1.9 % of the fuel energy achieved for the two-injector case using a flat bowl, showing its benefits compared to the standard bowl
- Increased exhaust energy of 5.6 % or 2.3 % of the fuel energy was achieved and can be used in an exhaust regeneration system such as the DCEE concept.
- Using bumps at the rim of the bowl to reduce head heat transfer gave little or no effect
- A total efficiency increase of 2.6 % from increased exhaust energy and IMEP is possible using two injectors with a flat bowl in the DCEE concept

## References

1. European Commission, "Reducing CO<sub>2</sub> emissions from heavy-duty vehicles", [https://ec.europa.eu/clima/policies/transport/vehicles/heavy\\_en](https://ec.europa.eu/clima/policies/transport/vehicles/heavy_en) (accessed 2018-05-10)
2. European Environment Agency, "Carbon dioxide emissions from Europe's heavy-duty vehicles" <https://www.eea.europa.eu/themes/transport/heavy-duty-vehicles/carbon-dioxide-emissions-europe> (accessed 2018-09-23)
3. Caton JA. Comparisons of Global Heat Transfer Correlations for Conventional and High Efficiency Reciprocating Engines. ASME. Internal Combustion Engine Division Fall Technical Conference, ASME 2011 Internal Combustion Engine Division Fall Technical Conference ();327-337. doi:10.1115/ICEF2011-60017.
4. Noehre, C., Andersson, M., Johansson, B., and Hultqvist, A., "Characterization of Partially Premixed Combustion," SAE Technical Paper 2006-01-3412, 2006, <https://doi.org/10.4271/2006-01-3412>.
5. Sjöberg, M. and Dec, J., "Combined Effects of Fuel-Type and Engine Speed on Intake Temperature Requirements and Completeness of Bulk-Gas Reactions for HCCI Combustion," SAE Technical Paper 2003-01-3173, 2003, <https://doi.org/10.4271/2003-01-3173>.
6. Manente, V., Johansson, B., Tunestal, P., and Cannella, W., "Effects of Different Type of Gasoline Fuels on Heavy Duty Partially Premixed Combustion," *SAE Int. J. Engines* 2(2):71-88, 2010, doi: 10.4271/2009-01-2668.
7. Bhavani Shankar, V., Lam, N., Andersson, A., and Johansson, B., "Optimum Heat Release Rates for a Double Compression Expansion (DCEE) Engine," SAE Technical Paper 2017-01-0636, 2017, doi:10.4271/2017-01-0636.
8. Lam, N., Tuner, M., Tunestal, P., Andersson, A. et al., "Double Compression Expansion Engine Concepts: A Path to High Efficiency," *SAE Int. J. Engines* 8(4):2015, doi:10.4271/2015-01-1260.
9. Lam, N., Andersson, A., and Tunestal, P., "Double Compression Expansion Engine Concepts: Efficiency Analysis over a Load Range", SAE Technical Paper 2018-01-0886, 2018, doi:10.4271/2018-01-0886.
10. Bhavani Shankar, V.S., Johansson, B., and Andersson, A., "Double Compression Expansion Engine: A Parametric Study on a High-Efficiency Engine Concept," SAE Technical Paper 2018-01-0890, 2018, doi:10.4271/2018-01-0890.
11. Okamoto, T. and Uchida, N., "New Concept for Overcoming the Trade-Off between Thermal Efficiency, Each Loss and Exhaust Emissions in a Heavy Duty Diesel Engine," *SAE Int. J. Engines* 9(2):2016, doi:10.4271/2016-01-0729.
12. Nyrenstedt, G, Al Turkestani, T, Im, H and Johansson, B, "CFD Study of Heat Transfer Reduction Using Multiple Injectors in a DCEE concept" SAE Technical Paper 2019-01-0070, 2019, doi: 10.4271/2019-01-0070
13. Reitz, R., and Diwakar, R., "Structure of High-Pressure Fuel Sprays," SAE Technical Paper 870598, 1987, doi:10.4271/870598.
14. Amsden, A. A., O'Rourke, P. J., and Butler, T. D., KIVA-II: A computer program for chemically reactive flows with sprays (No. LA-11560-MS). Los Alamos National Lab., NM (USA), 1989.
15. Richards, K. J., Senecal, P. K., and Pomraning, E., "CONVERGE (Version 1.4.1) Manual," Convergent Science, Inc., Middleton, WI, 2012.

16. Sivasankaralingam, V., Raman, V., Mubarak Ali, M., Alfazazi, A. et al., "Experimental and Numerical Investigation of Ethanol/Diethyl Ether Mixtures in a CI Engine," SAE Technical Paper 2016-01-2180, 2016, doi:10.4271/2016-01-2180.
17. Amsden, A. A., "KIVA-3V: A Block Structured KIVA Program for Engines with Vertical or Canted Valves," Los Alamos National Laboratory Report No. LA-13313-MS, 1997.
18. Babajimopoulos, A., Assanis, D. N., Flowers, D. L., Aceves, S. M., et. al., "A fully coupled computational fluid dynamics and multi-zone model with detailed chemical kinetics for the simulation of premixed charge compression ignition engines," International journal of engine research, 6:497-512, 2005, doi:10.1243/146808705X30503.
19. Zeuch, Thomas, Gladys Moréac, Syed Sayeed Ahmed, and Fabian Mauss. "A comprehensive skeletal mechanism for the oxidation of n-heptane generated by chemistry-guided reduction." *Combustion and Flame* 155, no. 4 (2008): 651-674.
20. Aronsson, U., Solaka, H., Lequien, G., Andersson, O. et al., "Analysis of Errors in Heat Release Calculations Due to Distortion of the In-Cylinder Volume Trace from Mechanical Deformation in Optical Diesel Engines," *SAE Int. J. Engines*5(4):1561-1570, 2012, <https://doi.org/10.4271/2012-01-1604>.

### Contact Information

Gustav Nyrenstedt  
 Ph.D. Student  
 Clean Combustion Research Center (CCRC)  
 King Abdullah University of Science and Technology (KAUST)  
 23955-6900 Thuwal, Saudi Arabia  
 sven.nyrenstedt@kaust.edu.sa  
 Phone no - +966 (0)56 045 8328

### Acknowledgments

This work was sponsored by King Abdullah University of Science and Technology (KAUST). The simulations in this work were performed with the computing resources at the KAUST Supercomputing Laboratories. The authors would like to thank Dr. Georgios Markomanolis, previously at KAUST Supercomputing Laboratory, for helpful guidance in post-processing, and Mr. Nhut Lam at Lund University for providing the experimental data for model validation.

### Abbreviations

<b>ATDC</b>	After top dead center
<b>BDC</b>	Bottom dead center
<b>CA50</b>	Crank angle degree at which 50 % of the heat is released
<b>CAD</b>	Crank angle degrees
<b>CO<sub>2</sub></b>	Carbon dioxide
<b>Cylinder Wall</b>	Liner, piston and head boundaries
<b>DCEE</b>	Double compression expansion engine
<b>EXMEP</b>	Exhaust mean effective pressure
<b>HCCI</b>	Homogenous charge compression ignition
<b>IMEPg</b>	Gross indicated mean effective pressure
<b>IMEPn</b>	Net indicated mean effective pressure
<b>N<sub>2</sub></b>	Nitrogen
<b>O<sub>2</sub></b>	Oxygen
<b>PPC</b>	Partially premixed combustion
<b>RANS</b>	Reynolds averaged Navier-Stokes
<b>RCCI</b>	Reactivity controlled compression ignition
<b>RoHR</b>	Rate of heat release
<b>SOI</b>	Start of injection
<b>TDC</b>	Top dead center



## Effect of different percentages of biodiesel–diesel blends on injection, spray, combustion, performance, and emission characteristics of a diesel engine



Subhash Lahane, K.A. Subramanian\*

Engines and Unconventional Fuels Laboratory, Centre for Energy Studies, Indian Institute of Technology Delhi, New Delhi 110 016, India

### HIGHLIGHTS

- In-line fuel injection pressure and spray penetration is higher with all biodiesel blends.
- Chance of wall impingement is to be critical with B20 but more with B25, B50, and B100.
- Ignition delay and rate of pressure rise decreased with all biodiesel blends.
- NOx emission increases with all biodiesel blends (B20: 15.6% and B100: 22.8%).
- B15 is the optimum blend based on change in NOx emission and no wall impingement.

### ARTICLE INFO

#### Article history:

Received 9 February 2014

Received in revised form 2 June 2014

Accepted 11 September 2014

#### Keywords:

In-line fuel pressure

Spray penetration

Wall impingement

NOx emission

Diesel engine

### ABSTRACT

A comparative study of effect of different biodiesel–diesel blends (B5, B10, B15, B20, B25, B50 and B100) on injection, spray, combustion, performance, and emissions of a direct injection diesel engine at constant speed (1500 rpm) was carried out. The penetration distance increased with increase in percentage of biodiesel in diesel due to enhanced in-line fuel pressure. The simulation results indicate the spray penetration with biodiesel–diesel blend up to B15 does not lead to wall impingement but B20 is to be a critical limit of wall impingement (within uncertainty  $\pm 1.3\%$ ). However, it is observed clearly from the simulation results that probability of wall impingement is more with higher blends (B25, B50 and B100). The ignition delay period decreased with all biodiesel blends due to higher cetane number resulting in less rate of pressure rise and the smooth engine running operation. The engine torque does not change significantly with biodiesel–diesel blends up to 20% (B20). However, the torque reduction is about 2.7% with B100 at the rated load. Carbon monoxide (CO), hydrocarbon (HC) and smoke emissions decreased with all biodiesel–diesel blends. However, oxides of nitrogen (NOx) emission increased in the range of 1.4–22.8% with all biodiesel–diesel blends at rated load due to oxygenated fuel, automatic advance in dynamic injection timing (DIT), higher penetration and higher in-cylinder temperature. A notable conclusion emerged from this study is the optimum biodiesel–diesel blend based on no wall impingement (B15: 0% and B20  $\pm 1.3\%$  uncertainty limit) and increase in NOx emission (B15: 4.1% and B20: 15.6%) in a conventional (unmodified) diesel engine is up to B15.

© 2014 Elsevier Ltd. All rights reserved.

### 1. Introduction

The main driving force behind the implementation of biodiesel in diesel engines is due to enhancement of fuel quality, self reliance of energy need, and boosting of rural economy. The higher cetane number of Karanja biodiesel (CN:58) could provide the easy starting of the engine, lesser white smoke, shorter ignition delay, less probability of knocking and smooth running of diesel engine as

compared to base diesel [1]. The sulfur and aromatics in biodiesel are lower as these properties would affect on formation of particulate matter in diesel engines. However, the bulk modulus is higher with biodiesel (1500 MPa) than base diesel (1350 MPa) as this property indicates the compressibility of the fuel that would effect on injection characteristics of diesel engines. In a diesel engine, the fuel spray characteristics which deal the interaction of the injected fuel with the surrounding hot air during ignition delay period and combustion, is mainly dependent on injection characteristics such as injection delay, in-line fuel injection pressure, dynamic injection timing (DIT), in-cylinder injection duration and injector nozzle con-

\* Corresponding author. Tel.: +91 11 26591247; fax: +91 11 26581121.

E-mail address: [subra@ces.iitd.ac.in](mailto:subra@ces.iitd.ac.in) (K.A. Subramanian).

<http://dx.doi.org/10.1016/j.fuel.2014.09.036>

0016-2361/© 2014 Elsevier Ltd. All rights reserved.

figuration. The fuel spray characteristics play an important role in the improvement of combustion and engine performance, because it influences the mixture formation process of fuel with air in the engine cylinder [2]. Some information on diesel fuel spray characteristics is available in literature. However, information on biodiesel spray is scanty.

### 1.1. Injection and spray characteristics of a diesel engine using biodiesel–diesel blends

Diesel engine process including injection, spray, mixing, ignition and combustion influences its performance and emission characteristics. Among these processes, injection and spray process are important as they are affected by the quality of fuel, resulting in alteration of combustion characteristics of diesel engines. As biodiesel has a different physico-chemical property (density, viscosity, distillation properties, bulk modulus, surface tension, etc.) as compared to base diesel, its effect on the injection [3] and spray characteristics of the engine need to be studied in order to find scopes for solving these problems.

Fuel injection system plays a vital role on enhancing engine efficiency and emission reduction of the modern diesel engine [4]. The injection characteristics of a diesel engine include injection delay, static injection timing, DIT and injection duration. The duration of injection delay is defined as the duration between DIT and static injection timing. DIT is defined as the actual injection timing where the fuel is started to inject into the cylinder. The fuel–injection process is important as it influences fuel spray characteristics (break-up length, spray cone angle, sauter mean diameter (SMD), penetration and air entrainment) and mixture formation process [2].

The numerical analysis of injection characteristics using biodiesel–diesel blends (B25, B50, B75 and B100) was carried out by Kegl and Hribernik [5] and Kegl [6]. They reported that the DIT advanced whereas injection duration and in-line pressure increased with all biodiesel–diesel blends. The process of atomization and fuel–air mixing rate could be enhanced by increasing the in-line fuel injection pressure [7]. However, it may increase penetration distance which results in more probability of wall impingement. National Renewable Energy Lab (NREL), USA reported that the automatic advance in injection timing is due to higher bulk modulus of biodiesel (1500 MPa) than diesel (1350 MPa) as it implies the compressibility of the fuel [8]. The bulk modulus of biodiesel is higher than base diesel resulting in significant increase in in-line fuel pressure. The fuel spray penetration distance increases with increase in the in-line fuel pressure resulting in increase of probability of wall impingement [9]. It may be noted that wall impingement is one of the main durable issues of a diesel engine that needs to be reduced. It could be reduced mainly by reducing the penetration distance.

Fuel quality parameters including viscosity, density, and surface tension influence the spray characteristics of diesel engines. High viscosity and surface tension of biodiesel increase SMD, which affects fuel atomization [7]. Gao et al. [10] studied the spray characteristics of three biodiesel fuels (Jatropha, palm and used fried oil). SMD and spray penetration increased with increasing percentage of biodiesel in diesel but the spray cone angle decreased resulting in poor atomization. It may be noted that the injection characteristics alter fuel spray and combustion which influence performance and emission characteristics of diesel engines for biodiesel–diesel blends. Hence, injection characteristics are a central theme of design of a diesel engine for biodiesel utilization.

### 1.2. Combustion characteristics of a diesel engine using biodiesel–diesel blends

The combustion characteristics are one of the important tools to optimize performance and emission characteristics of diesel

engines. Due to different properties of diesel and biodiesel, both fuels exhibit different combustion characteristics with respect to change in engine load. The main aim of optimization of fuel spray characteristics is improvement of mixture formation process which influences auto ignition and combustion process of diesel engines [11,12]. Biodiesel fuel comprises of 10–11% oxygen (by weight) which would enhance the heat release rate during combustion and reduces emissions (CO, HC, and Smoke/PM) significantly except NOx [13–15]. Combustion with biodiesel fueled diesel engine starts earlier at advanced dynamic injection timing due to higher bulk modulus. The peak rate of pressure rise is lower for biodiesel due to shorter ignition delay [16]. As high ignition delay leads to high rate of pressure rise, some extend to knocking, noise and NOx emission, it is necessary to lower the ignition delay. So, the combustion characteristics such as ignition delay, start of combustion, rate of pressure rise, etc. of a diesel engine for Karanja biodiesel–diesel blend need to be studied in detail in order to find the scopes for further improvement of the performance and emission reduction.

### 1.3. Performance and emission characteristics of a diesel engine using biodiesel–diesel blends

Biodiesel has low carbon content than diesel fuel (Diesel: 87 and Biodiesel: 77.2 wt.%). Hence, biodiesel fueled diesel engines will emit lower carbon based emissions than base diesel. Graboski and McCormick [17] studied the performance and emission characteristics of a diesel engine fueled with biodiesel–diesel blends (B10, B20, B30, B50 and B100) as compared to base diesel. The results indicated that CO, HC, PM, smoke and Poly-Aromatic Hydrocarbon (PAH) emissions decreased with the biodiesel–diesel blends whereas brake specific fuel consumption (BSFC) and NOx increased significantly [18,19]. Rakopoulos et al. [20] reported that the BSFC increases with the oxygen enrichment in the fuel but it does not affect with oxygen enrichment in the intake air. The percentage of torque reduction was reported as 0.85%, 1.25%, 2.33% and 5.90% with B20, B35, B65 and B100 respectively.

Experimental investigation was carried out to study the performance and emission characteristics of a diesel engine fueled with different percentages of Karanja biodiesel–diesel blends (B5, B10, and B15) [21]. They concluded that B10 (Karanja biodiesel–diesel blend) is the optimum blend for diesel engines. However, Mahanta et al. [22] concluded that B15 and B20 could be the optimum in terms of fuel efficiency and power developed. However, the optimum biodiesel–diesel blend would depend on particular feedstock [23,24]. It was reported that the appropriate biodiesel–diesel blend required for ensuring the optimum performance and low emission. As biodiesel is produced from different feed stocks, the physico-chemical properties of biodiesel will vary with the feed stock [25]. Lin et al. [23] reported the effect of biodiesel's feedstock on a diesel engine performance. They studied engine performance characteristics with biodiesel derived from different feed stocks including soybean oil methyl ester (SOME), peanut oil methyl ester (PNOME), corn oil methyl ester (COME), sunflower oil methyl ester (SFOME), rapeseed oil methyl ester (ROME), palm oil methyl ester (POME), palm kernel oil methyl ester (PKOME), and waste fried oil methyl ester (WFOME), and these results were compared with base diesel as given in Table 1. In general, they reported that carbon, hydrogen, oxygen, and sulfur content will influence the calorific value of a fuel and hence, it would also influence the engine performance and emission characteristics. Similarly, the combustion, performance and emission characteristics of a diesel engine fueled with biodiesel derived from wasting cooking oil were compared with base diesel [26,27]. The chance of wall impingement will be more for biodiesel fueled diesel engine due to higher injection pressure. Hence, the optimum biodiesel–diesel blend has to be

**Table 1**

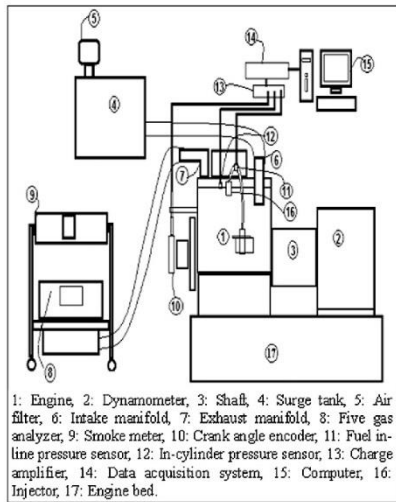
The experimental results of the engine performance and exhaust emissions from different feedstock fuels [23].

Item	PD	SOME	PNOME	COME	SFOME	ROME	POME	PKOME	WFOME
BSFC(g/MJ)	63.5	71.7	71.1	69.9	69.5	71.1	72.7	72.8	72
Power (kW)	7.22	7.18	7.13	7.18	7.32	7.25	7.28	7.2	7.14
Smoke (%)	22	9	11	10	9	10	9	6	11
NOx (ppm)	466	566	555	564	570	587	548	492	555
THC (ppm)	178	131	138	132	129	135	124	119	134
EGT (°C)	405	397	398	401	402	401	392	387	394

selected based on change in NOx emission and minimum probability of wall impingement. Therefore, the present study is aimed at the optimization of biodiesel–diesel blend based on injection, spray, combustion, performance and emission characteristics of a diesel engine.

## 2. Experimental details

A test diesel engine (single cylinder, four strokes, air cooled, constant speed (1500 rpm) with maximum power output of 7.4 kW (Swept volume: 947.38 cc; compression ratio: 19.5:1; nozzle diameter: 0.19 mm)) was used for the study (Fig. 1). The engine was equipped with cam-shaft driven fuel injector (mechanical fuel injector). An eddy current dynamometer was used for loading the engine. A piezoelectric strain gauge pressure transducer was mounted on the fuel line for measurement of in-line fuel pressure. A piezoelectric transducer was mounted (as flush mounted) in the cylinder head for in-cylinder pressure measurement (Measuring range: 0–250 bar, sensitivity: 45p C/bar and linearity:  $\leq \pm 0.3\%$ ). The crank angle encoder was mounted on the engine shaft for crank angle measurement with an accuracy of 0.05° CA. AVL indicom system comprised of in-built charge amplifier and data acquisition system was used for acquiring of pressure–crank angle data. The injection signals were processed using the system with the signal amplifier. The engine speed (1500 rpm) was maintained as constant throughout the tests. CO, CO<sub>2</sub> and HC emissions were measured using AVL Di-gas analyzer (Measurement principle: Infrared measurement). NOx emission was measured using CLD

**Fig. 1.** Experimental set-up.

analyzer (linearity:  $\pm 1\%$ ). Smoke opacity was measured using AVL smoke meter (Accuracy:  $\pm 1\%$ , measuring range: 0–100% Opacity). The Karanja methyl ester (biodiesel) was prepared in a laboratory scale and the biodiesel of 5%, 10%, 15%, 20%, 25%, 50% and 100% (B5, B10, B15, B20, B25, B50 and B100) by volume was blended with base diesel (Bharat stage IV (equivalent of Euro IV)). The physico-chemical properties were measured (density, viscosity, flash point, cloud point, pour point, and calorific value) whereas other physico-chemical properties such as thermal conductivity, surface tension and latent heat of fuels were taken from National Renewable Energy Laboratory (NREL) and BP websites (Table 2).

Experimental tests were conducted on the diesel engine in-order to assess injection, combustion, performance and emissions of the engine for base diesel and biodiesel–diesel blends. Each test was repeated at least three times to confirm the accuracy of measured data.

The measured injection and combustion characteristics (Injection duration, In-line fuel pressure, In-cylinder pressure) were given as input to the spray models/correlations. The measured swirl ratio of 2.20 was taken into account for calculation of spray characteristics. The spray characteristics are analyzed with respect to crank angle per cycle. The models, which are selected for calculating the spray characteristics for the present study, are based on our previous work published in literature [2]. These spray models are optimized/selected based on available measured data in the literature for spray characteristics. Furthermore, these selected models are also used by many researchers to calculate biodiesel spray characteristics. Even though the spray characteristics could be calculated with more accurate during the ignition delay period, it is very difficult to predict the spray characteristics after the start of combustion. The reasons could be due to fuel spray interaction with air at very high temperature, high pressure and unpredictable air motion (high velocity) resulting to complexity in nature of mixture formation with unburned reactant and burned product during the diffusion combustion phase. Wall impingement is defined that it would occur when the spray penetration distance is higher than the available length between piston bowl surface and nozzle tip. A study of probability wall impingement based on spray penetration and piston bowl motion with respect to crank angle was carried out. Spray penetration with respect to crank angle was calculated using model. Wall impingement would occur when the spray penetration is higher than the available length between piston bowl surface and nozzle tip. The volume of cylinder with respect to crank angle was calculated using Eqs. (1)–(4). From the known displacement volume, the stroke length can be calculated as given in Eq. (5). Injector angle was measured to predict the inclined length, i.e. actual distance from injector nozzle tip to piston bowl depth (Fig. 2) with respect to crank angle.

$$r_c = \frac{V_t}{V_c} = \frac{V_d + V_c}{V_c} \quad (1)$$

$$V_d = \frac{\pi}{4} \times D^2 \times L \quad (2)$$

where  $r_c$  = Compression ratio,  $D$  = Cylinder bore and  $L$  = Stroke length

**Table 2**  
Physico-chemical properties of diesel and biodiesel blends.

Property	Diesel	B5	B10	B15	B20	B25	B50	B100
Density (kg/m <sup>3</sup> )	821.5	823.1	827.5	831.3	835.6	838.9	860.7	893.6
Viscosity (cSt)	2.64	2.65	2.66	2.69	2.71	2.75	3.5	5.8
Flash point (°C)	76	85	96	101	110	117	129	147
Cloud point (°C)	6.5	7.2	8.3	9.1	10	10.3	11.1	13.6
Pour point (°C)	3.1	3.5	3.8	4.3	4.5	4.8	5.3	6.7
CV (MJ/kg)	44.05	43.89	43.25	42.90	42.60	42.00	41.73	40.750
Thermal condu. (W/mK)	0.061	–	–	–	–	–	–	0.018
Surface tension (N/m)	0.023	–	–	–	–	–	–	0.028
Latent heat (kJ/kg)	250	–	–	–	–	–	–	181

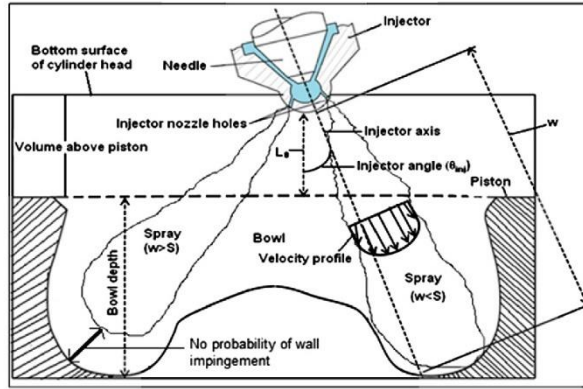


Fig. 2. Occurrence of wall impingement on the surface of piston bowl.

Cylinder volume ( $V$ ) at any crank angle position  $\theta$  can be calculated using Eq. (6).

$$V_{\theta} = V_c + \left[ \frac{\pi \times D^2}{4} (l + a - s) \right] \quad (3)$$

$$\text{where } s = a \times \cos \theta + (l^2 - a^2 \times \sin^2 \theta)^{1/2} \quad (4)$$

The available length ( $L_{\theta}$ ) between the nozzle tip to piston surface can be calculated using  $V_{\theta}$  as given in Eq. (5).

$$L_{\theta} = \frac{4 \times V_{\theta}}{\pi \times D^2} \quad (5)$$

The sum of bowl depth ( $B_L$ ) and  $L_{\theta}$  is known as total length ( $L_t$ ) as given in Eq. (6).

$$L_t = L_{\theta} + B_L \quad (6)$$

The maximum available inclined length ( $w$ ) can be calculated using Eq. (7). The entire representation of wall impingement is shown in Fig. 2.

$$w = \frac{L_t}{\cos(\theta_{inj})} \quad (7)$$

The actual maximum available length ( $w$ ) can be found from the distance between nozzle tip to bowl depth. If ' $w$ ' is greater than spray penetration ( $w > S$ ), wall impingement does not occur, whereas ' $w$ ' is lesser than spray penetration ( $w < S$ ), the probability of wall impingement would be more. If ' $w$ ' is equal to spray penetration ( $w = S$ ), it is a critical condition.

### 3. Results and discussion

#### 3.1. Analysis of injection characteristics for different biodiesel–diesel blends with comparison of base diesel

Figure 3 shows that the injection delay is lower with all biodiesel–diesel blends than base diesel due to lesser compressibility of biodiesel (higher bulk modulus) resulting in automatic advancement in dynamic injection timing (DIT). As the duration of injection delay decreased from 5.6° CA with base diesel to 5.5°, 5.4°, 5.3°, 5.2°, 5.1°, 5° CA with B10, B15, B20, B25, B50 and B100 respectively, DIT advanced from 0.4° CA before top dead center (BTDC) with base diesel to 0.5°, 0.6°, 0.7°, 0.8°, 1.1° and 1.5° CA BTDC with B10, B15, B20, B25, B50 and B100 respectively. However, there is no change in injection delay and DIT with B5. The drastic advancement can be observed from the figure for higher blends (B25, B50 and B100). It may be noted that bulk modulus is function of density (B5: 823.1, B10: 827.5, B15: 831.3, B20: 835.6, B25: 838.9, B50: 860.7 and B100: 893.6 kg/m<sup>3</sup>) and square of sound velocity resulting in higher bulk modulus of biodiesel. In general, the advanced DIT generally leads to higher NO<sub>x</sub> emission.

The in-line fuel injection pressure increases with increase the percentage of biodiesel in diesel. It may be noted that the in-line fuel pressure fluctuates as the pressure waves generated by the mechanical injection pump propagates more rapidly toward the injector [15]. Bulk modulus is the ratio of pressure ( $dP$ ) and volumetric strain ( $dV/V$ ). If the volumetric strain ( $dV/V$ ) is constant, the pressure ( $dP$ ) is directly proportional to bulk modulus ( $B$ ). Similarly, the peak in-line fuel injection pressure of all biodiesel–diesel blends (B5: 484.28, B10: 487.62, B15: 490.85, B20: 495.45,



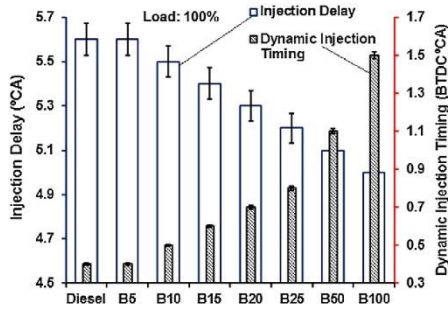


Fig. 3. Comparison of injection delay and DIT for base diesel and biodiesel blends.

B25: 493.48, B50: 496.32 and B100: 505.9 bar) is higher than base diesel (Diesel: 472.31 bar). In order to maintain same power output, the fuel flow rate needs to be enhanced more. The enhanced fuel flow rate may be one of the reasons to increase in-line fuel injection pressure with biodiesel–diesel blends.

The high in-line fuel pressure for biodiesel–diesel blends increases spray penetration distance which is discussed in latter section. The in-cylinder fuel injection duration is higher with all biodiesel–diesel blends than base diesel. In order to maintain same power output, the fuel flow rate needs to be enhanced more. The increased injection duration would affect performance characteristics of the engine mainly torque, BSFC and combustion characteristics negatively. The injection duration increases from 10.2° CA with base diesel to 10.5°, 10.7°, 10.8°, 10.9°, 11°, 11.2° and 11.4° CA with B5, B10, B15, B20, B25, B50 and B100 respectively at the rated load. The percentage change in injection duration is in the range of 5–10% for B20 to B100 whereas it is less than 5% up to B15. Hence, injection system including injection timing, plunger diameter, number of nozzle holes and its size and nozzle opening pressure has to be optimized for the overcoming of the problem of increased mass flow rate of biodiesel blends.

### 3.2. Analysis of spray characteristics for different biodiesel–diesel blends and base diesel

#### 3.2.1. Spray break-up length ( $L_b$ )

The break-up length (BUL) is calculated using Hiroyasu–Arai model as shown in Eq. (8).

$$L_b = 15.8 \times \left(\frac{\rho_l}{\rho_a}\right)^{0.5} \times D_n \quad (8)$$

where  $\rho_l$  is liquid density ( $\text{kg/m}^3$ ),  $\rho_a$  is air density ( $\text{kg/m}^3$ ),  $D_n$  is nozzle diameter (m).

As the density of biodiesel blends (B100: 893.6  $\text{kg/m}^3$ ) is higher than base diesel (821.5  $\text{kg/m}^3$ ), the break-up length for B100 fuel is higher than base diesel (Fig. 4(a)). The peak break-up length is higher with B100 (13.9 mm) as compared to base diesel (13.5 mm) at the rated load. There is no change in break-up length with biodiesel–diesel blend (B5 to B20) as the values are within uncertainty limit ( $\pm 1.3\%$ ) whereas there is a significant increase with B25, B50 and B100 blends. Break-up length preferably should be less whereas higher break-up length leads to the poor air entrainment into the fuel spray.

#### 3.2.2. Spray cone angle ( $\theta$ )

The spray cone angle (SCA) is calculated using Reitz model as given in Eq. (9).

$$\tan\left[\frac{\theta}{2}\right] = \left(\frac{1}{A}\right) \times 4 \times \pi \times \left(\frac{\rho_a}{\rho_l}\right)^{0.5} \times \left(\frac{3^{0.5}}{6}\right) \quad (9)$$

where  $A = 3 + \left(\frac{U_a D_n}{3.6}\right)$

The spray cone angle ( $\theta$ ) for biodiesel–diesel blends is lower than base diesel due to higher density of biodiesel–diesel blends than base diesel (Fig. 4(b)). At the end of spray, the spray cone angle is more divergent could be due to the momentum of spray decreases from upstream (injector tip) to downstream (spray tip). The peak spray cone angle decreased from 17.5° with base diesel to 16.8° with B100 at the rated load at 10° CA ATDC. It may be due to higher density and viscosity of biodiesel. At same spray penetration distance, if spray cone angle decreased, air entrainment would be less resulting to poor mixture formation. Even though biodiesel blend has higher in-line fuel pressure, spray cone angle does not change significantly with biodiesel because of spray cone angle is influenced mainly by fuel quality (density and viscosity).

#### 3.2.3. Sauter mean diameter (SMD)

Sauter mean diameter is the average diameter of droplet that has same volume to surface area ratio as that of the total spray. The average diameter of droplet is used to describe the quality of atomization and SMD is a main input to calculate other spray characteristics. Hiroyasu model was used to calculate SMD ( $X_{32}$ ) as given in Eqs. (10)–(12).

$$X_{32} = \text{Max}(X_{32}^{LS}, X_{32}^{HS}) \quad (10)$$

$$X_{32}^{LS} = 4.12 \times D_n \times \text{Re}^{0.12} \times \text{We}^{-0.75} \times \left(\frac{\mu_l}{\mu_a}\right)^{0.54} \times \left(\frac{\rho_l}{\rho_a}\right)^{0.18} \quad (11)$$

$$X_{32}^{HS} = 0.38 \times D_n \times \text{Re}^{0.25} \times \text{We}^{-0.32} \times \left(\frac{\mu_l}{\mu_a}\right)^{0.37} \times \left(\frac{\rho_l}{\rho_a}\right)^{-0.47} \quad (12)$$

where Re and We is Reynolds and Weber number,  $\mu_l$  and  $\mu_a$  is fuel and air viscosity (Pa s).

SMD is higher for the biodiesel–diesel blends than that of base diesel fuel and this is due to the higher density, viscosity and surface tension of biodiesel–diesel blends (Fig. 5). The change of increase in SMD up to B15 blend is within uncertainty limit whereas SMD increased beyond B20 blends. The Weber number is important parameter for SMD and it is function of density and surface tension. As the surface tension is higher with biodiesel [28], Weber number would be lower. Hence, lower Weber number would give larger SMD with biodiesel. A sharp peak of SMD is observed for B100 at 2° CA ATDC and it is due to change in in-line fuel pressure at particular crank angle. At the end of spray, SMD increases significantly during 9–11° CA ATDC due to decrease in in-line pressure. The larger SMD deprived the mixing rate of air and fuel.

#### 3.2.4. Spray penetration

Spray penetration calculated using Hiroyasu–Arai model is shown in Eqs. (13), (14) as these equations were used by other researchers to calculate the spray penetration distance of a diesel engine for biodiesel–diesel blends. The penetration distance with respect to crank angle is calculated using input of measured in-line fuel pressure, in-cylinder pressure, injection duration, nozzle diameter and air density for the biodiesel–diesel blends and the results are compared with base diesel. It is observed from the results that the penetration distance increased with all biodiesel–diesel blends (Fig. 5). The peak penetration distance increased from 34.24 mm with base diesel to 34.4, 34.8, 35.1, 36.28, 36.6, 36.9 and 37.5 mm with B5, B10, B15, B20, B25, B50 and B100 at the rated load. The change in increase of spray penetration is lower than 5% up to B20 blend whereas it is higher for B25, B50 and B100.

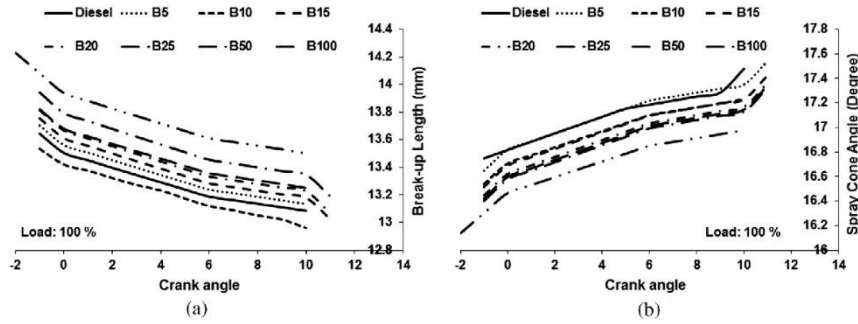


Fig. 4. Variation of (a) break-up length and (b) spray cone angle for base diesel and biodiesel blends.

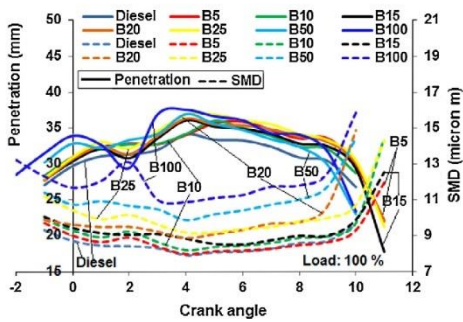


Fig. 5. Variation of SMD and spray penetration for base diesel and biodiesel blends.

In case of B100 at 2° CA ATDC, sudden drop was observed for penetration. It is mainly due to drop in in-line fuel pressure at 2° CA ATDC. At the downstream of the spray (tip), penetration decreases due to lesser momentum toward downstream. The higher penetration is beneficial for air entrainment but it may lead to wall impingement [29].

$$S = 2.95 \times \left( \frac{\Delta P}{\rho_a} \right)^{0.25} \times (D_n \times t)^{0.5} \quad \text{for } t > t_b \quad (13)$$

$$S = 0.39 \times \left( 2 \times \frac{\Delta P}{\rho_a} \right)^{0.5} \times t \quad \text{for } t < t_b \quad (14)$$

where  $S$  is spray penetration (m),  $t$  is injection time (s) and  $t_b$  is break-up time (s).

### 3.2.5. Air entrainment

Air entrainment is defined as the process of air drawn into the fuel spray. Air entrainment calculated using Rakopoulos model/correlation is given in Eq. (15). Air entrainment is calculated with respect to crank angle using input of calculated spray cone angle, penetration and air density.

$$m_a = \left( \frac{\pi}{3} \right) \times \left( \tan \left( \frac{\theta}{2} \right) \right)^2 \times S^3 \times \rho_a \quad (15)$$

It is observed from the results that the air entrainment increased for biodiesel–diesel blends due to higher in-line fuel pressure resulting in higher penetration distance as compared to

base diesel (Fig. 6). In case of B100, air entrainment suddenly drops at 2° CA ATDC as it is mainly due to sudden drop in in-line fuel pressure resulting in particular crank angle. At the end of the spray, air entrainment decreased due to decrease in penetration distance. In general, as the spray cone angle decreased, air entrainment also decreased. The net result is in increased air entrainment as the penetration distance is more influencing parameter to increase in air entrainment than spray cone angle.

### 3.2.6. Wall impingement

Spray wall impingement is also an important post process in spray combustion. It is observed from the simulation study that the probability of wall impingement is more with higher biodiesel–diesel blends (B25, B50 and B100). This is due to increased penetration distance. The distance between nozzle tip and piston bowl decreases as piston moves toward top dead center and vice versa. The distance between nozzle tip and piston bowl depth (0–1) is shown in Fig. 7. The distance ‘0–1’ is the highest distance as compared to the distance ‘0–2’ and ‘0–3’. The distance ‘0–1’ is considered for all calculations. When piston moves toward the top dead center (TDC), there may be a probability of fuel impingement on piston bowl at points ‘3’ and ‘2’ due to shorter distance of ‘0–2’ and ‘0–3’. The general mathematical form of wall impingement is explained in our study that was used to calculate the wall impingement [9]. There is no wall impingement for base diesel, B5, B10, B15 and B20 as shown in Fig. 7. As the uncertainty limit of penetration is  $\pm 1.3\%$ , there may be a probability of wall impingement with B20. However, wall impingement was observed clearly with higher

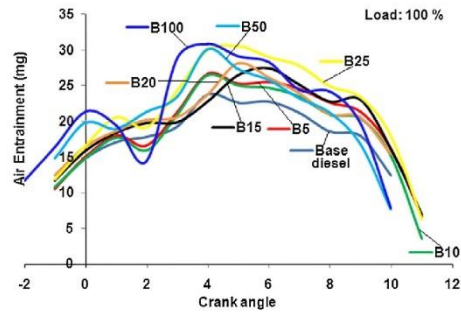


Fig. 6. Variation of air entrainment for base diesel and biodiesel blends.

biodiesel–diesel blends such as B25, B50 and B100. For B100, wall impingement is observed from 3° CA ATDC to 5° CA ATDC whereas for B25 and B50, it is observed from 3.8° CA ATDC to 4.3° CA ATDC. The wall impingement problem can be overcome by optimizing the nozzle hole size (diameter) and number of nozzle holes [29].

3.3. Analysis of combustion characteristics for different biodiesel–diesel blends and base diesel

Ignition delay, premixed combustion, mixing controlled (diffusion) combustion and late burning combustion are the vital parameters of combustion in diesel engines. The liquid fuel injected into the combustion chamber of an engine undergoes a set of physical and chemical process such as atomization, evaporation and mixing with air entrained into the spray. Ignition occurs in the periphery of the spray depending on the temperature and pressure of the in-cylinder air. The ignition delay was found lower with all the biodiesel–diesel blends (B5: 3.2°, B10: 3.2°, B15: 3°, B20: 2.9°, B25: 2.8°, B50: 1.7° and B100: 1.6° CA) as compared to base diesel (3.4° CA) due to higher cetane number of biodiesel. The start of combustion advanced for all biodiesel blends (B5: 2.8°, B10: 2.7°, B15: 2.4°, B20: 2.2°, B25: 2°, B50: 0.6° and B100: 0.1° CA ATDC) than diesel (3° CA ATDC). It is mainly due to the advance in injection timing and higher cetane number of biodiesel–diesel blends which improves the ignition quality.

The peak in-cylinder temperature increased with all biodiesel–diesel blends (B20: 1742, B100: 1810 K) as compared to base diesel (1687 K) (Fig. 8). It may be due to advance in DIT resulting in early combustion process initiated. In addition to this, the presence of oxygen molecule in biodiesel tends to advance the start of combustion. The comparison of heat release rate (HRR) for diesel and biodiesel blends is shown in Fig. 9. The endothermic reaction of fuel with air initially results in negative heat release rate. HRR is one of the important tools to optimize any internal combustion engine parameters. The heat release rate can be calculated using first law of thermodynamics. The adjustment of ignition delay can control the premixed combustion phase and this phase is responsible for NOx formation and knocking. Mixing controlled combustion phase (diffusion) is responsible for smoke formation. Premixed combustion phase duration increased marginally for all biodiesel–diesel blends as compared to base diesel. As the premixed combustion phase duration is higher for biodiesel–diesel blends, it could be one of the reasons for increase in NOx emission with biodiesel–diesel blends. Mixing controlled combustion phase duration increased

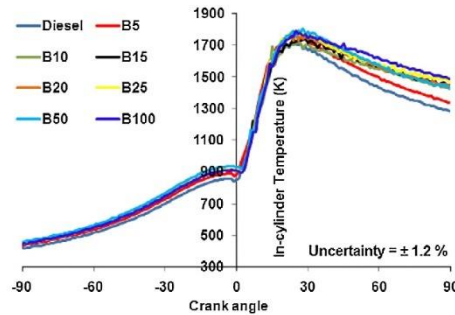


Fig. 8. Variation of in-cylinder temperature for base diesel and biodiesel blends.

marginally with all biodiesel–diesel blends as compared to base diesel.

The rate of pressure rise decreased with all biodiesel–diesel blends (B5: 5.9, B10: 5.4, B15: 4.35, B20: 4.3, B25: 4.26, B50: 3.25, B100: 2.2 bar/CA) as compared to base diesel (6.7 bar/CA) resulting in smoother engine running. The diesel engine with biodiesel–diesel blends has lesser ignition delay mainly due to higher cetane number resulting in lower rate of pressure rise [30]. The combustion duration is an important tool for optimizing performance and emission characteristics of the engine. The combustion duration is higher with all biodiesel–diesel blends (B20: 87.8° CA and B100: 89.9° CA) than base diesel (86° CA). The combustion duration increased marginally for lower biodiesel–diesel blends (up to B25) whereas it increased significantly for higher biodiesel–diesel blends (B50 and B100). It may be due to biodiesel has lower calorific value results in longer injection duration. In order to reduce combustion duration, a sustainable technology needs to be identified such as optimization of injection system and engine design parameters.

3.4. Analysis of performance and emission characteristics of the diesel engine for different biodiesel–diesel blends and base diesel

The brake specific energy consumption (BSEC) is calculated from the brake power output of the engine, calorific value and

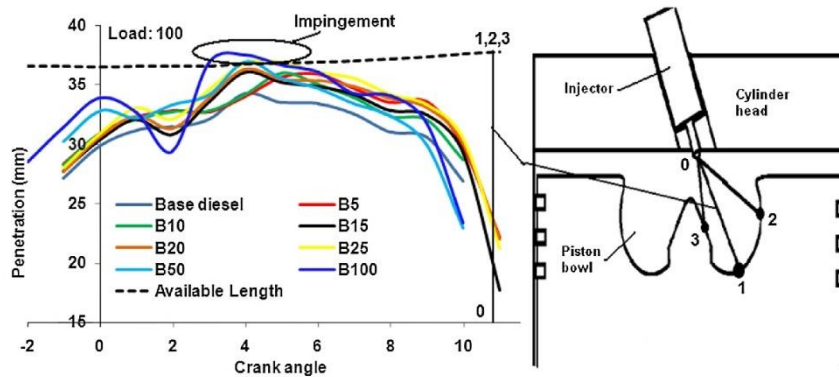


Fig. 7. Wall impingement for base diesel and biodiesel blends.

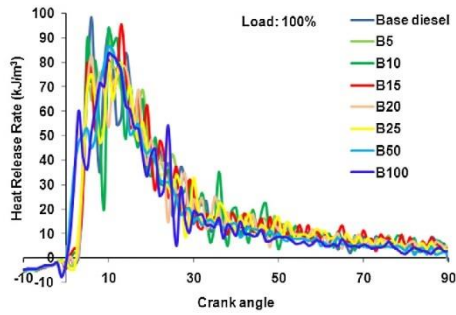


Fig. 9. Variation of heat release rate for base diesel and biodiesel blends.

the mass flow rate of the fuel. BSEC increases at lower and the rated load but it marginally decreases at 50%, 75% and 90% load (Fig. 10). The BSEC increases at lower load due to lower in-cylinder pressure and temperature. The BSEC increases with increase the biodiesel–diesel blends due to biodiesel having higher injection duration and combustion duration. BSEC increased from 12.7 MJ/kW-h with base diesel to 17.5 MJ/kW-h with B100 at the rated load. The increase in BSEC results in lower brake thermal efficiency (BTE) for biodiesel–diesel blends as compared to base diesel (Fig. 10). BTE decreased marginally with lower biodiesel–diesel blends (up to B25) whereas it decreased significantly with higher biodiesel blends (B50 and B100). It may be mainly due to biodiesel having higher density, viscosity and surface tension results in poor atomization and mixture formation (less spray cone angle) with air. It will lead to slower combustion and lower BTE. BTE at 50% and 75% loads marginally increased with all biodiesel blends as compared to diesel (within uncertainty limit). The percentage torque reduction was found to be 0.21, 0.63, 0.84, 0.9, 1.27, 2.33 and 2.76 for B5, B10, B15, B20, B25, B50 and B100 respectively as shown in Fig. 10. It is clearly seen from the figure that torque reduction is more for higher blends (B25, B50 and B100) whereas it is less for B5, B10, B15 and B20.

CO and HC emissions decreased with biodiesel–diesel blends due to higher oxygen content and lower C/H ratio (Fig. 11). The cleaner and complete combustion takes place due to oxygen content in biodiesel fuel which helps to reduce the CO and HC emissions. The automatic advancement of injection timing with biodiesel will provide more time for mixture formation resulting

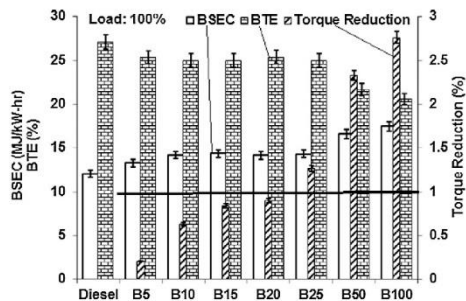


Fig. 10. Comparison of BSEC, BTE and torque reduction for base diesel and biodiesel blends.

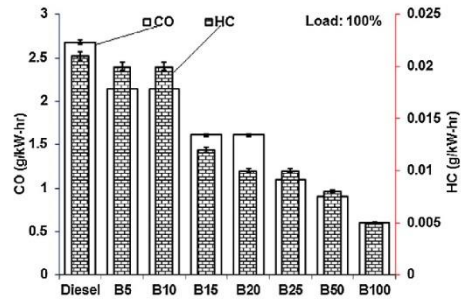


Fig. 11. Comparison of CO and HC emissions for base diesel and biodiesel blends.

in decrease in CO and HC emissions. CO and HC emissions decreased from 2.68 g/kW-h and 0.02 g/kW-h with base diesel to 0.5 g/kW-h and 0.005 g/kW-h with B100 respectively at the rated load.

NOx emission increased from 6.24 g/kW-h with base diesel to 8.07 g/kW-h with B100 (Fig. 12). This is one of the major problems for use of biodiesel in diesel engine. It is due to fuel containing oxygen (10%), automatic advance in injection timing and its formation around spray periphery due to larger penetration distance. NOx emission for lower biodiesel–diesel blends (up to B20) increased marginally at all loads whereas it increased significantly for higher biodiesel–diesel blends (B25, B50 and B100) at all loads. At rated load, NOx emission increased marginally up to B15, but beyond B15, NOx emission increased significantly. In pump-line-nozzle injection system, advanced injection timing increases the residence time of fuel which results in high reaction rate and more NOx formation. The problem can be overcome using NOx reduction techniques such as exhaust gas recirculation (EGR), injection timing optimization, nozzle opening pressure, nozzle size and number of nozzle holes optimization [29].

Smoke emission decreased drastically with all biodiesel–diesel blends (B100: 15.4% opacity) as compared to base diesel (51.9% opacity) as shown in Fig. 12. It decreased due to oxygen content of the biodiesel molecule, enables more complete combustion even in regions of the fuel-rich diffusion flames in combustion chamber. Biodiesel which is an oxygenated fuel provides oxygen in the core of the spray (rich fuel) during combustion process and hence enhancing reduction in smoke formation.

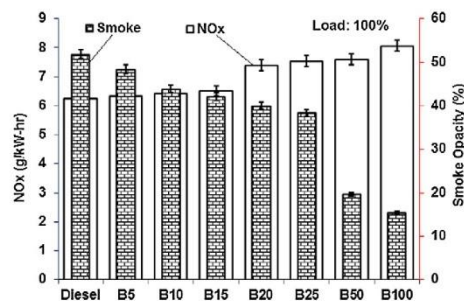


Fig. 12. Comparison of NOx and smoke emissions for base diesel and biodiesel blends.

#### 4. Conclusions

The following conclusions are drawn based on experimental and simulation results of spray, injection, combustion, performance and emission characteristics of a diesel engine fueled with biodiesel–diesel blends with comparison of base diesel.

Dynamic injection timing (DIT) of the engine advanced at all loads for all biodiesel–diesel blends due to higher bulk modulus of biodiesel. At the rated load, the DIT advanced from 0.4° CA BTDC with base diesel to 0.7° CA BTDC and 1.5° CA BTDC with B20 and B100 respectively. Spray penetration increased with all biodiesel–diesel blends (B20: 36.28 mm, B100: 37.5 mm) than base diesel (34.28 mm) due to higher in-line fuel pressure with biodiesel. No wall impingement was observed for B5, B10, and B15 whereas wall impingement probability was observed to be critical for B20 (within uncertainty  $\pm 1.3\%$ ). However, there is more probability of wall impingement with higher biodiesel blends (B25, B50 and B100) due to higher penetration distance.

Ignition delay and rate of pressure rise (RPR) decreased with all biodiesel–diesel blends due to higher cetane number of biodiesel than base diesel. At the rated load, the peak RPR decreased from 6.7 bar/°CA with diesel to 4.3 bar/°CA and 2.2 bar/°CA with B20 and B100 respectively. The reduction of torque was observed significantly beyond B20 blends. CO, HC and smoke emissions decreased drastically from 2.68 g/kW-h, 0.021 g/kW-h and 51.9% opacity with base diesel to 0.6 g/kW-h, 0.005 g/kW-h and 15.4% opacity with B100 respectively at the rated load. NOx emission increased with all biodiesel blends as compared to diesel due to oxygen content in biodiesel, advancement in DIT, higher penetration and in-cylinder temperature. NOx emission increased from 6.24 g/kW-h with base diesel to 7.39 g/kW-h and 8.07 g/kW-h with B20 and B100 respectively at the rated load. The optimum biodiesel–diesel blend based on no wall impingement and increase in NOx emission in unmodified diesel engine is up to B15.

#### References

- Subramanian KA, Lahane S. Comparative assessment of injection, combustion, performance and emission characteristics of a diesel engine for biodiesel–diesel blends. *Int J Renew Energy Tech* 2013;3(4):410–29.
- Subramanian KA, Lahane S. Comparative evaluations of injection and spray characteristics of a diesel engine using karanja biodiesel–diesel blends. *Int J Energy Res* 2013;37:582–97.
- Choi CY, Bower GR, Reitz RD. Effects of biodiesel blended fuels and multiple injections on DI diesel engines. *SAE* 970218; 1997.
- Kegl B. Biodiesel usage at low temperature. *Fuel* 2007. <http://dx.doi.org/10.1016/j.fuel.2007.06.023>.
- Kegl B, Hribernik A. Experimental analysis of injection characteristics using biodiesel fuel. *Energy Fuels* 2006;20:2239–48.
- Kegl B. Numerical analysis of injection characteristics using biodiesel fuel. *Fuel* 2006;85:2377–87.
- Ejimi CE, Fleck BA, Amirfazli A. Analytical study for atomization of biodiesels and their blends in a typical injector: surface tension and viscosity effects. *Fuel* 2007;86:1534–44.
- Tat ME, Gerpen JH. Measurement of biodiesel speed of sound and its impact on injection timing. Report by NREL/SR-510-31462-2003.
- Lahane S, Subramanian KA. Modelling and CFD simulation of effects of spray penetration on piston bowl impingement in a DI diesel engine for biodiesel–diesel blend (B20). In: *Proceeding of ASME ICED Spring Technical Conference*; 2012: 163–70.
- Gao Y, Deng J, Li C, Dang F, Liao Z, Wu Z, et al. Experimental study of the spray characteristics of biodiesel based on inedible oil. *Int J Biotechnol Adv* 2009;27:616–24.
- Sahoo PK, Das LM. Combustion analysis of Jatropha, Karanja and Polanga based biodiesel as fuel in a diesel engine. *Fuel* 2009;88:994–9.
- Rakopoulos DC. Heat release analysis of combustion in heavy-duty turbocharged diesel engine operating on blends of diesel fuel with cottonseed or sunflower oils and their bio-diesel. *Fuel* 2012;96:524–34.
- Sharma YC, Singh B, Upadhyay SN. Advancements in development and characterization of biodiesel: a review. *Fuel* 2008;87:2355–73.
- Zheng M, Mulenga MC, Reader GT, Wang M, Ting DSK, Tjong J. Biodiesel engine performance and emissions in low temperature combustion. *Fuel* 2008;87:714–22.
- Moon G, Lee Y, Choi K, Jeong D. Emission characteristics of diesel, gas to liquid, and biodiesel-blended fuels in a diesel engine for passenger cars. *Fuel* 2010;89:3840–6.
- Qi DH, Geng LM, Chen H, Bian YZH, Liu J, Ren XCH. Combustion and performance evaluation of a diesel engine fueled with biodiesel produced from soybean crude oil. *Renew Energy* 2009;34:2606–13.
- Graboski MS, McCormick RL. Combustion of fat and vegetable oil derived fuels in diesel engines. *Prog Energy Combust Sci* 1998;24(2):125–64.
- Sahoo PK, Das LM. Process optimization for biodiesel production from Jatropha, Karanja and Polanga oils. *Fuel* 2009;88:1588–94.
- Sahoo PK, Das LM, Babu MKG, Naik SN. Biodiesel development from high acid value polanga seed oil and performance evaluation in a CI engine. *Fuel* 2007;86:448–54.
- Rakopoulos CD, Hountalas DT, Zannis TC, Leventis YA. Operational and environmental evaluation of diesel engines burning oxygen-enriched intake air or oxygen-enriched fuels: a review. *SAE Paper No.* 2004-01-2924.
- Bajpai S, Sahoo PK, Das LM. Feasibility of blending karanja vegetable oil in petro-diesel and utilization in a direct injection diesel engine. *Fuel* 2009;88:705–11.
- Mahanta P, Mishra SC, Kushwah YS. An experimental study of pongamia pinnata L. oil as a diesel substitute. *IMEChE Part A: J Power Energy* 2006;20:803–8.
- Lin B, Huang J, Huang D. Experimental study of the effects of vegetable oil methyl ester on DI diesel engine performance characteristics and pollutant emissions. *Fuel* 2009;88:1779–85.
- Caresana F. Impact of biodiesel bulk modulus on injection pressure and injection timing, the effect of residual pressure. *Fuel* 2011;90:477–85.
- No SY. Inedible vegetable oils and their derivatives for alternative diesel fuels in CI engines: a review. *Renew Sustain Energy Rev* 2011;15:131–49.
- An H, Yang WM, Chou SK, Chua KJ. Combustion and emissions characteristics of diesel engine fueled by biodiesel at partial load conditions. *Appl Energy* 2012;99:363–71.
- An H, Yang WM, Maghbouli A, Li J, Chou SK, Chua KJ. Performance, combustion and emission characteristics of biodiesel derived from waste cooking oils. *Appl Energy* 2013;112:493–9.
- Som S, Longman DE, Ramirez AI, Aggarwal SK. A comparison of injector flow and spray characteristics of biodiesel with petrodiesel. *Fuel* 2010;89:4014–24.
- Lahane S, Subramanian KA. Impact of nozzle holes configuration on fuel spray, wall impingement and NOx emission of a diesel engine for biodiesel–diesel blend (B20). *Appl Therm Eng* 2014;64:307–14.
- Kuti OA, Zhu J, Nishida K, Wang X, Huang Z. Characterization of spray and combustion processes of biodiesel fuel injected by diesel engine common rail system. *Fuel* 2013;104:838–46.

2018-01-1693 Published 10 Sep 2018



## Spray Parameters of Fuel Blends of Recycled Lubricating Oil and Diesel

Marcos Gutierrez Tablet School

Andres Castillo, Juan Iniguez, and Gorky Reyes Universidad Internacional del Ecuador

**Citation:** Gutierrez, M., Castillo, A., Iniguez, J., and Reyes, G., "Spray Parameters of Fuel Blends of Recycled Lubricating Oil and Diesel," SAE Technical Paper 2018-01-1693, 2018, doi:10.4271/2018-01-1693.

### Abstract

The use of alternative fuels consisting of mineral and synthetic waste substances such as recycled lubricating oil blended with diesel is a measure to mitigate the environmental impact of the fossil fuels. However, to inject these fuel blends into contemporary engines without changes to their components, it must maintain or improve the fuel injection characteristics compared to neat diesel, in order to maintain or improve the engine performance. In the present research, the spray parameters of injected fuel, such as length, angle and atomization particle diameter in terms of the Sauter mean diameter (SMD), are modeled depending on the characterization of different concentration of the recycled

lubricating oil blended with diesel. It was found that the same nozzle geometry of the injectors can provide an equivalent fuel spray performance for different concentrations of these alternative fuel blends, and that the increase of the recycled lubricating oil in the fuel blend reduced the wear of the needle and nozzle of the injector. The densities and viscosities between each fuel type are very similar and any correction of injection duration or pressure is not required. Due to simple distillation and blending process, alternative and environmentally friendly fuel blends can be obtained to reduce the combustion of fossil diesel and reuse waste pollutant substances as a sustainable and immediately applicable solution for modern engines and fuel injection systems.

### Introduction

The use of fossil fuels represents around 78% of the global annual energy consumption; from this, 0.8% of biomass was used as an alternative fuel exclusively for transport from 2011 till 2017; while in 2018 an increase of this share was registered up to 0.9% [1]. Even when this reuse of vegetable-animal substances can be improved and raised to reduce the environmental impact being used as alternative fuels, the process of its transformation into fuel requires a complex process such as transesterification [2]. Among the waste substances, which can be transformed into fuel, there are synthetic and mineral substances such as lubricating oil that, depending on the population, and industrial growth, are more likely to become waste. The yield of reuse of lubricating oil can achieve up to 84%, however, an additional process to improve its lubricant properties is necessary [3]; while diesel-like fuel can be obtained as 60% of waste lubrication engine oil [4]. The use of this substances as a fuel has the advantage that after only filtration and simple distillation the lubricating oil can be used as a fuel blend with diesel for small to medium engines; while in a pure state it can be used as a fully compatible fuel instead of a heavy fuel oil (HFO) for heavy-duty engines [5].

One of the factors that condition the use of alternative fuels in order to be implemented as real and lasting alternatives are: the production cost, the ability to get into the combustion chamber well atomized with the required

quantity, length and angle of the spray, and reduced wear or damage possibilities like lack of lubrication capacity. Based on this, the present research focuses on the study of diesel blended with recycled lubricating oil, obtained by simple distillation with a yield of 50% under laboratory conditions, with a higher yield expected with the proper industrial process. The characterization of the studied fuel blends with recycled lubricating oil reveals small variations compared to neat diesel, that means high compatibility to be used as an alternative fuel. Finally, the durability of the fuel injection system, was higher, because of reduced wear under the effect of the lubricating action in the fuel blends, as the mass of the needle and nozzle of the tested injectors revealed, after endurance tests were performed.

The characterization of five fuel blends of diesel and recycled lubricating oil were compared to diesel, in order to evaluate the spray parameters depending mainly on the density and viscosity of each fuel blend.

Earlier investigations of biofuels showed that the difficulties of the fuel atomization due to higher viscosities are controlled with higher injections pressures [6], higher fuel consumption due to higher fuel densities are controlled by reducing the injection advance [7]; while in the present research, the goal is to offer fuel blends based on recycled lubricating oil with full compatibility without changes in the engine components or in the engine operation settings, to be used as substitutes of the neat diesel.

The present research analyzes the spray parameters of a common rail injector in terms of the injected quantity of fuel, with the use of alternative fuels from waste synthetic mineral substances as recycled lubricating oil, without any change in the engine components or control parameters of the fuel injection; later it will be compared with the use of neat diesel.

The recycling of lubricating oil to be reused as a fuel blend allows to effectively handle two issues: the first one is to minimize the disposal and re-refining process of waste substances, and the second one is to reduce the use of fossil fuels with fuel blends based on recycled waste substances. This approach can be successfully implemented, when the properties of the alternative fuel blends allow to maintain the spray parameters and delivered fuel quantity in equivalent ranges, between each fuel type and neat diesel, as the agreement of the calculated and experimental results of the present research reveals.

It is necessary to evaluate the effect of the fuel properties on the spray parameters that influence on the atomization and penetration characteristics of alternative fuel blends. There is a variety of sources and procedures to produce alternative fuels [8, 9], but it is fundamental that they can be injected into the engine to produce a performance equivalent or better than neat diesel.

## Main Section

### Materials and Equipment

The experimental characterization of five different concentrations of fuel blends consisting of diesel with recycled lubricating oil varying from 5% up to 25% (in terms of volume), gives the values of each property that condition the spray parameters of the fuel injection.

The fuel properties, such as density and viscosity, vary with temperature. For this reason, due to experimental and mathematical modeling, the values in the Table 1 were corrected to 37.8 °C [10], measured and calculated accordingly.

The characterized fuel was tested in a common rail test bench equipped with a diesel injector, able to control the rail pressure and injection duration into small periods, in order to perform tests under idle, pre-injection and main injection conditions (Table 2, Figure 1).

**TABLE 2** Test bench specification and operation settings.

Manufacturer	Speedmaq
Model	S200i
Power supply	220-380 V
Control system	Microcomputer to control the rail pressure and injection duration
Injection duration and pressure at idle condition	0.35 s @ 300 bar
Injection duration and pressure at pre-injection condition	0.10s @ 800 bar
Injection duration and pressure at main injection condition	0.70s @ 1000 bar
Temperature of the tested fuels	40 °C max.
Volume measurement accuracy	±0.5 mL

© SAE International

**FIGURE 1** Injector assembly in the test bench.



© SAE International

**TABLE 1** Properties of the diesel and fuel blends consisting of different diesel and recycled lubricating oil concentrations. \*Values measured experimentally at 15.55 °C and corrected to 37.8 °C [10]. \*\*Values measured experimentally. \*\*\*Calculated values.

Fuel type	Diesel	L5	L10	L15	L20	L25
Density @ 37.8 °C [kg/m <sup>3</sup> ]*	834.197	832.808	832.808	827.818	827.818	828.648
Kinematic viscosity @ 37.8 °C [cSt]**	4.02	4.07	4.09	4.16	4.25	4.75
Dynamic viscosity@ 37.8 °C [cP]***	3.353	3.390	3.406	3.444	3.518	3.936
Flash point [°C]**	62.3	63.4	53.1	52.0	48.3	47.8
Cetane number***	51.8	52.98	54.02	54.02	55.03	55.03
Heat value [MJ/kg]**	42.7817	42.7982	42.7986	42.7986	42.8453	42.8453
Superficial tension [N/m] @ 35 °C	0.0258	0.0260	0.0260	0.0270	0.0270	0.0270

© SAE International

© 2018 SAE International. All Rights Reserved.

The tank of the test bench must be cleaned refilled and cooled to test each fuel type. The temperature of the tested fuels was maintained at 38 °C by a radiator that maintained the temperature variation up to  $\pm 1$  °C.

The testing common rail injector specified in Table 3, is used for locomotive applications in a 4-stroke diesel engine (Table 4) and is able to perform multiple injections. In the present research, the injector performed pre-injection and main injection, as allowed by the test bench.

In order to make a proper and accurate calculation of the atomized fuel drops in terms of the Sauter mean diameter (SMD) (Eq. 5), the air properties correspond to the conditions inside of the combustion chamber at the end of the compression stroke and beginning of the injection, making reference to ideal gas law, as detailed in Table 5

**TABLE 3** Injector specification. \*Reference value.

Injector manufacturer	Bosch GmbH
Injector type	Common Rail
Injector model	095000652
Nozzle hole size [mm]	0.21
Nozzle hole length [mm]*	0.5
Nozzle hole angle [°]	155
Nozzle hole number [-]	8
Nozzle hole discharge coefficient*	0.85

© SAE International

**TABLE 4** Engine specification and fuel injection conditions. \*Referential value.

Engine manufacturer	Hino
Engine type	Diesel, four-cycle, four-cylinder in line, overhead valve, water cooled
Engine model	N04C US
Power	110 kW @ 2500 rpm
Torque	420 Nm @ 1400 rpm
Bore [mm]	104
Stroke [mm]	118
Piston displacement [cm <sup>3</sup> ]	4000
Fuel injection system	Electronic control, common rail type
Air intake system	Turbo intercooled
Specific fuel consumption [gr/kW h]*	210
Injection duration [°]*	22.5
Injection pressure range [bar]*	300-1000

© SAE International

**TABLE 5** Air properties. \*Calculated values with the ideal gas law. \*\*Values from Willi Bohl, Wolfgang Elmendorf [11].

Density @ 915 K & 61 bar [kg/m <sup>3</sup> ]*	23.23
Dynamic viscosity @ 915 K & 61 bar [cP]**	0.039

© SAE International

© 2018 SAE International. All Rights Reserved.

## Mathematical Formulation

The quality of the process of the fuel injection into the cylinder depends on the optimal diameter and geometry of the nozzle spray holes. Based on the equation to calculate the flow through a nozzle (Eq. 1) [14], the equation to determine the diameter of the spray holes (Eq. 2) can be expressed as a function of the specific fuel consumption, engine power, number of cylinders, injection duration, 4-stroke engine factor, number of nozzle holes, discharge coefficient of the nozzle holes, injection pressure, the pressure corresponding to the compression stroke and the density of the fuel.

$$Q = C_f \cdot A \cdot \sqrt{\frac{2 \cdot \Delta p}{\rho}} \quad (1)$$

$$D_n = \sqrt{\frac{4 \cdot SFC \cdot \frac{Pot}{z} \cdot \frac{360}{t_{inj}} \cdot K}{n \cdot C_f \cdot \pi \cdot \sqrt{\frac{2 \cdot (p_{inj} - p_{comp})}{\rho}}}} \quad (2)$$

The terms composed by the specific fuel consumption (SFC), the engine power (Pot), number of engine cylinders (z) and duration of the injection ( $t_{inj}$ ) in Eq. 2 represent the rate of flow (Q) in the Eq. 1; while the area (A) of the nozzle in the Eq. 1, is expressed in terms of the diameter of the nozzle hole (Dn) and the number of nozzle holes (n) in the Eq. 2; finally, the pressure difference ( $\Delta p$ ) in Eq. 1 represents the difference between the injection pressure ( $p_{inj}$ ) and the pressure corresponding to the compression stroke ( $p_{comp}$ ), shown in Eq. 2.

Once the diameter of the nozzle hole is calculated and compared with the specified nozzle hole diameter of the tested injector, the length reached by the atomized flow through the nozzle and the atomization angle is calculated with the Eq. 3 and Eq. 4 correspondingly [12]; while the size of the atomized fuel drops is calculated with the Eq. 5, in terms of the Sauter mean diameter (SMD) [13].

$$L_b = 15.8 \times \left( \frac{\rho_l}{\rho_a} \right)^{0.5} \cdot D_n \quad (3)$$

$$\tan \left[ \frac{\theta}{2} \right] = \left( \frac{1}{3 + \left[ \frac{L_b}{3.6} \right]} \right) \cdot 4 \times \pi \times \left( \frac{\rho_l}{\rho_a} \right)^{0.5} \times \left( \frac{3^{0.5}}{6} \right) \quad (4)$$

$$X_{32} = \text{Max} \left( X_{32}^{LS}, X_{32}^{HS} \right) \quad (5)$$

Where:

$$X_{32}^{LS} = 4.12 \times D_n \times Re^{0.12} \times We^{-0.75} \times \left( \frac{\mu_l}{\mu_a} \right)^{0.54} \times \left( \frac{\rho_l}{\rho_a} \right)^{0.18}$$

$$X_{32}^{HS} = 0.38 \times D_n \times Re^{0.25} \times We^{-0.32} \times \left( \frac{\mu_l}{\mu_a} \right)^{0.37} \times \left( \frac{\rho_l}{\rho_a} \right)^{-0.47}$$

$$Re = \frac{v_{inj} \cdot D_n}{\nu_l}$$

$$We = \frac{v_{inj}^2 \cdot D_n \cdot \rho_l}{\sigma_l}$$



According to Hiroyasu et al. [13],  $X_{32}^{LS}$  and the  $X_{32}^{HS}$  are the size of the atomized fuel drops for incomplete and complete sprays correspondingly; which mainly depend from the velocity of the injection and the ambient air conditions.  $X_{32}$  is the larger value of both. It means that  $X_{32}$  is bigger expected Sauter mean diameter of the atomized fuel drops.

The injected volume of the fuel is calculated with Eq. 6, based on Eq. 1, in terms of the number of the nozzle holes (n), the discharge coefficient of the nozzle ( $C_d$ ), the diameter of the nozzle hole ( $D_n$ ), the injection pressure ( $p_{inj}$ ), the density of the fuel ( $\rho$ ) and the injection duration ( $t_{inj}$ ). The results of this calculation are compared and evaluated with the volume measured in the test bench. The volume for this comparison is calculated only in function of the injection pressure ( $p_{inj}$ ), because the tested fuel is injected at the ambient pressure, without the effect of any compression or counter pressure.

$$v = n \cdot C_d \cdot \frac{\pi}{4} \cdot D_n^2 \cdot \sqrt{\frac{p_{inj}}{\rho}} \cdot t_{inj} \quad (6)$$

## Evaluation Procedure

The first stage of this research is to calculate the nozzle hole diameter (Eq. 2) with the characterization values of each fuel type (Table 1), under the operation conditions of the engine (Table 4). Afterwards the calculated diameter is compared with the diameter specified by the injector manufacturer (Table 3), in order to determine that all the analyzed fuel blends can be injected through the same nozzle without any significant differences.

The second stage consists in the calculation of the spray parameters like length, angle and Sauter mean diameter

(SMD) of the atomized fuel drops, depending on the calculated nozzle hole diameter, and on the properties of each fuel blend. This approach is performed in order to determine that the analyzed fuel blends are able to deliver a spray equivalent to the obtained with neat diesel.

The third and final stage consists in the measurement of the mass losses through wear of the nozzle and needle of six tested injectors, with each fuel concentration, after 250 hours of endurance test at 100 bar of injection pressure and 0.7 s of injection duration; in order to determine the lubricant benefits of the of the different concentrations of the recycled lubricating oil in each fuel blend.

## Results

The results of the delivered volume by the injector reveal that the injector works according to the specified calibration range values of the test bench (Table 6), with all the tested fuel blends. The injected volume during each injection was calculated (Eq. 6) and experimentally measured, giving small differences between each calculated and measured value with all the tested fuel blends.

The calculated nozzle hole diameters at each specified injection pressure, are the same for all the fuel types (Table 7). However, as the nozzle hole diameter is a fixed machined parameter, the larger value is selected to fulfill all the operation condition of the injection.

The spray length values (Table 8) are equivalent each other with all the fuel types, and the differences at each

**TABLE 6** Delivered injection volume at idle, pre-injection and main injection conditions at the common rail test bench, with different fuel blends based on recycled lubricating oil and neat diesel. \*Calibration range values for the specified injector at the common rail test bench.

Fuel type		Diesel	L5	L10	L15	L20	L25
Idle @ 300 bar (10-20) ml*	measured	15	15	15	15.5	15	15.5
	calculated	15.633	15.646	15.646	15.693	15.693	15.685
Pre-injection @ 800 bar (7-8.5) ml*	measured	7.5	7.5	8	8	8	8
	calculated	7.294	7.300	7.300	7.322	7.322	7.318
Full load @ 1000 bar (45-60) ml*	measured	52	52	52.5	52.5	53	52.5
	calculated	57.082	57.130	57.130	57.302	57.302	57.273

**TABLE 7** Calculated nozzle diameter at different injection pressures for each fuel blend based on recycled lubricating oil and neat diesel.

Fuel type	Diesel	L5	L10	L15	L20	L25
Nozzle holes diameter [mm] @ 300 bar	0.227	0.227	0.227	0.227	0.227	0.227
Nozzle holes diameter [mm] @ 800 bar	0.174	0.174	0.174	0.175	0.175	0.175
Nozzle holes diameter [mm] @ 1000 bar	0.165	0.165	0.165	0.165	0.165	0.165

**TABLE 8** Calculated spray length at different injection pressures for each fuel blend based on recycled lubricating oil and neat diesel.

Fuel type	Diesel	L5	L10	L15	L20	L25
Length of the atomized flow @ 300 bar [mm]	21.461	21.452	21.452	21.420	21.420	21.424
Length of the atomized flow @ 300 bar [mm]	16.509	16.502	16.502	16.478	16.478	16.481
Length of the atomized flow @ 1000 bar [mm]	15.583	15.576	15.576	15.553	15.553	15.556

specified injection pressure are not significant. The same consideration applies for the angle of the spray (Table 9); however, is observed that the angle tends to be wider for the fuels of the type L15 and L20. The difference between the fuel blends in comparison to diesel for the length and angle of the spray is less than 1%.

The diameter of the atomized fuel drops in terms of the Sauter mean diameter (SMD), tends to be higher as the concentration of the recycled lubricating oil in the fuel blend increases. This difference amounts a maximum of 10% and a minimum of 1% for the L25 and L5 fuel blends correspondingly.

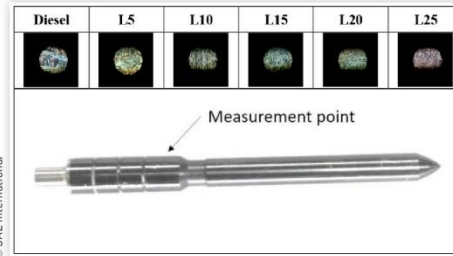
The marked section on the needle surface (Figure 2), was selected as the section to be analyzed regarding the wear with each fuel blend. After 250 hours of an endurance test, at 100 bar of injection pressure and 0.7 s of injection duration, is observed that the wear and mass losses are lower, as the concentration of the recycled lubricating oil in the fuel blend is higher.

## Analysis

From the characterization of each fuel blend, it is observed that there are no differences in the density between the L5 and L10, as well as between L15 and L20 fuel blends.

As the concentration of the fuel blend grows from 5 to 25%, the delivered volume by the injector at the common rail test bench (Table 6) shows that the values remain stable and inside the range specified by the injector set up values of the test bench. That means that all the fuel blends regarding the delivered volume are compatible and equivalent.

**FIGURE 2** Wear analysis of the injector needle.



The minimal differences of the delivered injected volume, the length, and angle of the spray are attributed to the minimal differences between the properties of the characterized fuel. However, the atomized diameter of the fuel drops in terms of the Sauter mean diameter (SMD), reveals that these differences amount up to 10% for the L25 fuel blend. This effect can be explained by the higher dynamic and kinematic viscosities as the concentration of the recycled lubricating oil in the fuel blend increases.

An additional benefit of the fuel blends based on recycled lubricating oil is the lubricating effect of the fuel for the injection system, as the results of the mass measurement of the injector needle showed, after the endurance test with each fuel blend (Table 11).

**TABLE 9** Calculated spray angle at different injection pressures for each fuel blend based on recycled lubricating oil and neat diesel.

Fuel type	Diesel	L5	L10	L15	L20	L25
Angle of the atomized flow @ 300 bar [°]	19.024	19.041	19.041	19.102	19.102	19.094
Angle of the atomized flow @ 800 bar [°]	18.118	18.135	18.135	18.194	18.194	18.186
Angle of the atomized flow @ 1000 bar [°]	17.889	17.915	17.915	17.974	17.974	17.966

**TABLE 10** Calculated diameter of the atomized fuel drops in terms of the Sauter mean diameter (SMD) for each fuel blend based on recycled lubricating oil and neat diesel.

Fuel type	Diesel	L5	L10	L15	L20	L25
Diameter of the atomized fuel drops SMD lower atomization @ 300 bar [μm]	26.82	26.946	26.962	27.421	27.491	27.851
Diameter of the atomized fuel drops SMD higher atomization @ 300 bar [μm]	34.936	35.289	35.361	36.512	36.842	38.621
Diameter of the atomized fuel drops SMD lower atomization @ 800 bar [μm]	17.126	17.207	17.217	17.510	17.555	17.785
Diameter of the atomized fuel drops SMD higher atomization @ 800 bar [μm]	15.372	15.527	15.559	16.065	16.210	16.993
Diameter of the atomized fuel drops SMD lower atomization @ 1000 bar [μm]	15.516	15.589	15.598	15.863	15.904	16.112
Diameter of the atomized fuel drops SMD higher atomization @ 1000 bar [μm]	12.83	12.959	12.986	13.408	13.529	14.183

**TABLE 11** Mass of the needle and nozzle of the injector after 250 hours of an endurance test at 100 bar of injection pressure and 0.7 s of injection duration with neat diesel and the fuel blends from recycled lubricating oil.

Fuel type	Diesel	L5	L10	L15	L20	L25
Needle mass [gr]	3.3075	3.2994	3.2996	3.3033	3.3034	3.3068
Nozzle mass [gr]	22.7030	22.5790	22.5792	22.6330	22.6335	22.6990

© SAE International

© 2018 SAE International. All Rights Reserved.

Unlike fuel blends from vegetable-animal substances that have a bigger variation in the properties of the characterization, making necessary correction on the pressure and duration of the injection, in order to compensate especially the density, viscosity and heat values variations; the fuel blends based on recycled lubricating oil and diesel are stable in concentrations from 5 up to 25% and practically fully compatible with neat diesel. However, it is necessary to remark that the quality of the fuel blend is conditioned by the accuracy of the recycling process of the used lubricating oil.

Normally, the collection process of used lubricating oil is a mixture of oils from different producers with own properties coming from engines, operating at different conditions, which may have impurities like carbon waste that may alter properties of the fuel blends and make difficult to have a narrow range for the variation of each property.

## Conclusions

The presented methodology allows to evaluate the spray parameters of any alternative fuel blend, as well as its compatibility with the fuel injection system. At the same time, if the variation in the fuel blend properties is considerable, the proposed evaluation method allows to locate the control parameters of the fuel injection, such as the pressure and duration of the injection, to achieve the required spray performance.

The calculation of fuel spray parameters determines if alternative fuel blends are able to operate with a diesel-based fuel injection system from the functional point of view.

Based on the characterization results of each fuel type, especially on the heat value and on the fact that between L5 and L10, as well as between L15 and L20, the densities are the same, it is recommended to use less diesel and burn more recycled lubricating oil. It means that the worthiest fuel blend concentrations are the L10, L20, and L25, disregarding the L5 and L15 blends.

The spray parameters such as the delivered fuel quantity, length and angle of the spray remain constant for each fuel blend, even when the concentration of the recycled lubricating oil with diesel varies from 5 up to 25%.

Regarding the atomization diameter of the fuel drops, in terms of the Sauter mean diameter (SMD), there is a significant difference between the use of the L25 fuel blend and neat diesel, where the atomized fuel drops are bigger for the alternative fuel. It can lead to the formation of soot and decreased engine performance, as the fuel is not well atomized in comparison with neat diesel or with the blends with less concentration of recycled lubricating oil.

The use of recycled lubricating oil as part of a blend for an alternative fuel solve problems like disposal and re-refining of this kind of waste substances. Furthermore, it improves the durability of the fuel injection system because of its lubricating effect.

## References

1. REN21 Renewable Energy Policy Network for the 21st Century, "Renewables 2013, 2014, 2015, 2016, 2017, 2018 Global Status Report," <http://www.ren21.net>, accessed June 2018.
2. Castellar, G., Angulo, E., and Cardozo, B., "Transesterification Vegetable Oils Using Heterogeneous Catalysts," *Prospect* 12(2):90-104, 2014.
3. Eman, A. and Shoaib, A., "Re-Refining of Used Lub Oil I by Solvent Extraction and Vacuum Distillation Followed by Hydrotreating," *Petroleum & Coal* 55(3):179-187, 2013, ISSN:1337-7027.
4. Arpa, O., Yumrutas, R., and Demirbas, A., "Production of Diesel-Like Fuel from Waste Engine Oil by Pyrolytic Distillation," *Applied Energy* 87(1):122-127, Jan. 2010, doi:10.1016/j.apenergy.2009.05.042.
5. Tajima, H., Takasaki, K., Nakashima, M., Yanagi, J. et al., "Combustion of Used Lubricating Oil in a Diesel Engine," SAE Technical Paper 2001-01-1930, 2001, doi:10.4271/2001-01-1930.
6. Banapurmath, N.R., Tewari, P.G., and Hosmath, R.S., "Effect of Biodiesel Derived from Honge Oil and its Blends with Diesel when Directly Injected at Different Injection Pressures and Injection Timings in Single-Cylinder Water-Cooled Compression Ignition Engine," *Proc. IMechE Part A: J. Power and Energy* 223, 2009, doi:10.1243/09576509JPE673.
7. Carraretto, C., Macor, A., Mirandola, A., Stoppato, A. et al., "Biodiesel as Alternative Fuel: Experimental Analysis and Energetic Evaluations," *Energy* 29:2195-2211, 2004, doi:10.1016/j.energy.2004.03.042.
8. Mahmudul, H.M., Hagos, F.Y., Mamat, R., Abdul, A.A. et al., "Production, Characterization and Performance of Biodiesel as an Alternative Fuel in Diesel Engines - A Review," *Renewable and Sustainable Energy Reviews* 72:497-509, 2017.
9. Rakopoulos, C.D., Antonopoulos, K.A., Rakopoulos, D.C. et al., "Comparative Performance and Emissions Study of a Direct Injection Diesel Engine Using Blends of Diesel Fuel with Vegetable Oils or Bio-Diesels of Various Origins," *Energy Conversion and Management* 47(2006):3272-3287, 2006.
10. Queiroz Santos, D., De Lima, A.L., De Lima, A.P., Borges Neto, W. et al., "Thermal Expansion Coefficient and Algebraic Models to Correct Values of Specific Mass as a Function of Temperature for Corn Biodiesel," *Fuel* 106:646-650, 2013, doi:10.1016/j.fuel.2012.10.048.
11. Bohl, W. and Elmendorf, W., *Technische Strömungslehre* Fifteenth Edition (Germany: Vogel Business Media GmbH, 2014). ISBN:978-3-8343-3329-2.
12. Lahane, S. and Subramanian, K.A., "Effect of Different Percentages of Biodiesel-Diesel Blends on Injection, Spray, Combustion, Performance, and Emission Characteristics of a Diesel Engine," *Fuel* 139:537-545, 2015, doi:10.1016/j.fuel.2014.09.036.
13. Hiroyasu, H., Arai, M., and Tabata, M., "Empirical Equations for the Sauter Mean Diameter of a Diesel Spray," SAE Technical Paper 890464, 1989, doi:10.4271/890464.

14. Streeter, V., Benjamin, W.E., and Bedford, K., *Fluid Mechanics* Ninth Edition (USA: McGraw Hill, 1998). ISBN:0-07-062537-9.
15. Reddy, S., Sharma, N., Gupta, N., and Kumar, A.A., "Effect of Non-edible Oil and its Biodiesel on Wear of Fuel Injection Equipment Components of a Genset Engine," *Fuel* 222:841-851, 2018.

## Contact Information

**Name:** Marcos Gutiérrez Ojeda PhD  
**Company:** Tablet School  
**Position:** Director  
**P.O. Box:** 05-01-444  
**Address:** General Maldonado and Belisario Quevedo  
**City:** Latacunga  
**Country:** Ecuador  
[marcosgutierrez@tablet-school.com](mailto:marcosgutierrez@tablet-school.com)

## Acknowledgments

We give our acknowledgments to Svyatoslav Cheranov from Moscow Polytechnic University in Moscow - Russia for his contribution to this work.

## Definitions/Abbreviations

**D100** - Neat diesel fuel  
**L5** - 5% recycled lubricating oil blended with 95% neat diesel  
**L10** - 10% recycled lubricating oil blended with 90% neat diesel  
**L15** - 15% recycled lubricating oil blended with 85% neat diesel  
**L20** - 20% recycled lubricating oil blended with 80% neat diesel  
**L25** - 25% recycled lubricating oil blended with 75% neat diesel  
**Q** - Rate of flow [L/min]  
**C<sub>r</sub>** - Discharge coefficient [-]  
**A** - Cross section [mm<sup>2</sup>]

**Δp** - Pressure difference [bar]  
**ρ** - Density [kg/m<sup>3</sup>]  
**D<sub>n</sub>** - Diameter of the nozzle holes [mm]  
**SFC** - Specific fuel consumption [g/kW h]  
**P<sub>ot</sub>** - Engine power [kW]  
**z** - Number of cylinders [-]  
**t<sub>inj</sub>** - Injection duration in terms of crankshaft rotation degrees [°]  
**K** - 4 stroke engine factor with value 2. [-]  
**n** - Number of nozzle holes [-]  
**p<sub>inj</sub>** - Injection pressure [MPa]  
**p<sub>comp</sub>** - Compression pressure in the combustion chamber [MPa]  
**SMD** - Sauter mean diameter  
**L<sub>s</sub>** - Length of the spray [mm]  
**ρ<sub>f</sub>** - Density of the fuel at the injection conditions [kg/m<sup>3</sup>]  
**ρ<sub>a</sub>** - Density of the air at the engine compression stroke conditions [kg/m<sup>3</sup>]  
**θ** - Spray angle [°]  
**L<sub>n</sub>** - Length of the nozzle holes [mm]  
**X<sub>32</sub>** - Sauter mean diameter of the atomized fuel drops, as the maximum value between  $X_{32}^{IS}$  and  $X_{32}^{HS}$   
**X<sub>32</sub><sup>IS</sup>** - Sauter mean diameter of the atomized fuel drops in terms of incomplete atomization  
**X<sub>32</sub><sup>HS</sup>** - Sauter mean diameter of the atomized fuel drops in terms of complete atomization  
**Re** - Reynolds number [-]  
**We** - Weber Number [-]  
**μ<sub>f</sub>** - Dynamic fuel viscosity [Pa-s]  
**μ<sub>a</sub>** - Dynamic fuel viscosity [Pa-s]  
**v<sub>inj</sub>** - Injection velocity [m/s]  
**v<sub>1</sub>** - Kinematic fuel viscosity [m<sup>2</sup>/s]  
**v** - Delivered volume [mm<sup>3</sup>]

All rights reserved. No part of this publication may be reproduced, stored in a retrieval system, or transmitted, in any form or by any means, electronic, mechanical, photocopying, recording, or otherwise, without the prior written permission of the copyright holder.

Positions and opinions advanced in this paper are those of the author(s) and not necessarily those of SAE International. The author is solely responsible for the content of the paper.

ISSN 0148-7191

# Requerimientos en el sistema de inyección de combustible para el uso de biodiésel



## Requirements for the fuel injection system to use of biodiesel

Marcos Gutiérrez-Ojeda<sup>1</sup>, Andrés Castillo-Reyes<sup>2</sup>, Juan Iñiguez-Izquierdo<sup>2</sup> y Gorky Reyes-Campaña<sup>2</sup>

<sup>1</sup> Tablet School, General Maldonado y Belisario Quevedo, Latacunga (Ecuador)

<sup>2</sup> Universidad Internacional del Ecuador, Av. Simón Bolívar y Av. Jorge Fernández, Quito (Ecuador)

DOI: <http://dx.doi.org/10.6036/8656> | Recibido: 20/11/2017 • Evaluando: 02/10/2017 • Aceptado: 21/12/2017

### ABSTRACT

Biodiesel, when used as an alternative fuel in its pure state or mixed with diesel, requires certain modifications of time and pressure of the fuel injection to the engine. In the present study, the properties and characteristics to fulfill by fuel injector nozzles when biodiesel is used as fuel, are determined. With the characterization results of neat diesel and neat biodiesel; as well as a blend of 20% biodiesel and 80% diesel, the main parameters of the fuel injection were calculated and simulated according to the power requirements of the engine. The purpose of the present investigation is to determine the fuel injection control parameters that allow equivalent use of diesel and biodiesel, without any change in its components. It was found that maintaining the diameter of the nozzle holes, the atomization characteristics of both type of fuels can be maintained by controlling the injection time and pressure; compensating in addition, differences in heat values, density and viscosity of biodiesel blends compared to neat diesel. Biodiesel is the alternative to pollution problems and sources of energy to operate internal combustion engines; however, to be established as a sustainable and immediately applicable solution, modifications to the engine must be at the level of fuel injection control, avoiding any kind of change or replacement of components.

**Keywords:** Biodiesel, Diesel, Nozzle, Flow rate, Density, Fuel injection.

combustibles controlando la duración y la presión de inyección de combustible; además de compensar las diferencias de poder calorífico, densidad y viscosidad de las mezclas combustibles de biodiésel en comparación con el diésel puro. El biodiésel es la alternativa a problemas de contaminación y de fuentes de energía para operar motores de combustión interna; sin embargo, para que se establezca como una solución sostenible e inmediatamente aplicable, las modificaciones en el motor deben ser a nivel del control de la inyección de combustible evitando todo tipo de cambio o sustitución de componentes.

**Palabras clave:** Biodiésel, Diésel, Tobera, Tasa de flujo, Densidad, Inyección de combustible.

### 1. INTRODUCCIÓN

El uso de biodiésel en estado puro o mezclado en diferentes concentraciones, en motores con sistemas de inyección de combustible diseñados para funcionar con diésel, hace necesario que antes de hacer modificaciones o de diseñar nuevos componentes, se identifiquen primero los requerimientos que garanticen un resultado equiparado con ambos combustibles. Estos requerimientos fundamentales son: el diámetro de los orificios de la tobera, para entregar la cantidad de combustible requerida por el motor; así como, la longitud y ángulo del chorro de atomización, para garantizar la distribución uniforme en la cámara de combustión de manera homogénea, para mejorar la calidad de la mezcla aire combustible.

En la presente investigación, por medio de cálculo y simulación con datos medidos experimentalmente de diésel y biodiésel puros; así como de una mezcla de 20% biodiésel y 80% diésel (B20), se determinaron: el diámetro de los orificios de la tobera, la longitud y ángulo del chorro de combustible atomizado. El biodiésel se obtuvo por medio de transesterificación de aceite reciclado de palma, considerando que los beneficios ecológicos y el rendimiento de producción [1], como un combustible alternativo, corresponden a la combustión de 100% y mínimo 20% de este tipo de combustible.

Los cálculos y simulaciones fueron realizados en función de la duración de la inyección a lo largo de diferentes valores de presión, con el fin de equiparar el rendimiento del motor con el uso de diésel y de mezclas de biodiésel. El objetivo consiste en determinar las condiciones que mantienen las características de rociado de combustible equivalentes al del diésel puro, para que el uso del biodiésel sea una alternativa directamente aplicable.

### RESUMEN

El biodiésel al ser usado como un combustible alternativo en estado puro o mezclado con diésel, necesita determinadas modificaciones en la duración y en la presión de la inyección de combustible en el motor. En el presente estudio se determinan las propiedades y las características que deben cumplir las toberas de un inyector para motores diésel, al momento de usar biodiésel como combustible. Con los datos de caracterización de diésel y biodiésel puros; así como de una mezcla de 20% de biodiésel con 80% diésel, se procedió a calcular y a simular los principales parámetros de la inyección de combustible en función de los requerimientos de potencia del motor. El propósito de la presente investigación consiste en determinar los parámetros de control de la inyección de combustible que permitan el uso equiparado de diésel y biodiésel, sin ningún cambio en sus componentes. Se encontró que, manteniendo el diámetro de los orificios de la tobera, se pueden mantener las características de atomización de ambos tipos de

Investigaciones anteriores señalan que, a pesar de los prometedores resultados en la reducción de emisiones, existe aún cierta resistencia al uso e implementación del biodiésel puro o mezclado como combustible alternativo, debido a una reducción de la potencia del motor e incremento en el consumo de combustible [2], e independientemente del origen de este tipo de combustible [3]. Esto se debe principalmente a un menor valor calorífico, alta viscosidad [4] y mayor densidad [5] del biodiésel. Estos efectos son incluso más notorios conforme aumenta la concentración de biodiésel en la mezcla combustible. El efecto que tiene un poder calorífico menor, es una reducción en la cantidad de energía química que se convierte en energía mecánica; mientras que, una mayor viscosidad trae como consecuencia una mayor profundidad de penetración del chorro atomizado de combustible, pero con un grado deficiente de mezclado con el aire en la cámara de combustión, debido a que un fluido con alta viscosidad tiene mayores dificultades para atomizarse en mayor grado. Finalmente, una mayor densidad trae como consecuencia un mayor consumo de combustible; ya que, el combustible se entrega al motor en función del volumen, y en el caso del biodiésel se entrega una mayor cantidad para compensar el reducido poder calorífico en comparación con el diésel puro [6].

El problema del alto consumo de combustible debido al re-

ducido poder calorífico y a la alta densidad del biodiésel se controla reduciendo el avance a la inyección [7]; mientras que, las dificultades en la atomización debido a la alta viscosidad pueden ser controladas con una mayor presión de inyección [8]. Se debe considerar además que la velocidad de inyección de combustible disminuye cuando se reduce también la presión de inyección [9].

Las propiedades de los combustibles, tales como la densidad y la viscosidad varían con la temperatura, por lo que se han realizado experimentos y modelos matemáticos que permiten corregir las mediciones a los valores de temperatura deseados [10], por esta razón en la presente investigación los valores medidos de la densidad a 15.55 °C se corrigieron a 37.8°C que es la temperatura a la que se midió la viscosidad cinemática, además de que es una temperatura cercana a la de la inyección del combustible en el motor.

Para cumplir con las expectativas de que el biodiésel sea un combustible alternativo y sustituto del diésel puro, se deben definir los parámetros y condiciones que deben controlarse en el sistema de inyección para que se cumplan los requerimientos de potencia del motor, manteniendo parámetros de eficiencia y reduciendo su impacto ambiental [19]. El enfoque de esta investigación consiste en determinar la duración de inyección; así como también la longitud y el ángulo del combustible atomizado, que permitan obtener una entrega de combustible totalmente equivalente entre biodiésel y diésel puro, para mantener la potencia del motor. El hecho de que la entrega de combustible dependa de la duración de la inyección, y no del diámetro de los orificios en las toberas del inyector, permite que el uso del biodiésel no requiera de cambios de diseño ni de construcción en el sistema de inyección, aparte de las modificaciones en los parámetros de control.

Propiedades del combustible			
Tipo de combustible	Diésel	Biodiésel	B20
Densidad @ 37.8°C [kg/m <sup>3</sup> ]	833.357	884.11	842.798
Viscosidad cinemática @ 37.8°C [mm <sup>2</sup> /s]	4.02	6.58	5.03
Viscosidad dinámica @ 37.8°C [cP]	3.35	5.817	4.239
Poder calorífico [MJ/kg]	42.7817	39.9254	42.5632
*Datos medidos experimentalmente a 15.55°C y calculados a 37.8°C con el método de Douglas Queiroz Santos, et. al, 2013 [10].			
**Datos medidos experimentalmente.			
***Datos calculados.			

Tabla I: Propiedades de diésel y del biodiésel

Datos de los motores analizados			
Tipo de motor <sup>*</sup>	8V 4000 M63	12V 4000 M63	16V 4000 M63
Potencia [kW] <sup>*</sup>	1000	1500	2000
Velocidad [rpm] <sup>*</sup>	1800	1800	1800
Número de cilindros <sup>*</sup>	8	12	16
Caudal de combustible [l/h] @ 42.8 MJ/kg de poder calorífico del combustible <sup>*</sup>	251.8	363.3	479.5
Presión de admisión turbo cargada [bar] <sup>**</sup>	1.2		
Relación de compresión <sup>**</sup>	16.5:1		
Presión de compresión [bar] <sup>***</sup>	61		
Temperatura de compresión [K] <sup>***</sup>	915		
*Datos tomados de <a href="http://www.mtu-online.com">http://www.mtu-online.com</a> [12,13, 14].			
**Datos estimados de referencia.			
***Datos calculados.			

Tabla II: Datos del motor para el cálculo de la inyección de combustible

Propiedades del comburente	Aire
Densidad @ 915K & 61bar [kg/m <sup>3</sup> ]	23.23
Viscosidad dinámica @ * 915K & 61bar [cP] <sup>**</sup>	0.039
<sup>*</sup> Dato calculado con la ecuación del gas ideal.	
<sup>**</sup> Dato tomado de Willi Bohl, Wolfgang Elmendorf. Technische Strömungslehre. 2014. [15].	

Tabla III: Propiedades del aire en las condiciones de la cámara de combustión del motor

## 2. MATERIALES Y MÉTODOS

### 2.1. MATERIAL Y EQUIPO UTILIZADO

El cálculo y simulación del sistema de inyección se basan en datos experimentales de caracterización de diésel y biodiésel puro; así como de una mezcla combustible de 20% biodiésel y 80% diésel (B20). Se toma como referencia, los datos de potencia, consumo de combustible y régimen de giro de motores diésel de aplicación marina, considerando que la duración de la inyección de combustible debe ser menor a los 25° de giro del cigüeñal para garantizar una tasa de combustión más alta [11].

La aplicación sostenible de los motores de combustión interna y del biodiésel como combustible alternativo, se concentra en aplicaciones en donde se genera o consume grandes cantidades de energía; por esta razón, para el cálculo y simulación, y con el fin de determinar los requerimientos del sistema de inyección con el uso de combustibles alternativos, se tomaron los datos de la especificación de tres motores de aplicación marina de la compañía MTU del tipo 8V, 12V y 16V de la serie 4000 M63 [12, 13, 14], como referencia para el cálculo de las características del rociado con los diferentes tipos de combustibles.

### 2.1.1. Formulación matemática

Para que un sistema de inyección de combustible sea apto para funcionar con fuentes alternativas como el biodiésel, deben tener el diámetro óptimo en los orificios de la tobera para que el combustible inyectado sea el necesario para alcanzar la potencia requerida por el motor. Se debe también considerar, que el combustible inyectado a través de la tobera debe mantener diferencias mínimas entre las variaciones de longitud y ángulo de atomizado; tanto para el diésel como para diferentes mezclas de biodiésel.

Mediante la ecuación de Bernoulli expresada en función de la presión (ecuación 1), se procede a deducir la ecuación que determina el diámetro de los orificios de las toberas, la misma que a su vez está en función de los requerimientos y características de funcionamiento del motor (ecuación 2).

$$\frac{1}{2} \cdot \rho \cdot c_1^2 + \rho \cdot g \cdot z_1 + p_1 = \frac{1}{2} \cdot \rho \cdot c_2^2 + \rho \cdot g \cdot z_2 + p_2 = cte. \quad (1)$$

Donde

$p_1, p_2$ : presión [MPa]  
 $\rho$ : densidad [ $\text{kg/m}^3$ ]  
 $c_1, c_2$ : velocidad del fluido [m/s]  
 $g$ : aceleración de la gravedad [ $\text{m/s}^2$ ]  
 $z_1, z_2$ : altura [m]

$$D = \sqrt{\frac{4 \cdot SFC \cdot \frac{Pot \cdot 360^\circ}{z \cdot t_{inj}} \cdot K}{n \cdot C_f \cdot \pi \cdot \sqrt{\frac{2 \cdot (p_{inj} - p_{comp})}{\rho}}}} \quad (2)$$

Donde

$D$ : Diámetro de los agujeros de la tobera [mm]  
 $SFC$ : Consumo específico de combustible [g/kWh]  
 $Pot$ : Potencia del motor [kW]  
 $z$ : Número de cilindros [-]  
 $t_{inj}$ : Duración de la inyección [° giro del cigüeñal]  
 $K$ : Factor de motor de 4 tiempos con valor 2. [-]  
 $n$ : Número de orificios de la tobera [-]  
 $C_f$ : Coeficiente de descarga de la tobera  
 $p_{inj}$ : Presión de inyección [MPa]  
 $p_{comp}$ : Presión de compresión del motor [MPa]

La longitud y el ángulo que alcanza la atomización del combustible [16], se calculan con las ecuaciones (3) y (4) respectivamente.

$$L_b = 15.8 \times \left(\frac{\rho_l}{\rho_a}\right)^{0.5} \cdot D_n \quad (3)$$

Donde

$L_b$ : Longitud del chorro de atomización [mm]  
 $\rho_l$ : Densidad del combustible a las condiciones de la inyección [ $\text{kg/m}^3$ ]  
 $\rho_a$ : Densidad del aire a la presión de compresión del motor [ $\text{kg/m}^3$ ]

$$\tan\left[\frac{\theta}{2}\right] = \left(\frac{1}{3 + \left[\frac{L_n}{3.6}\right]}\right) \cdot 4 \times \pi \times \left(\frac{\rho_l}{\rho_a}\right)^{0.5} \times \left(\frac{3^{0.5}}{6}\right) \quad (4)$$

Donde

$\theta$ : Ángulo del chorro de atomización [°]  
 $L_n$ : Longitud de los orificios de las toberas [mm]  
 $D_n$ : Diámetro de los orificios de las toberas [mm]  
 $\rho_l$ : Densidad del combustible a las condiciones de la inyección [ $\text{kg/m}^3$ ]  
 $\rho_a$ : Densidad del aire a la presión de compresión del motor [ $\text{kg/m}^3$ ]

### 2.2. PROCESO DE CÁLCULO

Para calcular las características de rociado de determinados combustibles y determinar su uso como una alternativa los unos de los otros, es necesario que todas sus propiedades sean medidas o corregidas a una misma temperatura. Ya que, al hacer el estudio de mezclas combustibles, se deben determinar por estudios específicos los diferentes coeficientes que permitan corregir las densidades y viscosidades a una temperatura determinada. Es recomendable tomar mediciones directas y reales, cercanas a los 40°C, que es la temperatura a la que tiene lugar la inyección de combustible en los motores diésel. En el presente estudio los valores de densidad medidos a 15.55°C se corrigieron al valor de temperatura de 37.8°C, que es a la que se midió la viscosidad, con la finalidad de que los valores de cálculo provengan de mediciones directas, y al mismo tiempo estén cercanas a los 40°C. Posteriormente se procede a calcular el diámetro requerido por las toberas del inyector; en función de la potencia del motor, las características de la inyección y las propiedades de cada tipo de combustible. Finalmente se procede a calcular la longitud y el ángulo de atomización de cada tipo de combustible para proceder a su comparación y de ser necesario, hacer las correcciones necesarias en el tiempo o en la presión de inyección. Para los cálculos se consideró una tobera con 5 orificios y con una longitud de cada orificio correspondiente de 3 a 6 veces el diámetro de los mismos [9].

La solución consiste en determinar la variación porcentual del combustible tipo biodiésel con respecto al diésel para que el combustible inyectado sea el necesario para cumplir con los requerimientos de potencia del motor y de atomización del sistema de inyección. Las variaciones que existan entre los tipos de combustibles estudiados, se pueden corregir, tanto con el tiempo, como con la presión de inyección. La metodología expuesta sirve para todo tipo de combustible alternativo al diésel, teniendo en cuenta que el objetivo es equiparar el funcionamiento y rendimiento en lo que se refiere a la potencia del motor y a las características de rociado del combustible. Es necesario exponer, que los efectos contaminantes resultantes de la combustión o los efectos en la durabilidad o estabilidad de los componentes del motor, necesitan de un estudio y metodología de evaluación propios.

### 3. RESULTADOS

Se encontró que sin hacer cambios en el motor ni en el sistema de inyección, y que para alcanzar la potencia requerida por el motor y para mantener en un rango adecuado las características de atomizado de combustible, tanto con diésel como con biodiésel puros; así como también mezclados, es necesario recortar la duración de la inyección en el caso del diésel y alargarla en el caso de las mezclas de biodiésel.

Datos de la tobera y características de la inyección			
Tipo de combustible	Diésel	Biodiésel	B20
Número de orificios	5		
Longitud de los orificios [mm]	2		
Coefficiente de descarga de la tobera	0.7		
Diámetro de los orificios de la tobera [mm]	0.44		
Presión nominal de inyección [bar]	1500		
Duración de la inyección en grados de giro del cigüeñal [°GC]	20	24	22
Consumo específico de combustible del motor 8V 4000 M63 @ 251.8 l/h [gr/kW-h] <sup>1</sup>	209.839	222.619	212.217
Consumo específico de combustible del motor 12V 4000 M63 @ 363.3 l/h [gr/kW-h] <sup>1</sup>	201.839	214.131	204.126
Consumo específico de combustible del motor 168V 4000 M63 @ 479.5 l/h [gr/kW-h] <sup>1</sup>	199.797	211.965	202.061

<sup>1</sup>Datos calculados en base al caudal de combustible especificado del motor con la densidad de cada combustible.

Tabla IV. Datos de la tobera y características de la inyección con diésel y biodiésel

Investigaciones anteriores demuestran que, con el uso de biodiésel, el aumento del consumo específico de combustible en relación al diésel aumentó en 12.9% [17], debido a que el biodiésel tiene un menor poder calorífico y una mayor densidad en una proporción de 18.5% más de masa y 13.5% menos de volumen [18]. A esto hay que añadir que, las diferencias porcentuales de los poderes caloríficos y el consumo de combustible entre el diésel y el biodiésel puro (ver Tabla I y IV), alcanzan el 7%; mientras que, en el caso de la mezcla combustible de 20% biodiésel y 80% diésel (B20), esta diferencia alcanza el 1%.

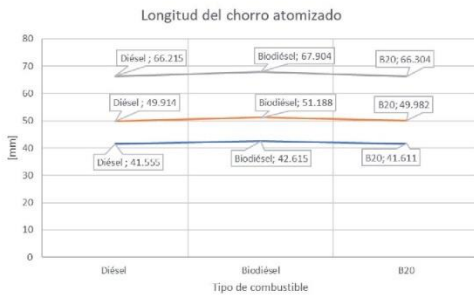


Fig. 1: Longitud del chorro de atomización calculado a 1500 bar

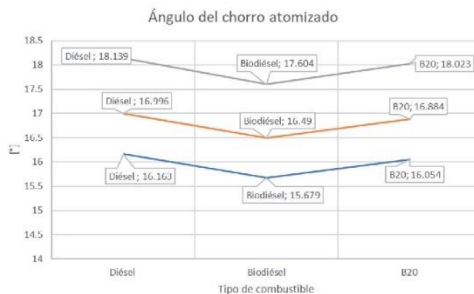


Fig. 2: Ángulo del chorro de atomización calculado a 1500 bar

Las ecuaciones descritas en la formulación matemática, fueron implementadas con el uso del software matemático Mathcad®, tanto para el cálculo de valores específicos, como para simular diferentes condiciones dentro del cálculo. La selección del software mencionado se debe a su versatilidad para desplegar resultados en función de un rango determinado de una variable. En este caso se calculó el diámetro de los orificios de las toberas, la longitud y el ángulo del chorro atomizado, en función de la presión de inyección. Para el cálculo, se consideró una presión nominal de inyección de 1500 bar.

Con la finalidad de mantener las mismas características de la inyección, en lo referente a la longitud y al ángulo del chorro atomizado de combustible, y haciendo uso de la misma geometría de la tobera del inyector con el uso de diferentes combustibles; es necesario corregir la duración de la inyección entre 2 y 4° de giro del cigüeñal.

Para mantener la misma longitud del chorro de combustible es necesario corregir la presión de inyección entre 150 y 200 bar; y para mantener los mismos ángulos de atomización con los combustibles analizados y dependiendo de la potencia del motor, las correcciones en la presión de inyección se encuentran en el rango de 500 a 800 bar (ver Tabla V).

#### 4. DISCUSIÓN

De los resultados obtenidos se observa que es posible alcanzar los requerimientos de potencia del motor usando diésel o biodiésel como combustibles, sin la necesidad de hacer cambios en los componentes del motor o del sistema de inyección, pero sí en los parámetros de control, como son el tiempo y la presión de inyección.

Manteniendo la presión y reduciendo la duración del tiempo de inyección del diésel en 4° de giro del cigüeñal en comparación con el biodiésel puro, y en 2° en comparación con la mezcla del 20% de biodiésel y 80% de diésel (B20); se logra además, que las características de atomización del combustible se mantengan con diferencias del 3% para la longitud y el ángulo de atomización con el uso del biodiésel puro; mientras que, las diferencias con el uso de la mezcla combustible B20 son del 1%.

Para reducir las variaciones porcentuales de la longitud y el ángulo del chorro atomizado, que alcanzan máximo el 3%; es necesario hacer correcciones relativamente grandes en la presión de inyección, que llegan alcanzar hasta un 37.5%. Ya que, conforme aumenta la presión del sistema, el ángulo del chorro de atomización tiende a disminuir, en el caso del biodiésel en estado puro es necesario reducir la presión de inyección hasta 900 bar, para tener el mismo ángulo del chorro atomizado con diésel inyectado a 1700 bar.

El uso del biodiésel como un combustible alternativo y como una solución ecológica, debe tener la flexibilidad de ser usado en los motores y con los sistemas de inyección actuales. Diferencias entre el 1 y 3% en las características de atomización de la inyección hacen que, con la configuración correcta de la duración del tiempo de inyección de acuerdo a las características del motor, el biodiésel puro o mezclado, pueda ser usado como un absoluto sustituto del diésel en lo que respecta al mantener los requerimientos de potencia y características de atomización.



Características de la inyección en función de la presión de inyección				
Tipo de combustible		Diésel	Biodiésel	B20
Duración de la inyección en grados de giro del cigüeñal [°GC]				
		20	24	22
Motor 8V 4000 M63	Longitud del chorro atomizado [mm]	41.555	41.571	41.611
	Presión de inyección corregida [bar]	1500	1650	1500
	Ángulo del chorro atomizado [°]	16.163	16.159	16.054
	Presión de inyección corregida [bar]	1500	1000	1500
Motor 12V 4000 M63	Longitud del chorro atomizado [mm]	49.914	49.549	49.982
	Presión de inyección corregida [bar]	1500	1700	1500
	Ángulo del chorro atomizado [°]	17.073	17.043	17.002
	Presión de inyección corregida [bar]	1400	900	1350
Motor 16V 4000 M63	Longitud del chorro atomizado [mm]	66.215	66.241	66.304
	Presión de inyección corregida [bar]	1500	1650	1500
	Ángulo del chorro atomizado [°]	18.019	18.075	18.09
	Presión de inyección corregida [bar]	1700	900	1400

Datos calculados en base al caudal de combustible especificado del motor con la densidad de cada combustible  
Tabla V: Datos de las características de inyección en función de la presión de inyección para cada tipo de combustible para una geometría definida de la tobera del inyector

### 5. CONCLUSIONES

En el presente trabajo se ha presentado una metodología teórica de cálculo con datos experimentales para evaluar las características del sistema de inyección de combustible con el uso de diésel y de biodiésel.

Se ha evidenciado que por medio del control de la duración de la inyección de combustible es posible mantener las características de atomización y el rendimiento del motor con combustibles alternativos.

La densidad del combustible está estrechamente relacionada con la cantidad de su volumen inyectado; mientras que, la viscosidad determina su calidad de atomización. Al mismo tiempo, la cantidad de combustible inyectado depende también del poder calorífico; ya que, en función de esta propiedad, se debe inyectar más o menos cantidad del mismo.

La calidad y las características de atomización del combustible no solo dependen de la tobera del inyector, sino también de las condiciones en la cámara de combustión bajo las cuales el combustible es inyectado. Las variaciones de la densidad y viscosidad del aire son altas, cuando se comparan sus valores en condiciones normales (1 atm – 293K) y en las condiciones a la que se encuentra en el interior de la cámara de combustión al final del ciclo de compresión e inicio de la inyección; en el caso del presente estudio, a 61bar y 915 K.

Los valores de la densidad y viscosidad varían drásticamente con la temperatura; del mismo modo las características de la inyección como la longitud y el ángulo del chorro atomizado de combustible, dependen de la temperatura del combustible y pueden ser controlados mediante el tiempo y la presión de inyección.

El diésel y la mezcla combustible de 20% de biodiésel y 80% diésel, son prácticamente compatibles, requiriendo únicamente cambios en la duración de la inyección de combustible, mientras que el uso de biodiésel puro necesita cambios considerables en los valores de presión de inyección desde 500 hasta 800 bar, dependiendo de la potencia del motor, además de los cambios en la duración de la inyección.

La metodología propuesta ha demostrado ser adecuada para definir los parámetros de control de inyección de diferentes tipos de combustibles, con el fin de que su uso produzca el mismo

rendimiento del motor y variaciones mínimas en los parámetros que determinan la calidad de la inyección.

### BIBLIOGRAFÍA

[1] Vidal-Benavides, A. I., Quintero-Díaz, J. C., and Herrera-Orozco, I., Análisis de ciclo de vida de la producción de biodiésel a partir de aceite vegetal usado. DYNA 84(201), pp. 155-162, 2017. (doi: <http://dx.doi.org/10.15446/dyna.v84n201.54469>)

[2] Jinlin Xue, Tony E. Grift a, Alan C. Hansena. "Effect of biodiesel on engine performances and emissions". Renewable and Sustainable Energy Reviews 15 (2011) 1088-1116. (doi: <http://dx.doi.org/10.1016/j.rser.2010.11.016>)

[3] Bai-Fu Lin, Jun-Han Huang, Dao-Yi Huang. "Experimental study of the effects of vegetable oil methyl ester on DI diesel engine performance characteristics and pollutant emissions" Fuel 88 (2009) 1779-1785. (doi: <http://dx.doi.org/10.1016/j.fuel.2009.04.006>)

[4] Hüseyin Aydın, Hasan Bayındır. "Performance and emission analysis of cottonseed oil methyl ester in a diesel engine". Renewable Energy 35 (2010) 588-592. (doi: <http://dx.doi.org/10.1016/j.renene.2009.08.009>)

[5] Magin Lapuerta, José M. Herreros, Lisbeth L. Lyons, Reyes García-Contreras, Yolanda Briceño. "Effect of the alcohol type used in the production of waste cooking oil biodiesel on diesel performance and emissions". Fuel 87 (2008) 3161-3169. (doi: <http://dx.doi.org/10.1016/j.fuel.2008.05.013>)

[6] D.H. Qi, L.M. Geng, H. Chen, Y.Z.H. Bian, J. Liu, X.C.H. Ren. "Combustion and performance evaluation of a diesel engine fueled with biodiesel produced from soybean crude oil". Renewable Energy 34 (2009) 2706-2713. (doi: <http://dx.doi.org/10.1016/j.renene.2009.05.004>)

[7] C. Carraretto, A. Macor, A. Mirandola, A. Stoppato, S. Tonon. "Biodiesel as alternative fuel: Experimental analysis and energetic evaluations". Energy 29 (2004) 2195-2211. (doi: <http://dx.doi.org/10.1016/j.energy.2004.03.042>)

[8] N.R. Banapurmath, P. C.Tewari, and R.S. Hosmath. "Effect of biodiesel derived from Honge oil and its blends with diesel when directly injected at different injection pressures and injection timings in single-cylinder water-cooled compression ignition engine". Proc. IMechE Vol. 223 Part A: J. Power and Energy, 2009. (doi: <http://dx.doi.org/10.1243/09576509JPE673>)

[9] Hiroyasu, H., Arai, M., and Tabata, M. "Empirical Equations for the Sauter Mean Diameter of a Diesel Spray," SAE Technical Paper 890464, 1989. (doi: <http://dx.doi.org/10.4271/890464>)

[10] Douglas Queiroz Santos, Ana Lúcia de Lima, Ana Paula de Lima, Waldomiro Borges Neto, José Domingos Fabris. "Thermal expansion coefficient and algebraic models to correct values of specific mass as a function of temperature for corn biodiesel". Fuel 106 (2013) 646-650. 2013. (doi: <http://dx.doi.org/10.1016/j.fuel.2012.10.048>)

[11] Günter P. Merker, Christian Schwarz, Rüdiger Teichmann. Grundlagen Verbrennungsmotoren. 6ta. Ed. Berlin Vieweg+Teubner Verlag, Springer Fachmedien Wiesbaden GmbH, 2012. ISBN 978-3-8349-1987-1

[12] MTU Friedrichshafen GmbH. "Engine Program / Diesel engines for work boats / 8V 4000 M63" [en línea], [citado 05.11.2017]. Disponible en Internet: [http://www.mtu-online.com/mtu/products/engine-program/diesel-engines-for-marine-main-propulsion-dieselelectric-drives-and-ona-board-power-generation/diesel-engines-for-work-boats/detail/7bx\\_mcgshop\\_shop%5Bengine%5D=4376tx\\_mcgshop\\_shop%5Baction%5D=show6tx\\_mcgshop\\_shop%5Bcontroller%5D=Shop6txHash=51726abb958789f9a929f676ae7a5](http://www.mtu-online.com/mtu/products/engine-program/diesel-engines-for-marine-main-propulsion-dieselelectric-drives-and-ona-board-power-generation/diesel-engines-for-work-boats/detail/7bx_mcgshop_shop%5Bengine%5D=4376tx_mcgshop_shop%5Baction%5D=show6tx_mcgshop_shop%5Bcontroller%5D=Shop6txHash=51726abb958789f9a929f676ae7a5)

[13] MTU Friedrichshafen GmbH. "Engine Program / Diesel engines for work boats / 12V 4000 M63" [en línea], [citado 05.11.2017]. Disponible en Internet: [http://www.mtu-online.com/mtu/products/engine-program/diesel-engines-for-marine-main-propulsion-dieselelectric-drives-and-ona-board-power-generation/diesel-engines-for-work-boats/detail/7bx\\_mcgshop\\_shop%5Bengine%5D=4446tx\\_mcgshop\\_shop%5Baction%5D=show6tx\\_mcgshop\\_shop%5Bcontroller%5D=Shop6txHash=6572550c3197e9894505971e98d8](http://www.mtu-online.com/mtu/products/engine-program/diesel-engines-for-marine-main-propulsion-dieselelectric-drives-and-ona-board-power-generation/diesel-engines-for-work-boats/detail/7bx_mcgshop_shop%5Bengine%5D=4446tx_mcgshop_shop%5Baction%5D=show6tx_mcgshop_shop%5Bcontroller%5D=Shop6txHash=6572550c3197e9894505971e98d8)

[14] MTU Friedrichshafen GmbH. "Engine Program / Diesel engines for work boats / 16V 4000 M63" [en línea], [citado 05.11.2017]. Disponible en Internet: [http://www.mtu-online.com/mtu/products/engine-program/diesel-engines-for-marine-main-propulsion-dieselelectric-drives-and-ona-board-power-generation/diesel-engines-for-work-boats/detail/7bx\\_mcgshop\\_shop%5Bengine%5D=4446tx\\_mcgshop\\_shop%5Baction%5D=show6tx\\_mcgshop\\_shop%5Bcontroller%5D=Shop6txHash=6572550c3197e9894505971e98d8](http://www.mtu-online.com/mtu/products/engine-program/diesel-engines-for-marine-main-propulsion-dieselelectric-drives-and-ona-board-power-generation/diesel-engines-for-work-boats/detail/7bx_mcgshop_shop%5Bengine%5D=4446tx_mcgshop_shop%5Baction%5D=show6tx_mcgshop_shop%5Bcontroller%5D=Shop6txHash=6572550c3197e9894505971e98d8)

[15] Willi Bohl, Wolfgang Elmendorf. Technische Strömungslehre. 15. Ed. Würzburg. Vogel Business Media GmbH, 2014. ISBN 978-3-8343-329-2

[16] Subhash Lahane, K.A. Subramanian. "Effect of different percentages of biodiesel-diesel blends on injection, spray, combustion, performance, and emission characteristics of a diesel engine". Fuel 139 (2015) 537-545. (doi: <http://dx.doi.org/10.1016/j.fuel.2014.09.036>)

[17] Octavio Armas, Kuen Yehliu, André L. Boehman. "Effect of alternative fuels on exhaust emissions during diesel engine operation with matched combustion phasing". Fuel 89 (2010) 438-456. (doi: <http://dx.doi.org/10.1016/j.fuel.2009.09.022>)

[18] J.M. Luján, V. Bermúdez, B. Tormos, B. Pla. "Comparative analysis of a DI diesel engine fuelled with biodiesel blends during the European IMVEG-A cycle: Performance and emissions (II)" BIOMASS AND BIOENERGY 33 (2009) 948-956. (doi: <http://dx.doi.org/10.1016/j.biombioe.2009.02.003>)

[19] Reyes-Leon, A., Quintero-Díaz, P., Sanchez-Silva, F., Barbosa-Saladaña, J. (2016). ANALYSIS OF THE FUEL INFLUENCE IN ENERGY, EXERGY AND ECOLOGICAL EFFICIENCIES OF A POWER PLANT. DYNA Energía y Sostenibilidad, 5(1), 111 p. (doi: <http://dx.doi.org/http://dx.doi.org/10.6036/ES7993>)

### AGRADECIMIENTOS

Se agradece y se reconoce la contribución de Svyatoslav Cheranov, del Moscow Polytech en Moscú - Rusia, por su valioso aporte en este trabajo.

**SAE** *The Engineering Society  
For Advancing Mobility  
Land Sea Air and Space*® 400 COMMONWEALTH DRIVE, WARRENDALE, PA 15096-0001 U.S.A.

---

# SAE Technical Paper Series

890464

## Empirical Equations for the Sauter Mean Diameter of a Diesel Spray

**Hiroyuki Hiroyasu and Masataka Arai**  
University of Hiroshima

**Michihiko Tabata**  
Mazda Motor Corp.

Reprinted from SP-774 —  
Diesel Combustion and Emissions — Part V

International Congress and Exposition  
Detroit, Michigan  
February 27 — March 3, 1989



The papers included in this volume  
are abstracted and indexed in the  
SAE Global Mobility Database.

No part of this publication may be reproduced in any form, in an electronic retrieval system or otherwise, without the prior written permission of the publisher.

ISSN 0148-7191  
Copyright 1989 Society of Automotive Engineers, Inc.

Positions and opinions advanced in this paper are those of the author(s) and not necessarily those of SAE. The author is solely responsible for the content of the paper. A process is available by which discussions will be printed with the paper if it is published in SAE Transactions. For permission to publish this paper in full or in part, contact the SAE Publications Division.

Persons wishing to submit papers to be considered for presentation or publication through SAE should send the manuscript or a 300 word abstract of a proposed manuscript to: Secretary, Engineering Activity Board, SAE.

Printed in U.S.A.

890464

## Empirical Equations for the Sauter Mean Diameter of a Diesel Spray

Hiroyuki Hiroyasu and Masataka Arai  
University of Hiroshima

Michihiko Tabata  
Mazda Motor Corp.

### ABSTRACT

New empirical equations to represent the Sauter mean diameter of a spray injected by a diesel nozzle are presented in this paper. In order to determine the new equations, drop sizes of a diesel spray were analyzed by a laser diffraction technique. Liquids with different viscosities and different surface tensions were tested to obtain the generalized empirical equations. The maximum injection and maximum ambient pressures were 90 MPa and 3.0 MPa respectively. Both the minimum value of the injection pressure to produce a fine spray and the Sauter mean diameter increase the greater the viscosity and the surface tension of the liquid. At a high injection velocity, the Sauter mean diameter increases with an increase in ambient pressure, but it decreases when ambient pressure is increased at a low injection velocity. According to the effect of injection velocity and ambient pressure on break-up length and the drop size of the spray, spray formation mechanisms can be divided into two categories, the function of the injection velocity and the physical properties of the liquid. Finally, dimensionless analysis of each category leads to the general empirical equations for the Sauter mean diameter.

THE AIM OF FUEL INJECTION in a diesel engine is to atomize liquid fuel into a multitude of drops or a spray and to supply it to high pressure, high temperature air that is compressed by a piston to start a self-ignition of the fuel spray. The fuel injection process plays a primary part in the formation of a combustible mixture that controls the overall combustion process in a diesel engine. Therefore, in our efforts to improve diesel engines, a more

\*Numbers in parentheses designate references at end of paper.

accurate knowledge of this atomization process and the characteristics of the diesel spray itself are needed. Therefore, a study of spray injected by a diesel nozzle has been performed by many engine researchers as a basic study of diesel combustion.

The measurements of drop size in diesel spray were first carried out by Woltjen (1)<sup>\*</sup> and Sass (2). Sass obtained the drop size distribution for three different nozzle hole diameters under an air pressure of 1.1 MPa. He showed that the mean diameter increased linearly with the nozzle hole diameter, and increased with an increase of air pressure.

The drop size distribution in fuel spray was also given by Mehleg (3) for a spray under an air pressure of 0.27 MPa. Other works dealing with spray under atmospheric pressure have been conducted by Tanasawa and Hiroyasu (4,5). They showed the effects of parameters which included fuel viscosity, type of nozzle, rack position and speed of the fuel pump.

Tanasawa and Toyoda's studies show the effects of injection velocity and liquid properties on drop size in a diesel spray at atmospheric pressure under a wide range of injection conditions, leading to an experimental equation for the mean drop size (6).

The size distribution of fuel drops injected by a diesel nozzle into a high pressure environment has also been studied by Hiroyasu and Kadota (7). They reported the experimental equations related to the Sauter mean diameter and operating parameters of an injection pump. The transient characteristics of the drop size distribution in an injection period had been researched by Hiroyasu et al. (8).

Numerous atomization studies have generally been made on a liquid like the low viscosity fuel that is currently used in diesel engines. As a result, correlations relating drop size distribution to fuel properties and injection conditions have been obtained as mentioned above. Such correlations, however, have not been obtained for high speed diesel sprays and for the

highly viscous residual oil that is now of growing interest to marine users of diesel engines. In other words, because of the difficulty in taking measurements of a high speed spray which is fully developed at high ambient pressures and which corresponds to a diesel spray, many points have not yet been clarified regarding the break-up mechanism and the disintegration process of a diesel spray. Consequently, fundamental information on the atomization of a high speed spray is insufficient when considering the effects of liquid kinematic viscosity and surface tension on the mean drop size of a diesel spray at high ambient pressure and on the changes in the mean drop size in relation to changes in ambient pressure.

The main contents of this report are concerned with determining general equations for a diesel spray injected under various conditions. The main purpose of this experimental work is to investigate the effects of viscosity and the surface tension of fuel, the effect of nozzle diameter and injection pressure at various ambient pressures on the mean drop size, and the drop size distribution, in order to get the data base for the new equations. Several kinds of liquids, for example, residual oils and glycerine water solutions, etc., were prepared to widely change the physical properties of the liquids.

Measurements of the drop size were carried out over a wide range of injection pressures (3 to 90 MPa), nozzle diameters (0.2, 0.3 and 0.4 mm), kinematic viscosities of liquid ( $1 \times 10^{-6}$  to  $200 \times 10^{-6}$  m<sup>2</sup>/s), and surface tensions ( $30 \times 10^{-3}$  to  $75 \times 10^{-3}$  N/m) under the various ambient pressures (0.1 to 3.0 MPa).

EXPERIMENTAL APPARATUS

A schematic diagram of the experimental apparatus is given in Fig. 1. This apparatus consisted of a pressure vessel, a liquid injection system, an injection nozzle and measuring equipment for the drop size distribution of a diesel spray.

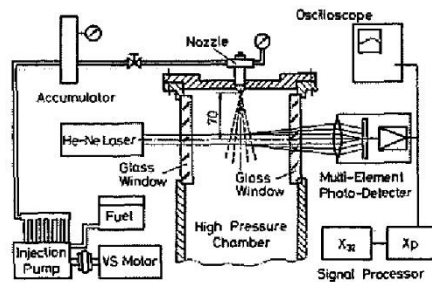


Fig.1 - Experimental apparatus

Most of the data reported here was obtained at an ambient pressure of 3.0 MPa and at room temperature. For this purpose, diesel nozzles of single-hole type with nozzle diameter of 0.2, 0.3 and 0.4 mm were tested in a large cylindrical pressure vessel. In order to provide optical access for drop size measurement, transparent windows were fitted on diametrically opposite sides of the vessel.

The liquid was continuously injected from the nozzle into the vessel by an injection system. This system was designed for an injection pressure from 0.1 MPa to 90 MPa. It consisted of an injection pump and a pressure accumulator for reducing the pressure pulsation. The injection pressure was here represented by the absolute pressure in the injection nozzle.

The drop size was measured using an optical technique that is based on Fraunhofer diffraction. This technique, reported by Swithenbank (9) and Felton (10), has been developed for the on-line measurement of drop size distribution.

The monochromatic and coherent light of the He-Ne gas laser beam illuminated the spray. The diffracted light from a spray, thus giving information on the drop size distribution, was gathered by using a Fourier transform lens and was detected by a multi-photodetector. The detected signal was analyzed by the program developed by Gomi (11). This program can calculate the most suitable chi-square volumetric distribution function (Nukiyama-Tanasawa eq.). In this work, the Sauter mean diameter  $X_{32}$  was printed out as the final output of the data processing (12).

The sampling location and volume illuminated by the laser beam are shown in Fig. 2. The laser beam of 6 mm dia. passed through the spray major axis at a right angle.

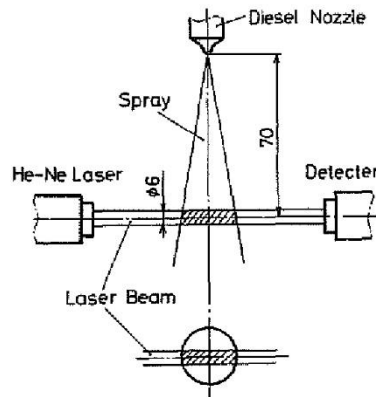


Fig.2 - Measuring location and sampling volume

The Sauter mean diameter measured by this optical system represented the average value in the cylindrical sampling volume. However, it also contains the weighted spatial value of the Sauter mean diameter of the spray. The distance Lh that shows the distance between the sampling location and the nozzle fixed at 70mm, because the multi-diffracted light from the extremely highly dense spray caused the wrong SHD data for the representative value to be produced.

**PHYSICAL PROPERTIES OF USED LIQUIDS** - In order to separate the effects of fuel viscosity on the Sauter mean diameter from the effects of the surface tension, three types of liquid groups with different surface tensions were prepared.

These groups were heavy oils, glycerine-water solutions and glycerine-alcohol-water solutions. Each group of liquids has almost the same surface tension value, but shows marked differences in kinematic viscosity. Table 1 shows both the types and the range of properties of liquids used in this study. The physical properties of heavy oil and glycerine-water solution at a temperature of 285 K are shown in Figs.3 and 4.

Table 1 - Kinematic viscosity and surface tension for the test liquids

	Kinematic Viscosity (m <sup>2</sup> /s)	Surface Tension (N/m)
Heavy Oil	8.0 x 10 <sup>-6</sup> - 209.4 x 10 <sup>-6</sup>	31.5 x 10 <sup>-3</sup> - 33.5 x 10 <sup>-3</sup>
Glycerine Solution + Alcohol	26.4 x 10 <sup>-6</sup> - 63.7 x 10 <sup>-6</sup>	51.5 x 10 <sup>-3</sup> - 53.5 x 10 <sup>-3</sup>
Glycerine Solution	0.7 x 10 <sup>-6</sup> - 61.1 x 10 <sup>-6</sup>	72.5 x 10 <sup>-3</sup> - 65.5 x 10 <sup>-3</sup>

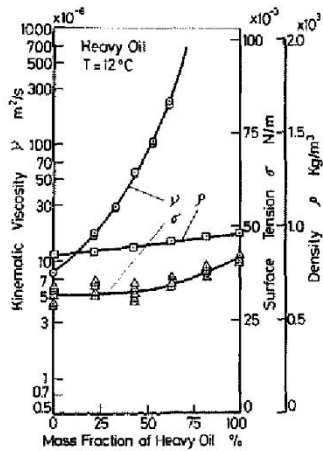


Fig.3 - Physical properties of heavy oil

Comparing the heavy oil with the glycerine-water solution, at the same kinematic viscosity, we can see that the heavy oil has about half the surface tension value of the glycerine-water solution. Therefore, the effects of surface tension can be analyzed separately from the effects of kinematic viscosity by measuring the respective Sauter mean diameters for the liquids of the same kinematic viscosity.

**EXPERIMENTAL RESULTS**

**EFFECT OF KINEMATIC VISCOSITY** - It is commonly considered that it is high viscosity in an injected liquid which causes an increase in Sauter mean diameter. But there are few measured results to this effect under high ambient pressure. Figure 5 shows the effect of the kinematic viscosity of heavy oil on the Sauter mean diameter.

The relative velocity between the injected jet and the ambient air decreases with the decrease in injection pressure. As the relative velocity decreases, generally, the injected liquid does not come to be as well atomized as a fine spray. The Sauter mean diameter gradually increases by decreasing the injection pressure from 90 MPa. However, when it decreases below a certain critical value, ( that can cause fine drops to be produced and is called the low pressure limit for a fine spray in this report ), the Sauter mean diameter shows a rapid increase. Both the Sauter mean diameter and the low pressure limit for a fine spray increase with an increase in fuel viscosity.

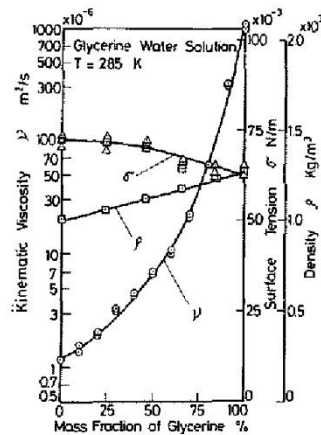


Fig.4 - Physical properties of glycerine-water solution

Even if the injection pressure is higher than 80 MPa, the effect of fuel viscosity on the Sauter mean diameter still holds to some extent. This occurs because the viscosity has a direct effect upon the final atomization process by which drops are formed, and this final process directly affects the Sauter mean diameter.

The effect of the kinematic viscosity of the glycerine-water solution on the Sauter mean diameter was also measured under the same injection conditions as shown in Fig.5. The summarized results are shown in Fig.6. The Sauter mean diameter and the low pressure limit for a fine spray also increase with an increase in the viscosity of the liquid.

Both Figures 5 and 6 show the same increase tendency in Sauter mean diameter when the kinematic viscosity of the liquids is increased. However, the low pressure limit for a fine spray is lower in the heavy oil than in the glycerine-water solution. This is a result of the surface tension of heavy oil being half that of the glycerine-water solution at the same kinematic viscosity, as shown in Fig. 3 and Fig. 4. Therefore, it must be considered that the effect of surface tension on the Sauter mean diameter can not be neglected where these fuels are concerned.

Figure 7 shows the effects of kinematic viscosity and nozzle diameter on the Sauter mean diameter when the glycerine-water solution was injected at an injection pressure of 11 MPa under an ambient pressure of 3 MPa. The Sauter mean diameter increases with an increase in kinematic viscosity at each nozzle diameter. The Sauter mean diameter increases rapidly when the kinematic viscosity rises above a certain value. It also increases with a decrease in nozzle diameter. It is apparent from this figure that the larger the diameter of the nozzle, the larger the Sauter mean diameter becomes and that this tendency becomes more remarkable with increased kinematic viscosity.

**EFFECT OF SURFACE TENSION** - The three liquid groups, that is, the heavy oils, the glycerine-water solutions and the glycerine-alcohol-water solutions, with different surface tension values but with the same value of kinematic viscosity, were used to study the pure effects of surface tension. Figure 8 shows an effect of surface tension on the Sauter mean diameter at a kinematic viscosity of  $\nu = 49 \times 10^{-6} \text{ m}^2/\text{s}$ . The Sauter mean diameter decreases with an increase in injection pressure for each of the three liquids. For the same injection pressure, the Sauter mean diameter increases with an increase in surface tension. When the injection pressure is relatively low, the effect of surface tension on the Sauter mean diameter is great. However under higher injection pressure conditions, the surface tension has a smaller effect on the Sauter mean diameter. There is also a low pressure limit for a fine spray. This limit increases with an increase in surface tension.

Further, the Sauter mean diameter was also measured for another value of kinematic viscosity

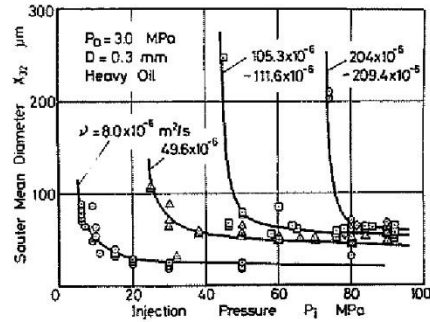


Fig.5 - Effect of kinematic viscosity on the Sauter mean diameter (heavy oil)

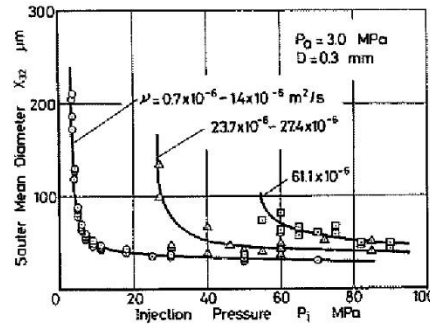


Fig.6 - Effect of kinematic viscosity on the Sauter mean diameter (glycerine-water solution)

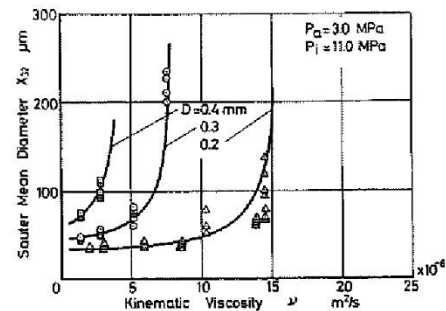


Fig.7 - Effect of kinematic viscosity and nozzle hole diameter on the Sauter mean diameter

in much the same way. It became clear that surface tension had a small effect on the Sauter mean diameter under high injection velocity conditions. This is because when the injection velocity, through a high injection pressure, is high enough to produce fine drops, the relative velocity between the jet and the ambient air controls to a great extent the liquid atomization. However, under a low injection pressure, that is, when the injection velocity is not so high, the surface tension has a stronger effect on the Sauter mean diameter than under a high injection pressure.

**EFFECT OF AMBIENT PRESSURE** - The ambient pressure was varied from 0.1 MPa to 3.0 MPa in order to study its effects on the Sauter mean diameter. Figure 9 summarizes for a study of the effect of ambient pressure on the relationship between effective injection pressure and the Sauter mean diameter in the case of a liquid viscosity of  $\nu = 1 \times 10^{-6} \text{ m}^2/\text{s}$ . The effective injection pressure is represented by a differential pressure between the injection and ambient pressures. Under a low effective injection pressure, an increase in ambient pressure causes a significant decrease of the Sauter mean diameter. However, on the contrary, under a high effective injection pressure, the Sauter mean diameter increases with an increase in ambient pressure.

To summarize both results, an increase in ambient pressure has a positive effect on the atomizing process at a low effective injection pressure but has a negative effect at a high one. There is a critical effective injection pressure where the effect of the ambient pressure on the Sauter mean diameter changes from positive to negative.

From these results, it can be considered that the effect of ambient pressure on the Sauter mean diameter reverses when effective injection pressure rises above a certain value and that an increase in ambient pressure promotes liquid

atomization under low injection velocity, while, under high injection velocity, an increase in the ambient pressure impedes liquid atomization. In other words, the liquid break-up mechanism and its process at high injection velocity can be considered to be different from those at low injection velocity.

**CORRELATION OF DATA**

To provide the general correlation of the descriptions obtained from Fig.5 to 9 concerning the different physical properties of liquid and various injection conditions, fundamental consideration based on dimensional analysis shown in the following equations is introduced

$$X_{32} = f(D, V_i, \nu, \rho, \rho_a, \rho_l, \sigma) \quad (1)$$

where, D is the diameter of the nozzle,  $V_i$  is the injection velocity calculated by volumetric flow rate,  $\nu$  is the kinematic viscosity,  $\rho$  is the density and  $\sigma$  is the surface tension on the liquid surface. Further, subscript a and l represent the ambient gas and injected liquid as shown in the previous sections. According to the dimensional analysis, eq.(1) is modified to

$$\frac{X_{32}}{D} = C_1 Re^{-n_1} We^{-n_2} \left(\frac{\nu_l}{\nu_a}\right)^{n_3} \left(\frac{\rho_l}{\rho_a}\right)^{n_4} \quad (2)$$

Where, the Reynolds number, Re, is expressed by

$$Re = \frac{V_i D}{\nu_l} \quad (3)$$

and Weber number, We, is written by

$$We = \frac{V_i^2 D \rho_l}{\sigma} \quad (4)$$

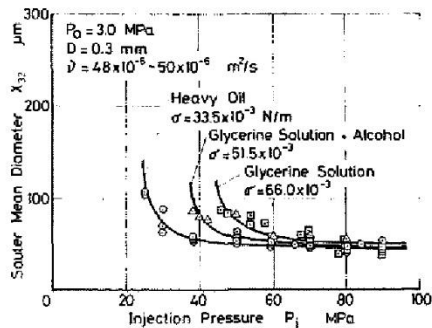


Fig.8 - Effect of surface tension on the Sauter mean diameter

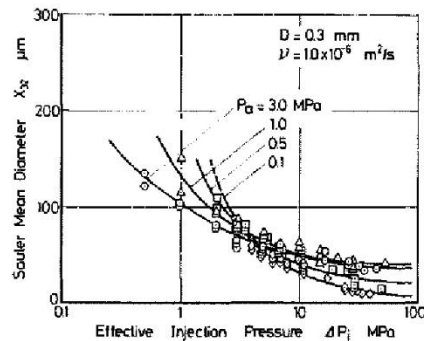


Fig.9 - Effect of ambient pressure on the Sauter mean diameter



Equation (2) means that the Sauter mean diameter for all of the different conditions can be expressed by using five dimensionless numbers and five empirical parameters. However, eq.(2) does not mean that the mean diameter can be expressed by a unique set of these parameters. For example, the Tanasawa's expression of the Sauter mean diameter for a diesel spray was well known by the following equation (the equation was rewritten in SI Unit).

$$X_{32} = 47 \times 10^{-3} \left( \frac{D}{V_i} \right) \left( \frac{\sigma}{\rho_l} \right)^{0.25} g^{0.2} \left( 1.331 \times 10^{15} \frac{\mu}{10^6 \rho_l D} \right) \quad (5)$$

where,  $g$  is the gravitational acceleration and  $\mu$  is the viscosity of the liquid. Figures 10 and 11 are comparisons between values predicted by eq.(5) and our experimental data. The discrepancy in the Sauter mean diameters between predicted and measured values ( shown in Fig.10 )

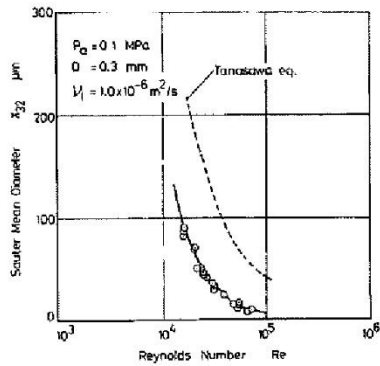


Fig.10 - Comparison between predicted and measured Sauter mean diameters under atmospheric condition

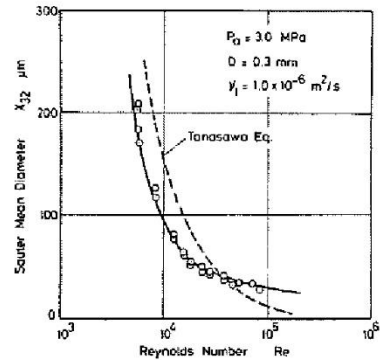


Fig.11 - Comparison between predicted and measured Sauter mean diameters under high pressure (3.0 MPa)

mainly comes from the difference in the methods for measuring velocity and drop size, because the inclines of both curves are essentially the same. However, the discrepancy, which is shown in Fig.11, shows that the Sauter mean diameter of the spray injected into high ambient pressure suggests another aspect of this difference. The predicted mean diameter in a high  $Re$  number region is much smaller than the measured value. This is because the eq.(5) was obtained from experimental data taken under atmospheric pressure conditions. Then this equation can not explain a pressure effect on the Sauter mean diameter. In other words, Tanasawa's equation can not express the positive and negative effects of the ambient pressure on the Sauter mean diameter. This fact suggests that two sets of empirical parameters in eq.(2) are needed to express the Sauter mean diameter of a spray injected in a different pressure environment.

To obtain a new parameter that was not taken into account by Tanasawa's equation, further observation of the spray were made under high pressure conditions. Figure 12 shows the change in atomization quality and Sauter mean diameter in a relation to the Reynolds number. Observations were conducted on glycerine-water solution at an ambient pressure of 3 MPa for two levels of kinematic viscosity.

Irrespective of kinematic viscosity, as injection velocity increases, the atomization state shifts from (A) to (B) and (B) to (C) as shown in the photographs in Fig.12. The spray

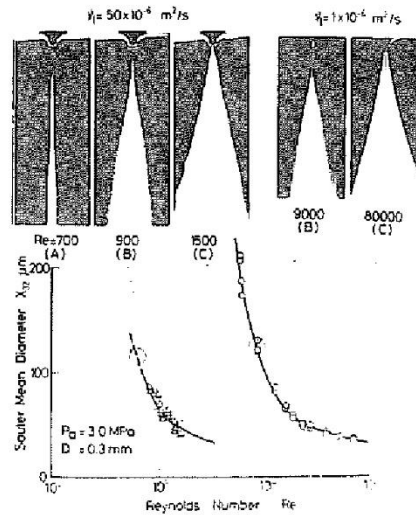


Fig.12 - Relation between spray formation processes and the Sauter mean diameter

cannot be formed in (A) due to insufficient atomization caused by low injection velocity. As injection velocity increases, the atomization state shifts to (B) where a smooth liquid jet is ejected from the exit of the nozzle hole to subsequently form a spray through a relatively slow disintegration process. In other words, the process of transformation from liquid column to drops might be developed along the liquid jet and fine drops were only made at a distance from the nozzle exit. The atomization state shown in (B) is hereinafter referred to as an incomplete spray. As injection velocity increases further, the smooth liquid column is shortened gradually to form a fully-atomized spray. In the atomization state (C), a disintegration process from jet to fine spray appeared as soon as the liquid was injected. This atomization status is hereinafter referred to as a complete spray. From the results observed above, it is considered that the spray may be classified into two categories according to the difference in the spray photography.

Corresponding to the shift from an incomplete to a complete spray, the decreasing ratio of the Sauter mean diameter in relation to injection velocity changes. Therefore, the Sauter mean diameter, as a function of the injection velocity or the Reynolds number, can be represented by two curves, each of which corresponds to one spray category. Figure 12 also shows that the shift point from incomplete to complete spray differs according to the difference in kinematic viscosity and that the shift occurs at a lower Reynolds number for higher than for lower kinematic viscosity.

Other evidence of the change in the spray formation mechanisms can be observed in the experimental data on break-up length obtained by the authors (13). The typical break-up of the

high speed jet injected into various pressure environments is shown in Fig. 13. In the wavy atomization region that is shown in  $2 \times 10^3 < Re < 2 \times 10^4$ , the break-up length increased with an increase in the Reynolds number. However, if the Re was increased beyond  $2 \times 10^4$ , the break-up length tended to decrease.

The wavy flow region of the spray corresponds to the spray photograph shown as (A) in Fig.12 and the decreasing region of the break-up length corresponds to (B). The photograph (C) in Fig.12 shows the complete spray indicated in the hatching area in Fig.13, where the break-up length was short and was not affected by the Reynolds number. When the jet was injected into the ambient gas of atmospheric pressure, the complete spray jet region could not be observed, but it was observed in the wide region under elevated pressure conditions. It can therefore easily be considered that the respective process of break-up and spray formation mechanisms for (B) and (C) in Fig. 12 differ from each other and it was the main reason why eq.(5) could not predict the Sauter mean diameter of the spray injected into an elevated pressure environment.

With reference to the two categories of sprays, the measurement results so far obtained on the Sauter mean diameter can be summarized as follows:

For an incomplete spray with a relatively low injection velocity, the Sauter mean diameter decreases with an increase in ambient pressure and rapidly decreases with a decrease in injection velocity, due to the strong influence of liquid kinematic viscosity and surface tension.

For a complete spray with a high injection velocity, the Sauter mean diameter increases with an increase in ambient pressure and decreases slowly with a decrease in injection velocity due to the slight influence of liquid kinematic viscosity and surface tension.

The shift from incomplete to complete spray is dependent upon kinematic viscosity and surface tension. The higher the kinematic viscosity and surface tension, the higher the injection velocity at which the shift occurs.

#### DERIVATION OF EMPIRICAL EQUATIONS

Dimensionless analysis was conducted based on equation (2) and discussions in the previous session. Dimensionless parameters of  $X_b/D$ ,  $Re$ ,  $We$ ,  $\mu/\mu_a$ ,  $\rho/\rho_a$ , were combined to produce the following two dimensionless groups of parameters.

$$\left(\frac{X_b}{D}\right) \left(\frac{Re}{We}\right)^{-0.3} \left(\frac{\mu}{\mu_a}\right)^{-0.3} \quad (6)$$

$$Re^{-0.3} We^{-1} \left(\frac{\mu}{\mu_a}\right)^{0.4} \left(\frac{\rho}{\rho_a}\right)^{1.2} \quad (7)$$

An index number for every dimensionless term was chosen by a trial and error method to produce the best correlation of the data obtained at an ambient pressure of 3.0 MPa.

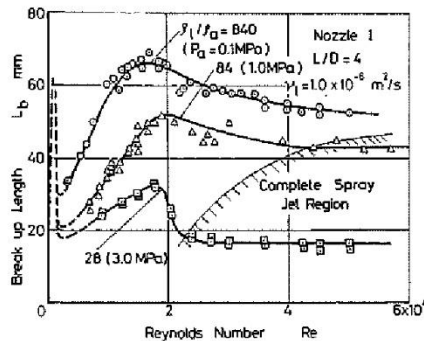


Fig.13 - Break-up length of a diesel spray

Figure 14 shows how these two dimensionless groups relate. From this figure, we could obtain the following two relationships. For incomplete sprays,

$$\frac{X_{50}}{D} = 4.12 \text{Re}^{0.12} \text{We}^{-0.075} \left(\frac{\mu_1}{\mu_a}\right)^{0.54} \left(\frac{\rho_1}{\rho_a}\right)^{0.18} \quad (8)$$

was obtained; and eq.(9) for complete sprays.

$$\frac{X_{50}}{D} = 0.14 \text{Re}^{0.25} \text{We}^{-0.32} \left(\frac{\mu_1}{\mu_a}\right)^{0.37} \left(\frac{\rho_1}{\rho_a}\right)^{0.17} \quad (9)$$

The correlation of data measured under different ambient pressure conditions is shown in Fig.15. The data for incomplete sprays appears in good correlation, though the Sauter mean diameters of complete sprays are not well correlated by these two dimensionless groups.

Therefore the equation (9) had to be modified by the density ratio  $\rho_1/\rho_a$  to apply the wide range of ambient pressure conditions. Then, the following equation to express the Sauter mean diameter of the complete spray could be obtained.

$$\frac{X_{50}}{D} = 0.38 \text{Re}^{0.25} \text{We}^{-0.32} \left(\frac{\mu_1}{\mu_a}\right)^{0.37} \left(\frac{\rho_1}{\rho_a}\right)^{-0.47} \quad (10)$$

Comparison of eq.(8) and the measured results for glycerine-water solution is shown in Fig.16. The deviation of the measured data from the predicted value shows that this equation can only apply to incomplete sprays that have relatively large Sauter mean diameters. Figure 17 indicates the deviation of the predicted results obtained by eq.(10) from the same measured data as Fig.16. In this case, the discrepancy appears in the relatively large  $X_{50}/D$ .

The critical conditions for the applicable limits of both equations are the same and expressed by the following equation.

$$\text{Re}^{0.3} \text{We}^{0.3} = 10.84 \left(\frac{\mu_1}{\mu_a}\right)^{0.17} \left(\frac{\rho_1}{\rho_a}\right)^{0.55} \quad (11)$$

This equation can also give the low pressure limit for a fine spray, because this limit means the shifting point from incomplete to complete spray.

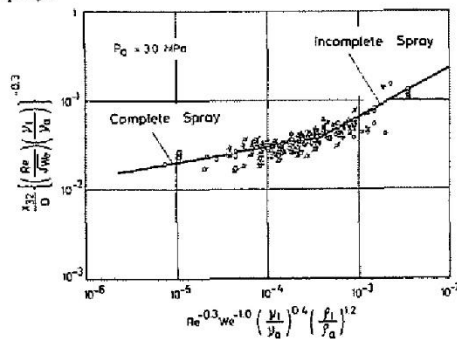


Fig.14 - Correlation of the measured results from the dimensionless parameters (data for 3.0 MPa)

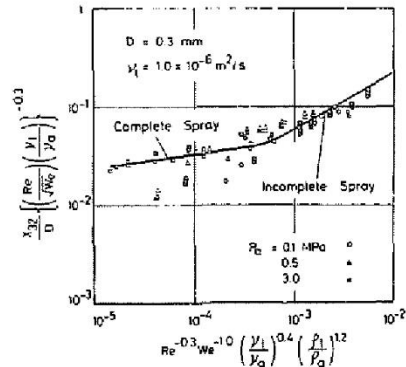


Fig.15 - Correlation of the measured results from the dimensionless parameters (data for different ambient pressure)

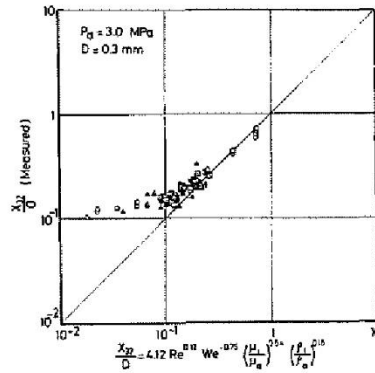


Fig.16 - Comparison between measured results and predicted Sauter mean diameters by eq.(8)

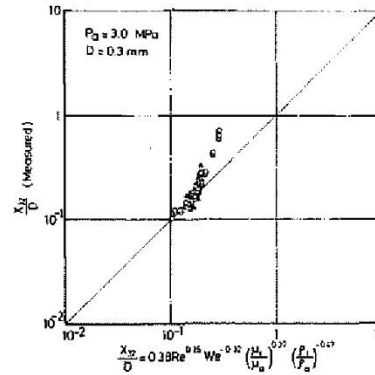


Fig.17 - Comparison between measured results and predicted Sauter mean diameters by eq.(10)

Finally from the above discussion we derive a general equation for the Sauter mean diameter of a diesel spray as follows

$$\frac{X_{32}}{D} = \text{MAX} \left[ \frac{X_{32}^{LS}}{D}, \frac{X_{32}^{HS}}{D} \right] \quad (12)$$

$$\left\{ \begin{aligned} \frac{X_{32}^{LS}}{D} &= 4.12 \text{Re}^{0.12} \text{We}^{-0.25} \left(\frac{\mu_l}{\mu_a}\right)^{0.54} \left(\frac{\rho_l}{\rho_a}\right)^{0.18} & (12-a) \\ \frac{X_{32}^{HS}}{D} &= 0.38 \text{Re}^{0.25} \text{We}^{-0.32} \left(\frac{\mu_l}{\mu_a}\right)^{0.37} \left(\frac{\rho_l}{\rho_a}\right)^{-0.47} & (12-b) \end{aligned} \right.$$

Where MAX[ , ] means the larger value of the two

$X_{32}/D$  = ratio of Sauter mean diameter to nozzle diameter

Re = Reynolds number of liquid

We = Weber number of liquid

$\mu_l/\mu_a$  = viscosity ratio of liquid to ambient air

$\rho_l/\rho_a$  = density ratio of liquid to ambient air

Equation (12-a) shows the Sauter mean diameter for the incomplete spray with a low injection velocity, and Eq.(12-b) for the complete spray. Concerning the effect of an ambient pressure on the Sauter mean diameter, the upper equation shows the positive density ratio of a liquid to ambient air ( $\rho_l/\rho_a$ ). This is well in agreement with the experimental result that the Sauter mean diameter decreases with an

increase in ambient pressure (or density). The lower equation showing a negative density ratio also agrees well with the experimental result that the Sauter mean diameter increases with an increase in ambient pressure (or density).

In Figure 18, the values of  $X_{32}/D$  calculated by equation (12) are plotted against all the measured values of the Sauter mean diameter. From this figure, it is apparent that by using equation (12) the change in the Sauter mean diameter is predictable in relation to each of such factors as injection pressure, ambient pressure, liquid kinematic viscosity and surface tension, and nozzle diameter.

The applicable range of equation (12) is given below.

- 1) Injection velocity 19 ~ 300 m/s  
(Injection pressure 3.5 ~ 90.0 MPa)
- 2) Density of ambient air 1.3 ~ 3.9 kg/m<sup>3</sup>  
(Ambient pressure 0.1 ~ 3.0 MPa)
- 3) Nozzle diameter 0.2 x 10<sup>-3</sup> ~ 0.4 x 10<sup>-3</sup> m  
(Length-to-hole diameter ratio = approx. 3 ~ 6)
- 4) Kinematic viscosity 0.8 x 10<sup>-6</sup> ~ 210 x 10<sup>-6</sup> m<sup>2</sup>/s
- 5) Surface tension 33 x 10<sup>-3</sup> ~ 75 x 10<sup>-3</sup> N/m
- 6) Density of liquid 0.8 x 10<sup>3</sup> ~ 1.3 x 10<sup>3</sup> kg/m<sup>3</sup>

### CONCLUSIONS

The influence of ambient pressure, liquid kinematic viscosity, surface tension and nozzle diameter on the Sauter mean diameter of a diesel spray was studied over a wide range of injection pressures from 3 to 90 MPa, using equipment to measure drop size developed from the Fraunhofer diffraction technique. The results of the study are summarized as follows:

1. According to the difference in break-up mechanism, the atomization state of a diesel spray can be classified into two categories. One is the incomplete spray where liquid disintegration progresses gradually from the exit of the nozzle as the jet advances, due to relatively low injection velocity. The other is the complete spray where atomization is fully developed. The shift from the incomplete to complete spray occurs as injection velocity increases.
2. The higher the liquid kinematic viscosity and surface tension, the higher the injection velocity at which the shift occurs.
3. The Sauter mean diameter decreases with an increase in ambient pressure for the incomplete spray, whereas the Sauter mean diameter increases with an increase in ambient pressure for the complete spray.
4. The higher the liquid kinematic viscosity and surface tension, the larger the Sauter mean diameter becomes. The Sauter mean diameter also increases with an increase in nozzle diameter.
5. Based on the above results, a dimensionless analysis of the measurement results on the Sauter mean diameter was conducted for each of the two spray categories, leading to equation (12) for the Sauter mean diameter.

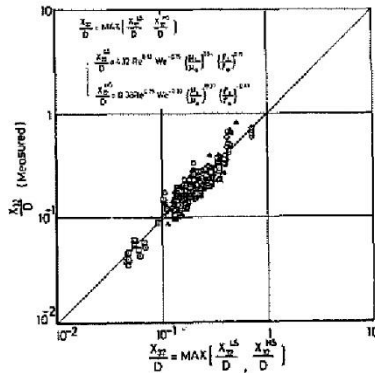


Fig.18 - Comparison between measured results and the Sauter mean diameters predicted by the final equation

REFERENCES

1. Woltjen, A., "Über die Feinheit der Brennstoffzerstaubung in Oelmotoren," Drmstat, Diss T.H., 1925.
2. Sass, F., "Kompressorlose Dieselmotoren," Berlin, Julius Springer, 1929.
3. Mehleg, H., "Zur Physik der Brennstoffstrahlen in Diesel Motoren," ATZ 37, 1934.
4. Tanasawa, Y. and Hiroyasu, H., "Measurement of Size Distribution of Sprayed Drops by Means of Molton Wax," Trans. of JSME (in Japanese), pp.26-162, 1960.
5. Tanasawa, Y. and Hiroyasu, H., "On the Drop Size Analyzer for Liquid Spray by Sedimentation," The Technology Reports of Tohoku University, 27-1, 1962.
6. Tanasawa, Y. and Toyoda, S., "On the Atomization of Liquid Jet Issuing from a Cylindrical Nozzle," Tech. Report of Tohoku Univ. 19-2, 1955.
7. Hiroyasu, H. and Kadota, T., "Fuel Droplet Size Distribution in Diesel Combustion Chamber," SAE Paper, No.740715, 1974.
8. Hiroyasu, H., Toyota, Y. and Kadota, T., "Transient Characteristics of Droplet Size Distribution in Diesel Sprays," 1st Int. Conference on Liquid Atomization and Spray Systems ICLASS-78 Tokyo, 1978.
9. Swithenband, J., et al, "A Laser Diagnostic Technique for the Measurement of Droplet and Particle Size Distribution," AIAA Paper 76-69, 1976.
10. Felton, P.G., "In-Stream Measurement of Particle Size Distribution," Int. Symp. on In-stream Measurements of Particle Solid Properties IIC, 1978.
11. Gomi, H., "Data Reductions of Drop Size Distribution from Diffracted Light Energy Distribution," The 12th Conference on Liquid Atomization and Spray Systems in Japan, 1984.
12. Tabata, M., Arai, M. and Hiroyasu, H., "Atomization of High Viscosity Liquid by a Diesel Nozzle," Bulletin of JSME, Vol.29, No.252, 1986.
13. Arai, M., Tabata, H., Hiroyasu, H. and Shimizu, H., "Disintegrating Process and Spray Characterization of Fuel Jet Injected by a Diesel Nozzle," SAE Paper, No. 840275, 1984.

ENERGY TECHNOLOGY CENTER  
LULEÅ UNIVERSITY OF TECHNOLOGY

CFD WITH OPENSOURCE SOFTWARE, ASSIGNMENT 3

---

## Tutorial dieselFoam

---

*Author:*  
Per CARLSSON

*Peer reviewed by:*  
NAIXIAN LU  
HÅKAN NILSSON

February 17, 2009

## Chapter 1

# Tutorial dieselFoam

### 1.1 Introduction

This tutorial describes how to pre-process, run and post-process a case involving compressible reacting flow with Lagrangian evaporating particles in a three-dimensional domain. It also describes how to copy the solver, copy an evaporation model and how to add a second material to the discrete particles.

The geometry consists of a block filled with air, with a 0.01x0.01 meter base and a length of 0.1 meter (figure 1.1). An injector is centrally placed on the top boundary where n-Heptane ( $C_7H_{16}$ ) is injected. When the discrete droplets enter the domain they evaporate and combustion takes place in the gas phase. There are several gas phase reaction schemes supplied with the case ranging from a reaction scheme with 5 species and one reaction up to a reaction scheme involving  $\sim 300$  reactions and 56 species.

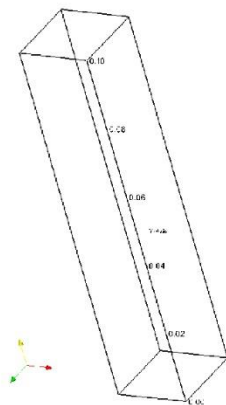


Figure 1.1: Geometry of the dieselFoam tutorial case.

## 1.2 Pre-processing

This section covers the necessary setup needed to get the dieselFoam case running with chemistry, the tutorial also covers a brief introduction to reacting flows in numerical simulations.

### 1.2.1 Getting started

Copy the dieselFoam tutorial to the run directory.

```
cp -r $FOAM_TUTORIALS/dieselFoam/aachenBomb $FOAM_RUN
cd $FOAM_RUN/aachenBomb
```

The file structure of the dieselFoam case is similar to other OpenFOAM tutorials where the case directory has a `/0`, `/constant` and `/system` directory. The dieselFoam case also has a `/chemkin` directory where the gas phase reaction schemes are specified. As usual in OpenFOAM tutorials; the solver-, write- and time-control can be found in the `/system` directory and the mesh setup in `/constant/polyMesh`.

### 1.2.2 Boundary and initial conditions

Since there are neither outlets nor inlets, apart from the injector, the boundary conditions for the dieselFoam tutorial are very simple. All walls are modeled as adiabatic. The boundary conditions for the injector can be found in `/constant/injectorProperties` file see example below.

```
injectorType      unitInjector;

unitInjectorProps
{
    position      (0 0.0995 0);
    direction     (0 -1 0);
    diameter      0.00019;
    Cd            0.9;
    mass          6e-06;
    temperature   320;
    nParcels      5000;

    X
    (
        1.0
    );
    massFlowRateProfile
    (
        (0 0.1272)
        (4.16667e-05 6.1634)
        (8.33333e-05 9.4778)
        ...
    );
}
```

In the `/constant/injectorProperties` file it can be seen that the injector is located 0.5 mm from the top of the domain and injects in the negative y direction. Furthermore, the injector nozzle diameter, the nozzle discharge coefficient, mass and temperature of the parcels can be found here as well as the total number of injected parcels. The X is the mass fraction of a specific specie which will be described further in section 1.5. The `massFlowRateProfile` specifies how the mass flow rate should vary over time. From time  $t_0 \rightarrow t_1$  the mass flow rate is  $\dot{m}_0$ . This done in order to simulate opening and closing of the injector. The left column of the `massFlowRateProfile` is  $t_i$  and the right,  $\dot{m}_i$ .



It is possible to define different kinds of injectors, however, in this tutorial only the `unitInjector` will be used. In the `/constant/sprayProperties` file the user can specify what will happen to the droplets as they enter the domain, see table 1.1.

Model	General meaning
<code>subCycles</code>	Minimum number of Lagrangian sub cycles
<code>atomizationModel</code>	How atomization is treated
<code>includeOscillation</code>	Droplet deformation; will effect droplet drag coefficient
<code>breakupModel</code>	If secondary break up is used
<code>injectorModel</code>	Which injector model to use
<code>collisionModel</code>	Particle - particle interaction
<code>evaporationModel</code>	Which evaporation model to use
<code>heatTransferModel</code>	Particle heat transfer model
<code>dispersionModel</code>	If turbulent dispersion is used or not
<code>dragModel</code>	Particle drag model
<code>wallModel</code>	What happens to particles hitting the walls

Table 1.1: Spray sub-models for the dieselFoam tutorial

The initial conditions are found in the `/0` directory and are summarized in table 1.2. Not all initial conditions are specified here since they are not necessary to get the case running. Note that the initial mass fractions for  $N_2$  and  $O_2$  corresponds to air and that the initial condition for `spray` is empty since it is specified in the `/constant/injectorProperties`-file.

Variable	Initial conditions
$\epsilon$	internalField uniform 90.0, walls zeroGradient
$k$	internalField uniform 1.0, walls zeroGradient
$N_2$	internalField uniform 0.766, walls zeroGradient
$O_2$	internalField uniform 0.233, walls zeroGradient
$p$	internalField uniform 5e+06, walls zeroGradient
<code>spray</code>	empty
$T$	internalField uniform 800, walls zeroGradient
$U$	internalField uniform ( 0 0 0 ), walls uniform ( 0 0 0 )

Table 1.2: Initial conditions for the dieselFoam tutorial

### 1.2.3 Physical properties

In the `/constant` directory the properties files for chemistry, environment, spray, combustion, injector, RAS and thermophysical. The spray and injector properties are described in section 1.2.2 and the RAS properties are thoroughly described in the OpenFOAM user guide and are therefore not described here. The properties files are summarized in table 1.3.

Properties file	General content
chemistryProperties	Chemical reactions are included if <code>chemistry</code> is switched on Specification and settings for the discretization scheme used to solve the chemistry ODEs
environmentalProperties	Gravity
combustionProperties	Ignition point on or off, timing and duration of ignition point
thermophysicalProperties	Specify the mixture type and which gas phase reaction scheme to use as well as thermodynamic database

Table 1.3: Properties files and general content for the dieselFoam tutorial

A certain mixture type may be more or less suited for a combustion problem and depends on if the flame is non-, partly or full-premixed. In the `thermophysicalProperties` file it is possible to specify the mixture types, several are available<sup>1</sup>. Parts of the `thermophysicalProperties` file is listed below, notice that the location of the `CHEMKINThermoFile` has been changed from `"OpenFOAM/thermoData/therm.dat"` to `"$FOAM_CASE/chemkin/therm.dat"`.

```
thermoType hMixtureThermo<reactingMixture>;
CHEMKINfile      "$FOAM_CASE/chemkin/chem.inp";
CHEMKINThermoFile "$FOAM_CASE/chemkin/therm.dat";
```

In this tutorial we will use the predefined `reactingMixture` together with the thermophysical model `hMixtureThermo` which calculates enthalpy for combustion mixture. The choice of mixture and thermo physical model depends both on the physics of the flame and which variables that are needed for the combustion model. The `thermophysicalProperties` file also contains information on where the gas phase reactions are defined as well which thermo dynamic data base to use. The gas phase reactions are specified in the `"$FOAM_CASE/chemkin/chem.inp"` file and the thermo dynamic data base in the `"$FOAM_CASE/chemkin/therm.dat"` file. The `therm.dat` and `chem.inp`-file will be described further in section 1.2.4 as well as the combustion model.

### 1.2.4 Chemistry

When the droplets enter the domain they start to evaporate. The  $C_7H_{16}(g)$ <sup>2</sup> then reacts with oxygen forming  $CO_2$  and  $H_2O$ . However, this reaction can be called a global reaction and is not what would happen if  $C_7H_{16}(g)$  would burn with air in a real combustor or burner. As an example, think about hydrogen burning with pure oxygen, see reaction 1.1.



However, in order for the hydrogen to react with oxygen, the bond between the atoms first have to be broken and a more complex reaction scheme is required, see reaction 1.2 to 1.6.



<sup>1</sup><http://www.openfd.co.uk/openfoam/doc/thermophysicalModels.html>

<sup>2</sup>Notation  $(g)$  meaning that the specie is in gas phase. Similar notation is  $(s)$  for solid and  $(l)$  for liquid. The notation is used here to emphasize that no heterogeneous reactions are taking place.



So, instead of having two reactions (backward and forward) with three species we have ten reactions (backward and forward) with six species (the scheme described above is *ad hoc* and is just used to describe the difficulties describing chemistry in numerical simulations). The transport equations for these species have to be solved as well as the ODEs for the reactions. In this tutorial the gas phase reactions are specified in the `/chemkin/chem.inp`-file, see below.

```

REACTIONS
C7H16 + 11O2          => 7CO2 + 8H2O          5.00E+8  0.0  15780.0!  1
      FORD / C7H16 0.25 /
      FORD / O2 1.5 /
END

```

The entries behind the reaction in the `/chemkin/chem.inp`-file are Arrhenius coefficient that are used to calculate the chemical reaction rate. FORD is the forward reaction order. The chemical reaction rate will be calculated according to equations 1.7 and 1.8

$$k_f = AT^b \cdot \exp\left(\frac{-E_a}{RT}\right) \quad (1.7)$$

Where  $k_f$  is the forward reaction coefficient,  $A$  pre exponential factor,  $b$  temperature exponent,  $E_a$  activation energy,  $R$  ideal gas coefficient and  $T$  temperature.

$$\dot{\omega}_i = \frac{d[\text{product}]}{dt} = -k_f * [\text{fuel}]^c [\text{oxidizer}]^d \quad (1.8)$$

Where  $\dot{\omega}_i$  is the chemical reaction rate,  $t$  time,  $c$  and  $d$  the forward reaction order and,  $[C]$  is concentration of specie  $C$ . In simplified terms the `/chemkin/chem.inp`-file can thus be written as:

```

REACTIONS
fuel + oxidizer          => product          A  b  Ea
      FORD / fuel c /
      FORD / oxidizer d /
END

```

Due to the numerical cost only the simplest scheme (`chem.inp`) will be used in this tutorial but the user is encouraged to look in the `chem.inp.full` file to see how a complex but still reduced reaction scheme might look like.

With out going into great detail regarding thermodynamics in combustion processes<sup>3</sup>, it is possible to realize that when a fuel and an oxidizer react, they will produce heat. The amount of heat released from the flame as well as the flame temperature can be predicted using thermodynamics. The thermodynamic data base is located in the `/chemkin/therm.dat`-file. An example from the `/chemkin/therm.dat`-file is listed below.

```

C7H16          P10/95 C  7H  16    0    0G  200.000 5000.000 1391.000  1
2.22148969e+01 3.47675750e-02-1.18407129e-05 1.83298478e-09-1.06130266e-13  2
-3.42760081e+04-9.23040196e+01-1.26836187e+00 8.54355820e-02-5.25346786e-05  3
1.62945721e-08-2.02394925e-12-2.56586565e+04 3.53732912e+01  4

```

<sup>3</sup>Combustion 4th edition, Chapter 4, J.Warnatz et al. Springer 2006

- The first row contains species name, date (not used in the code), atomic symbols and formula, phase of species (S, L, or G for gas), low temperature, high temperature and common temperature (if needed).
- The second row contains coefficients  $a_1 - a_5$  in equation 1.9 for upper temperature interval.
- The third row contains coefficients  $a_6, a_7$  for upper temperature interval, and  $a_1, a_2,$  and  $a_3$  for lower.
- The fourth row contains coefficients  $a_4, a_5, a_6, a_7$  for lower temperature interval.

From these constants, (NASA) polynomials for specific heat  $C_p$ , enthalpy  $H$  and entropy  $S$  can be calculated.

$$\frac{C_p}{R} = a_1 + a_2 \cdot T + a_3 \cdot T^2 + a_4 \cdot T^3 + a_5 \cdot T^4 \quad (1.9)$$

$$\frac{H}{RT} = a_1 + \frac{a_2 T}{2} + \frac{a_3 T^2}{3} + \frac{a_4 T^3}{4} + \frac{a_5 T^4}{5} + \frac{a_6}{T} \quad (1.10)$$

$$\frac{S}{R} = a_1 \ln T + a_2 T + \frac{a_3 T^2}{2} + \frac{a_4 T^3}{3} + \frac{a_5 T^4}{4} + a_7 \quad (1.11)$$

The specific heat  $C_p$ , enthalpy  $H$  and entropy  $S$  are then used in the code to solve the conservation equations.

The combustion model for this tutorial is a partially stirred reactor concept model developed at Chalmers Gothenburg described by equations 1.12 and 1.13

$$CST_i = \frac{\tau_{chem}}{\tau_{mix} + \tau_{chem}} \dot{\omega}_i \quad (1.12)$$

Where  $CST_i$  is the chemical source term,  $\tau_{chem}$  chemical time  $\propto \frac{1}{k_f}$  and  $\tau_{mix}$  mixing time. The mixing time  $\tau_{mix}$  is calculated according to

$$\tau_{mix} = C_{mix} \sqrt{\frac{\mu_{eff}}{\rho \epsilon}}. \quad (1.13)$$

Where  $C_{mix}$  is a constant specified in the `/constant/combustionProperties`-file,  $\mu_{eff}$  is the effective viscosity,  $\rho$  density and  $\epsilon$  rate of dissipation of turbulent kinetic energy. The combustion model can be found on lines 81-95 in `$FOAM_SOLVERS/combustion/dieselFoam/dieselFoam.C`

### 1.3 Running the code

Remove `ft` and `fu` and in the `aachenBomb/0` directory since these are not needed for this setup (keeping them will result in post-processing problems).

```
cd $FOAM_RUN/aachenBomb/0
rm ft fu
```

Turn chemistry on in the `/constant/chemistryProperties` file

```
chemistry          on;
```

and ignition on in the `/constant/combustionProperties` file. This step is not necessary, the mixture will still ignite when the species are properly mixed due to the high temperature.

```
ignite            on;
```

Mesh the geometry using `blockMesh`, and start the `dieselFoam` solver.

```
cd $FOAM_RUN/aachenBomb
blockMesh
dieselFoam
```

The solution is only 0.01 seconds long, however, due to the fast chemistry a minimum of 4000 time steps are needed to resolve it. Furthermore, there is a total of 5000 parcels ( $parcel_{mass} = N * Droplet_{mass}$  where  $N$  is the statistical number of drops in the parcel) that enter the domain and the source term from these all have to be calculated.

## 1.4 Post-processing in ParaView

Since paraFoam can not handle Lagrangian particles use foamToVTK and then ParaView.

```
cd $FOAM_RUN/aachenBomb
foamToVTK
paraview
```

In the /VTK directory open the case file ( `aachenBomb\1.vtk` ) and also, open the particles in the /Lagrangian/defaultCloud\_2.vtk file. Create glyphs for the particles, see figure 1.2 for settings.

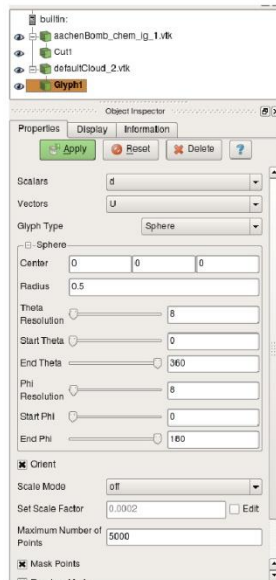


Figure 1.2: Settings for glyphs in ParaView to visualize the Lagrangian particles

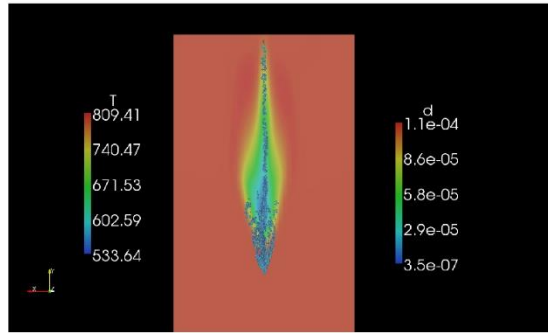


Figure 1.3: Droplets entering the domain, droplets colored by diameter and cut plane by temperature

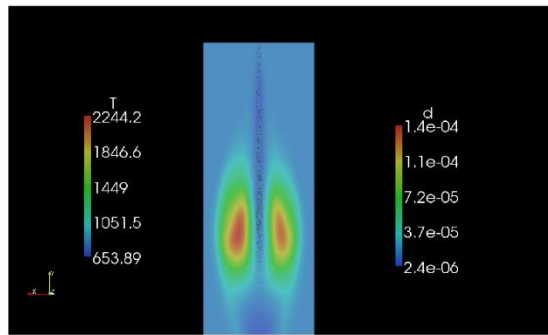


Figure 1.4: Gas phase ignition, droplets colored by diameter and cut plane by temperature

## 1.5 Adding a second liquid

To add a second liquid to the droplets follow these step-by-step instructions.

Remove `ft` and `fu` in the `aachenBomb/0` directory since these are not needed for this setup.

```
cd $FOAM_RUN/aachenBomb/0
rm ft fu
```

Turn chemistry on in the `/constant/chemistryProperties` file

```
chemistry          on;
```

and ignition on in the `/constant/combustionProperties` file.

```
ignite            on;
```

In `aachenBomb/constant/thermophysicalProperties` add an extra liquid material, here  $C_6H_{14}$  is used as an example.

```
liquidComponents
(
    C7H16
    C6H14
);

liquidProperties
{
    C7H16  C7H16  defaultCoeffs;
    C6H14  C6H14  defaultCoeffs;
}
```

In `aachenBomb/chemkin/chem.inp` add the  $C_6H_{14}$  in species.

```
ELEMENTS
H O C N AR
END
SPECIE
C6H14 C7H16 O2 N2 CO2 H2O
END
REACTIONS
C7H16 + 11O2          => 7CO2 + 8H2O          5.00E+8  0.0  15780.0!  1
      FORD          / C7H16 0.25 /
      FORD          / O2 1.5 /
END
```

In `aachenBomb/constant/injectorProperties` change the mass fractions for  $C_7H_{16}$  and  $C_6H_{14}$ .

```
X
(
    0.8
    0.2
);
```

The droplets will now consist of 80 weight percent  $C_7H_{16}$  and 20 percent  $C_6H_{14}$ . Mesh the geometry using `blockMesh`, and start the `dieselFoam` solver.

```
cd $FOAM_RUN/aachenBomb
blockMesh
dieselFoam
```

Post in ParaView as described in section 1.4. Notice the difference in evaporation pressure between the two species  $C_6H_{14}$  and  $C_7H_{16}$ .

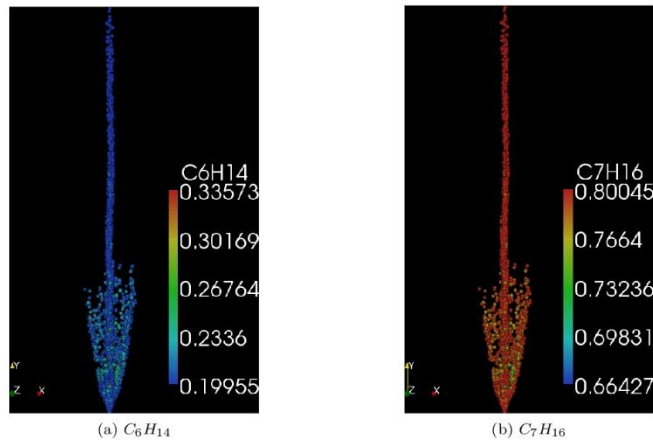


Figure 1.5: Droplets colored by mass fractions

## 1.6 Your own evaporation model

To copy and create your own evaporation model follow these step-by-step instructions.

### 1.6.1 Copy the dieselFoam solver

Copy the dieselFoam solver to your working directory.

```
mkdir -p $WM_PROJECT_USER_DIR/applications/solvers/combustion
cp -r $FOAM_SOLVERS/combustion/dieselFoam $WM_PROJECT_USER_DIR\
/applications/solvers/combustion/mydieselFoam
```

Rename solver to mydieselFoam.

```
cd $WM_PROJECT_USER_DIR/applications/solvers/combustion/mydieselFoam/Make
```

Change in the `/Make/files` so it reads.

```
dieselFoam.C
```

```
EXE = $(FOAM_USER_APPBIN)/mydieselFoam
```

Change in the `/Make/options` so the second line reads.

```
-I$(LIB_SRC)/../applications/solvers/combustion/dieselEngineFoam \
```

### 1.6.2 Copy the dieselSpray library

Copy the `src/lagrangian/dieselSpray` dictionary to your user dictionary and rename it to `mydieselSpray`.

```
cd $WM_PROJECT_DIR
cp -riuv --parents --backup src/lagrangian/dieselSpray \
$WM_PROJECT_USER_DIR
cd $WM_PROJECT_USER_DIR/src/lagrangian
mv dieselSpray mydieselSpray
```



Copy the `standardEvaporationModel` dictionary to `my_standardEvaporationModel`.

```
cd $WM_PROJECT_USER_DIR/src/lagrangian/mydieselSpray/spraySubModels/evaporationModel
cp -r standardEvaporationModel my_standardEvaporationModel
```

Change `standardEvaporationModel` to `my_standardEvaporationModel` in the `.C` and `.H` file using `sed` and rename the files to `my_standardEvaporationModel`.

```
cd $WM_PROJECT_USER_DIR/src/lagrangian/mydieselSpray/spraySubModels/evaporationModel
cd my_standardEvaporationModel
sed s/standardEvaporationModel/my_standardEvaporationModel/g \
standardEvaporationModel.C >my_standardEvaporationModel.C
sed s/standardEvaporationModel/my_standardEvaporationModel/g \
standardEvaporationModel.H >my_standardEvaporationModel.H
rm standardEvaporationModel.C standardEvaporationModel.H
```

Add `my_standardEvaporationModel.C` to the list of evaporation models in `/mydieselSpray/Make/files` line 59.

```
.
.
$(evaporationModels)/saturateEvaporationModel/saturateEvaporationModel.C
$(evaporationModels)/my_standardEvaporationModel/my_standardEvaporationModel.C
```

Also, change the name of the library at the bottom of the `/mydieselSpray/Make/files` file to

```
LIB = $(FOAM_USER_LIBBIN)/libmydieselSpray
```

### 1.6.3 Adding mydieselSpray library to mydieselFoam solver

Go to your `mydieselFoam` directory

```
cd $WM_PROJECT_USER_DIR/applications/solvers/combustion/mydieselFoam/Make
```

Open the `options` file and change line 6 from

```
-I$(LIB_SRC)/lagrangian/dieselSpray/lnInclude \
```

to:

```
-I$(WM_PROJECT_USER_DIR)/src/lagrangian/mydieselSpray/lnInclude \
```

At the end of the `options` file change so it reads:

```
-lpdf \
-L$(WM_PROJECT_USER_DIR)/lib/$(WM_OPTIONS) \
-lmydieselSpray
```

### 1.6.4 Update case files

Update the `sprayProperties` so it includes the coefficients for your evaporation model in `aachenBomb/constant/sprayProperties`.

```
cd $FOAM_RUN/aachenBomb/constant
```

Edit `sprayProperties` so the evaporation model is set to:

```
evaporationModel my_standardEvaporationModel;
```

Also, add model coefficients for your evaporation model in then `sprayProperties` file

```
my_standardEvaporationModelCoeffs
{
    evaporationScheme explicit;
    preReScFactor 0.6;
    ReExponent 0.5;
    ScExponent 0.333333;
}
```

### 1.6.5 Customizing the evaporation model

Go back to the `my_standardEvaporationModel` directory.

```
cd $WM_PROJECT_USER_DIR/src/lagrangian/mydieselSpray/spraySubModels/\
evaporationModel/my_standardEvaporationModel
```

Take a closer look in `my_standardEvaporationModel.C`. On line 98 to 104 it reads,

```
scalar my_standardEvaporationModel::Sh
(
    const scalar ReynoldsNumber,
    const scalar SchmidtNumber
) const
{
    return 2.0 + preReScFactor_*pow(ReynoldsNumber,ReExponent_)\
    *pow(SchmidtNumber,ScExponent_);
}
```

That is, the Sherwood number is calculated according to the *Ranz-Marshall* correlation<sup>4</sup>, see equation 1.14, observe that the `my_standardEvaporationModelCoeffs` are used here.

$$Sh = 2 + 0.6Re_r^{0.5}Sc^{0.33333} \quad (1.14)$$

Where  $Sh$  is the Sherwood number,  $Re_r$  relative Reynold number and  $Sc$  Schmidt number.

In this tutorial we will make changes to the evaporation time, located in `my_standardEvaporationModel.C`, on line 142 to 163.

```
scalar Xratio = (Xs - Xf)/max(SMALL, 1.0 - Xs);

if (Xratio > 0.0)
{
    lgExpr = log(1.0 + Xratio);
}

scalar denominator =
6.0 * massDiffusionCoefficient
* Sh(ReynoldsNumber, SchmidtNumber)
* rhoFuelVapor * lgExpr;

if (denominator > SMALL)
{
    time = max(VSMALL, liquidDensity * pow(diameter, 2.0)/denominator);
}

return time;
```

<sup>4</sup>Multiphase flows with droplets and particles, Crowe et al. (1998) CRC Press LLC

We want the evaporation time  $\tau_m$  to be calculated by a  $D^2$ -law showed in equations 1.15 and 1.16

$$\lambda = \frac{4Sh\rho_c D_v}{\rho_d} (\omega_{A,s} - \omega_{A,\infty}) \quad (1.15)$$

Where  $\lambda$  is the evaporation constant,  $\rho_c$  film density,  $\rho_d$  droplet density,  $D$  diameter,  $D_v$  diffusion coefficient for species  $A$ ,  $\omega_{A,s}$  mass fraction of species  $A$  at the droplet surface and  $\omega_{A,\infty}$  for the free stream.

$$\tau_m = \frac{D^2}{\lambda} \quad (1.16)$$

Make changes in the `my_standardEvaporationModel.C` file, according to the equations showed. Start by removing `scalar lgExpr = 0.0;` on line 123. Edit the `my_standardEvaporationModel.C` file and change `scalar Xratio` and `scalar denominator`. Remove the `if (Xratio > 0.0)` statement completely.

```
scalar Xratio = (Xs - Xf);

scalar denominator =
4.0 * massDiffusionCoefficient
* Sh(ReynoldsNumber, SchmidtNumber)
* rhoFuelVapor*Xratio;

if (denominator > SMALL)
{
    time = max(VSMALL, liquidDensity * pow(diameter, 2.0)/denominator);
}

return time;
```

### 1.6.6 Compile library and solver

Compile the `mydieselSpray` library and your solver.

```
cd $WM_PROJECT_USER_DIR/src/lagrangian/mydieselSpray
wclean
rm -r lnInclude
rm -r Make/linux*
wmake libso

cd $WM_PROJECT_USER_DIR/applications/solvers/combustion/mydieselFoam
wclean
rm -r Make/linux*
wmake
```

### 1.6.7 Running the case

Start the solver with `mydieselFoam` and post in ParaView as described in section 1.4. When the solver starts check that your evaporation model is being used.

```
cd $FOAM_RUN/aachenBomb
blockMesh
mydieselFoam
```